Check for updates

View Article Online
View Journal

Materials Advances

Accepted Manuscript

This article can be cited before page numbers have been issued, to do this please use: A. Zafar, Y. Altaf, A. Zafar and M. A. Hashmi, *Mater. Adv.*, 2026, DOI: 10.1039/D5MA01210D.

This is an Accepted Manuscript, which has been through the Royal Society of Chemistry peer review process and has been accepted for publication.

Accepted Manuscripts are published online shortly after acceptance, before technical editing, formatting and proof reading. Using this free service, authors can make their results available to the community, in citable form, before we publish the edited article. We will replace this Accepted Manuscript with the edited and formatted Advance Article as soon as it is available.

You can find more information about Accepted Manuscripts in the Information for Authors.

Please note that technical editing may introduce minor changes to the text and/or graphics, which may alter content. The journal's standard Terms & Conditions and the Ethical guidelines still apply. In no event shall the Royal Society of Chemistry be held responsible for any errors or omissions in this Accepted Manuscript or any consequences arising from the use of any information it contains.

ROYAL SOCIETY OF CHEMISTRY

rsc.li/materials-advances

View Article Online
DOI: 10.1039/D5MA01210D

Structural Modulation of Hexagonal Boron Nitride: Surface Chemistry, Defect Control, and Emerging Applications

Aiman Zafar[1], Yasir Altaf[1*], Ayesha Zafar[1], Muhammad Ali Hashmi[1,2**]

[1]*Department of Chemistry, Division of Science and Technology, University of Education, Lahore 54000, Pakistan*

[2]*School of Chemical and Physical Sciences, Victoria University of Wellington, Wellington 6012, New Zealand*

*Corresponding authors: *yasir.altaf@ue.edu.pk*, *Muhammad.hashmi@vuw.ac.nz*

Open Access Article. Published on 24 June 2026. Downloaded on 6/26/2026 4:24:14 PM.
This article is licensed under a Creative Commons Attribution 3.0 Unported Licence.

Materials Advances Accepted Manuscript

Abstract

This review presents a systematic examination of surface chemistry and advanced modulation of hexagonal boron nitride (*h*-BN) and its derivatives, emphasizing the unique structural, electronic, and optical properties that have enabled a wide range of applications. First, we discuss the inherent properties of *h*-BN, including high thermal stability, mechanical strength, and excellent electrical insulation. Next, we address chemical functionalization, doping, and the methods used to form heterostructures, which significantly enhance surface performance in various fields such as catalysis, sensing, and nanocomposites. We further explore the role of DFT in predicting the electronic structure and modifying the reactivity of *h*-BN surfaces, aiming to optimize these modifications for specific applications. This review critically analyzes synthesis methods for h-BN and its derivatives, with particular focus on chemical vapor deposition (CVD) as a scalable technique that ensures high-quality material production. We also examine potential synergies through heterostructures, emphasizing interactions between *h*-BN and two-dimensional material systems. The review highlights current challenges, such as achieving uniform functionalization of layers and maintaining surface stability under operational conditions. Finally, we outline promising areas for future research to overcome these challenges and facilitate new applications of *h*-BN derivatives in emerging technologies.

View Article Online
DOI: 10.1039/D5MA01210D

Contents

Open Access Article. Published on 24 June 2026. Downloaded on 6/26/2026 4:24:14 PM.
This article is licensed under a Creative Commons Attribution 3.0 Unported Licence.

Materials Advances Accepted Manuscript

View Article Online
DOI: 10.1039/D5MA01210D

Open Access Article. Published on 24 June 2026. Downloaded on 6/26/2026 4:24:14 PM.
This article is licensed under a Creative Commons Attribution 3.0 Unported Licence.

Materials Advances Accepted Manuscript

View Article Online
DOI: 10.1039/D5MA01210D

Open Access Article. Published on 24 June 2026. Downloaded on 6/26/2026 4:24:14 PM.
This article is licensed under a Creative Commons Attribution 3.0 Unported Licence.

Materials Advances Accepted Manuscript

View Article Online
DOI: 10.1039/D5MA01210D

Open Access Article. Published on 24 June 2026. Downloaded on 6/26/2026 4:24:14 PM.
This article is licensed under a Creative Commons Attribution 3.0 Unported Licence.

Materials Advances Accepted Manuscript

1. Introduction

Nanomaterials with enhanced efficiency have been used in the industrial, biomedical and environmental applications[1-3] some of the potent nanoscale materials are carbon based including fullerenes, graphene and its modifications, carbon nanotubes CNTs and diamond compounds.[4-6] Other than carbon-rich materials, molybdenum disulphide MoS_2, molybdenum sulphate $MoSO_4$, carbon nitride and boron nitride materials have attracted much of the attention due to one dimension expansion at the Nano-scale.[7-9] However, amongst these low dimensional materials,

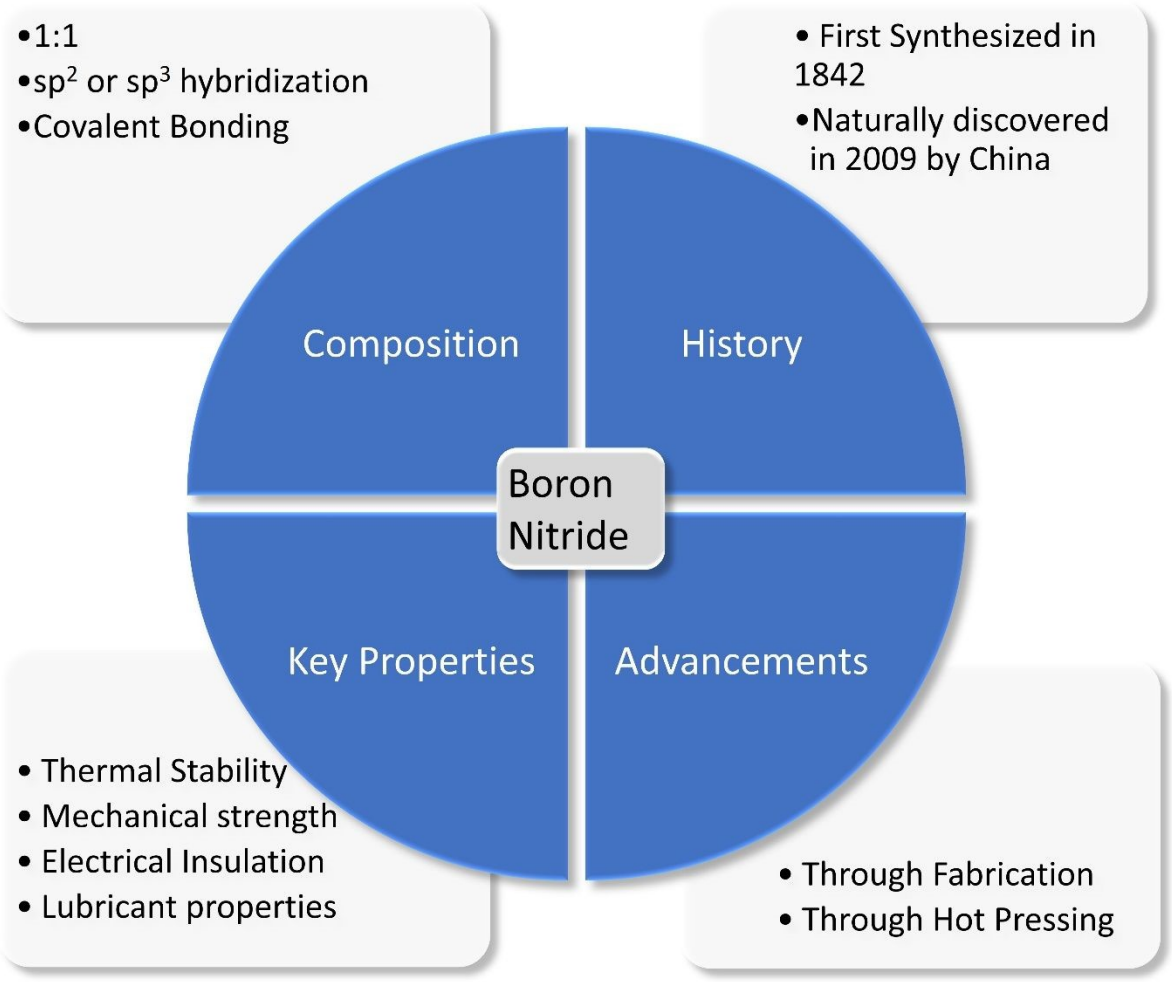

Figure 1: Overview of Boron Nitride: Composition, History, Properties, and Technological Advancements

BN had a massive influence attributing to the enhanced thermal stability and surface sensitivity. These materials are superior as well and have advantages over the conventional and traditional materials.[5, 6, 10-13] The rapid expansion of interest in low-dimensional nanomaterials was catalyzed by the successful synthesis and characterization of carbon nanotubes.[14]

View Article Online
DOI: 10.1039/D5MA01210D

Open Access Article. Published on 24 June 2026. Downloaded on 6/26/2026 4:24:14 PM.
This article is licensed under a Creative Commons Attribution 3.0 Unported Licence.

Boron nitride chemically written as BN comes under the category of low-dimensional ceramic materials. It has two elements nitrogen and boron.[15] Nitrogen is the most abundant monoatomic element comprising of 78% of atmosphere while boron is less abundant in nature and can only be found in the borates and its related minerals. The ratio of boron and nitrogen atom in BN is 1:1 which are overlapped via sp^2 or sp^3 hybridizations forming covalent bonds.[16, 17] These overlaps between the atomic orbitals of boron and nitrogen do not require any specific conditions rather works well in the normal conditions. Two monolayers in BN are attached together in place via weak type of Van der Waals interactive forces. The packing of adjacent layers occurs in such manner that B is facing N either from the top or the bottom which confirms the slight ionic nature of the covalent bonds between boron and nitrogen.[18] This stacking confers the polarity between the alternating boron and nitrogen.[19] Overview of Boron Nitride is graphically presented in Figure 1.

At first, BN was considered as the synthetic materials because no traces of it were found in the nature until 2009 when natural BN mineral was discovered in China.[20] BN has a long history and now can be synthesized from advanced techniques. It was Balmain in 1842 that first reported the synthesis of BN through the reaction of potassium cyanide with boric acid.[21, 22]

In the past years, there have been significant adaptations, fabrications, modifications and the improvements in the properties of BN more specifically after passing the BN through the procedure of hot pressing.[22-24] Thanks to the extensive research on BN, there are various crystal structures which are similar to carbon in their structures.[25]

A considerable number of reviews over the past couple of years have contributed to the understanding of h-BN and related two-dimensional materials and while these studies have advanced the field immaculately owing to substantial body of review literature but certain topics and aspects about h-BN are still dispersed across separate bodies of work. So, after carefully going through the literature and given the rapid, multi-disciplinary evolution and advancement of nanoscale material, there is a need for more recent and unified perspective that further understanding in h-BN literature. To give more context, Weng *et al.*[26] comprehensive work of 2016 on hexagonal boron nitride provides a chemically rigorous survey of physical and chemical functionalisation strategies for h-BN and it gives a catalogue of hydroxyl, amino, alkoxy, alkyl, and halogen surface groups alongside the carbon and oxygen heteroatom doping which adds to the value in terms of their usage in biological, polymer composite, and photocatalytic applications.

Materials Advances Accepted Manuscript

View Article Online
DOI: 10.1039/D5MA01210D

Open Access Article. Published on 24 June 2026. Downloaded on 6/26/2026 4:24:14 PM.
This article is licensed under a Creative Commons Attribution 3.0 Unported Licence.

The scope, however, is confined by literature that is available prior to that time. Some p-block elements, transition metal, and rare-earth substitutional dopants that have subsequently been shown by first-principles calculations to provide systematic control over the h-BN band gap through orbital hybridisation at B and N vacancy sites and it presents a gap in literature, left to be filled.[27-29] More recently though, Roy *et al.*[30] review of h-BN, specifically the structure, synthesis, and device applications, has exceptional depth in chemical vapour deposition growth strategies and van der Waals heterostructure physics. The consolidated discussion of dopant systems that are backed by DFT simulations remains notably scarce although the review does provide detailed commentary on dopants that are experimentally validated.

In this regard, the present review complement and extend on prior work by taking a different route and giving an integrated treatment of how structural defects, surface chemistry, and electronic properties are mutually coupled across all major BN configurations. The effect of dopant alongside the attention to DFT predicted mechanisms that underly the band gap engineering is what distinguishes the present review from its predecessors and it gives a unified surface chemistry perspective on emerging applications in environmental sensing, catalysis, and drug delivery to give researchers with a comprehensive framework for the rational design of h-BN-based functional materials.

2. Structural Details of Boron Nitride

BN structure is usually held together in place via sp^2 and sp^3 bonding patterns under room temperature and normal conditions. Many of the BN crystal structure exists but four forms are majorly used including hexagonal (h), cubic (c), rhombohedral (r) and wurtzite (w).[31, 32]

Hexagonal and rhombohedral configurations are structurally similar to graphite. Remaining forms (c) and (w) build up their crystal lattice via sp^3 hybridizations between atomic orbitals of nitrogen and boron and show resemblance with the crystals of diamond.[33, 34]

Both (c) and (w) crystalline structures are different based on the stacking parameters angles of tetrahedron containing BN_3 unit. Cubic form is appreciated for its chemical hardness. Among these structures, (h) and (r) BN lattices are formed by the intricate ordered sp^2 bonding.[35]

Materials Advances Accepted Manuscript

View Article Online
DOI: 10.1039/D5MA01210D

Open Access Article. Published on 24 June 2026. Downloaded on 6/26/2026 4:24:14 PM.
This article is licensed under a Creative Commons Attribution 3.0 Unported Licence.

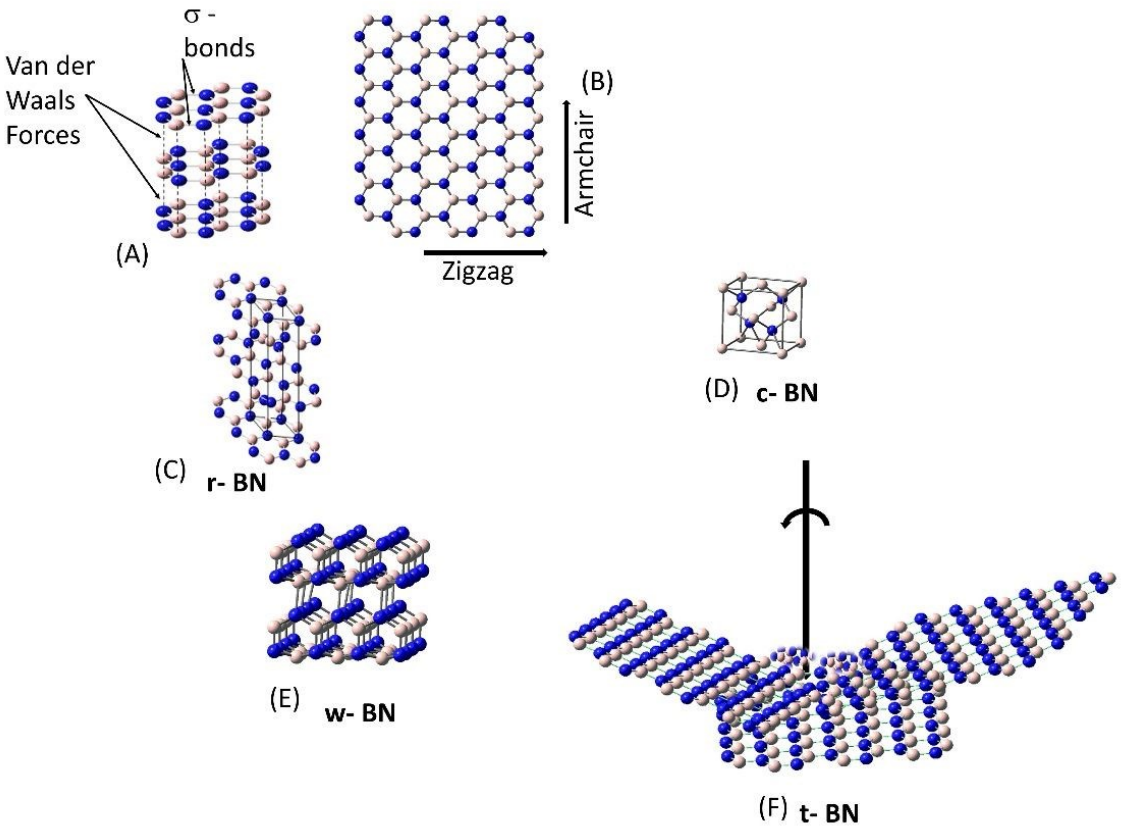

Figure 2: Forms of BN (A) Interactions between corresponding layers of BN (B) Zigzag and armchair BN (C) r-BN, (D) c-BN, (E) w-BN, (F) t-BN

Visual representations of various forms of BN are well presented in Figure 2. Less ordered allotropes with sp^2 bonded configurations are also present which are mostly produced as the by-products in the synthesis of hexagonal and rhombohedral BN. These allotropes are known amorphous boron nitride which is an atomic level structural defect and turbostratic boron nitride which arises as a defect between the basal planes of overlapping BN layers. Amorphous form is hygroscopic, highly disordered structure and possesses instability in the air which means it results in the formation of borate oxides and hydroxides. On the other side, the reported turbostratic boron nitride has found to be unstable due to long term exposure in the air and upon reaction it creates ammonium borates. Although all forms are important still cubic and hexagonal are employed in most of the industries due to high structural stability.[36]

Materials Advances Accepted Manuscript

View Article Online
DOI: 10.1039/D5MA01210D

Open Access Article. Published on 24 June 2026. Downloaded on 6/26/2026 4:24:14 PM.
This article is licensed under a Creative Commons Attribution 3.0 Unported Licence.

Table 1: Properties and Applications of Forms of BN

Form of BN	Nature of bonding	Hybridization pattern	Structural Stability	Synthesis process	Potential use	Reference
Cubic	Hydrogen Bonding	sp^2		phase transformation, solvothermal reaction, and laser ablation	Super hard materials and hydrogen generation	[37]
Hexagonal	Chemical nature	sp^2		CVD	Promising material to serve as a charge-blocking layer for graphene.	[38]
Sphalerite		sp^2				[39]
Wurtzite	Covalent Hard like Diamond	sp^3	97K	hexagonal-to-wurtzite phase transformation at high pressure and high temperature	Hard material can be used to replace diamond	[40, 41]
Rhomohedral	Strong B–N bond	sp^2	1100–1500°C, 1000–10000 Pa	CVD	Electronic Application	[41]

Properties and applications of Forms of BN are listed in Table 1. These crystalline forms are useful in the manufacturing of lubricants and abrasives particularly the layered and sphalerite BN**.** Furthermore, BN is a much-needed ingredient in the cosmetic industry because without it the cosmetic products cannot retain their integrity.

BN is isostructural and isomorphic with carbon and its analogues. But the major difference in both is that the electronic distributions are symmetrical in graphene due to zero difference of electronegativity while in BN, there is significant difference in the electronegativity because nitrogen is more electronegative than boron.[42] Attributing to this, BN have the unsymmetrical distribution of electrons and majority of the electronic charge is directed to the nitrogen atoms in the form of the lone pairs. These lone pairs on nitrogen are not fully localized, hence can move towards boron.

The crystalline structures of BN can be expanded in the zero-dimensional space such as cage configurations, one-dimensional space including diatomic molecules and nanotubes, two-dimensional space as in the monolayer structure of hexagonal boron nitride and finally the three

Materials Advances Accepted Manuscript

View Article Online
DOI: 10.1039/D5MA01210D

Open Access Article. Published on 24 June 2026. Downloaded on 6/26/2026 4:24:14 PM.
This article is licensed under a Creative Commons Attribution 3.0 Unported Licence.

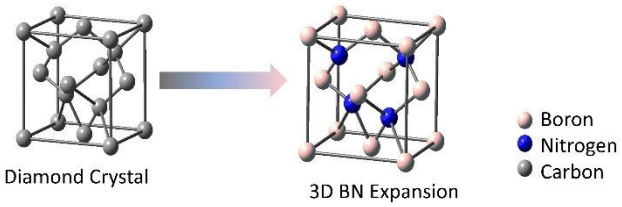

Figure 3: Similarity between diamond crystal and 3D BN

dimensional expansion of BN i.e. diamond crystals. Both diamond crystal and 3D BN structure are presented in Figure 3.

Nanotubes and fullerenes configurations have less surface area (<100m^2 g^{-1}), possess less surface reactivity therefore BN based nanosheets having high specific surface area 170m^2 g^{-1} are employed in most of the studies.[43] Thereby the following discussion is based on 2D h-BNNS, its decorated structure and their potential applications.

3. Morphology of 2D h-BN

Nanomaterials, nanostructure and heterostructures derived from the boron nitride are highly capable of administering in diverse applications. All these attributes and utility comprehend to the unique properties of boron nitride. In particular, electronic, thermal and optical properties are the main reason of their promising capabilities in technological fields. In particular, 2D hexagonal boron nitride h-BN and its structural alteration including the decorations with the dopants are employed in various settings as ongoing research on graphene unfolds the exceptional surface properties. Therefore, two-dimensional h-BN is known as white graphene[17] because of notable structural similarity index of BN with graphene even the reported bond lengths and distance between neighboring layers are same. Few similarities and differences from the reported literature are given in the Table 2.

Table 2: Similarities and differences between BN and Graphene

BN	Graphene	Similarities/Differences	Reference
Both have a 2D structure with lattice arrangement.		Similarities	[44]
Both have excellent mechanical properties but BN is slightly harder due to higher Young's Modulus which is 270 Nm^{-1}		Similarities	[45]
h-Bn has polar surface.	Graphene has non-polar surface.	Differences	[46]
Wide band gap	Zero band gap	Differences	[44]

Materials Advances Accepted Manuscript

View Article Online
DOI: 10.1039/D5MA01210D

Good optical properties	Zero optical properties in visible region, but have good absorption in deep ultraviolet range	Differences	[44]
Composed of Carbon atoms only	Composed of Boron and Nitrogen	Differences	[44]
BN has high thermal conductivity is 400 $Wm^{-1} K^{-1}$	Graphene has excellent thermal conductivity from 3000 – 6000 $Wm^{-1} K^{-1}$	Differences	[45]

Open Access Article. Published on 24 June 2026. Downloaded on 6/26/2026 4:24:14 PM.
This article is licensed under a Creative Commons Attribution 3.0 Unported Licence.

Alongside, other similar characteristics are the anisotropic behaviour in basal planes either in parallel or perpendicular orientation, high tensile strength and good thermal conductivity. Despite of the similar nature, BN has individual and characteristic features as well. Such features include colorless nature, good insulator material[47] and high asymmetry due to the partial delocalization of the electronic charges in the π bonds which cause the significant broadening in the band gaps. The reported wider band gaps in boron nitride are ~5 – 6 eV.[48] These structural features make BN applicable as insulating fillers. Hexagonal BN has honeycomb lattice configuration and is an excellent semiconductor material.[49, 50]

The crystallographic parameters concerning the hexagonal boron nitride nanosheet includes both a=b=0.250 nm and c=0.666 nm. The bond length of boron and nitrogen in plane are 0.144 nm while three bond angles alpha, beta and gamma of the crystal's sides are of 90°, 90° and 120° respectively. Furthermore, the useful interlayer differences and spacing of 0.333 nm gives BN a competitive edge against graphene.[42] As similarity with the graphene and other allotropes of carbon, h-BN also exhibits variety of configurations which includes BN nanosheets, BN nanotubes, BN octahedral fullerenes and other nanoscale level structural configurations such as nanoribbons,[51, 52] nanoplates,[53, 54] nanowires,[55] nanofibers,[56] nanoropes,[57] nanocups,[58] nanoscrolls,[59] nanomikes,[60] microbelts[61] and BN foams.[62] The structural dimensions of the hexagonal boron nitride differ as there are two types of termination namely zigzag and armchair. These structures are visually represented in Figure 2 (a).

The thermodynamic and energetic favorability in termination depends on the configuration of BN. In this regard, armchair termination was reported to be more favorable in nanoribbons of BN when compared to the nitrogen and boron zigzag edge from the perspective of the first principle and density functional analysis.[63, 64] The triangular growth pattern of BNNS on copper surface reflects that among nitrogen and boron zigzag end, N termination is more feasible whereas the B zigzag edge becomes more efficient and stable when nickel is employed as a substrate material.[65, 66]

Materials Advances Accepted Manuscript

View Article Online
DOI: 10.1039/D5MA01210D

Open Access Article. Published on 24 June 2026. Downloaded on 6/26/2026 4:24:14 PM.
This article is licensed under a Creative Commons Attribution 3.0 Unported Licence.

4. Stacking Patterns in BNNSs

There is a significant difference in the stacking parameters between different monolayers of h-BN in BNNSs. Generally, BN is stacked in the AA' mode in a bulk state which is characterized by the presence of boron atom on topside of each nitrogen atom, reverse can be true as well. There is also prediction that boron nitride nanosheets particularly adopt other stacking orders but their favorable stacking modes are AB and AC bernal pattern in relation with the graphite.[67-69] AB stacks particularly characterize the detection of the impurities in fresh exfoliated layers from bulk material which is responsible for the transformation of a good AA' stack into AB stacking mode as adapted from literature given in Figure 4 (b).[70] These stacking patterns are detected via the chemical vapor deposition methods and growth of the structures occurs under dark field transmission electron microscopy as shown in Figure 4 (a).[71]

The AA stacks have such a pattern that each boron atom being partial positive charge prefer to reside on the top of other boron (partial positive) in nearby monolayer of BN. This configuration causes repulsion thus is not favorable. On other hand its counter C has Boron facing the nitrogen in adjacent layers. In AA' stack, nitrogen is being partial negative charge while the boron is partial positive, thus creating the stability of structure by causing an apparent reduction in the electrostatic energy of the BNNSs system.

The AB stacking has boron in monolayer resting on center of the hexagonal structure on neighboring layer while AB' mode prefer to keep nitrogen towards the exact central position of hexagon. Furthermore, it can be observed that AC stacks are quite similar to AB' whereas its counterpart AC' shows similarity with AB except that nitrogen are in eclipsed setup rather than boron. Although, there should be equivalence in the energetic feasibility of AB, AC stacks and their counterparts AB' and AC', however due to the dominance of Pauli repulsions in the AB' and AC' stacks, the electrostatics forces failed to manage the integrity of the structure. Therefore, only AB and AC modes are largely favorable and employed.[68, 69]

Prior, it was believed that BN layers are strongly held together via electrostatic interaction build up by oppositely partial charged B and N atom which boast off the interlayer distance of (0.330–0.333 nm).[72-76]

Materials Advances Accepted Manuscript

View Article Online
DOI: 10.1039/D5MA01210D

Open Access Article. Published on 24 June 2026. Downloaded on 6/26/2026 4:24:14 PM.
This article is licensed under a Creative Commons Attribution 3.0 Unported Licence.

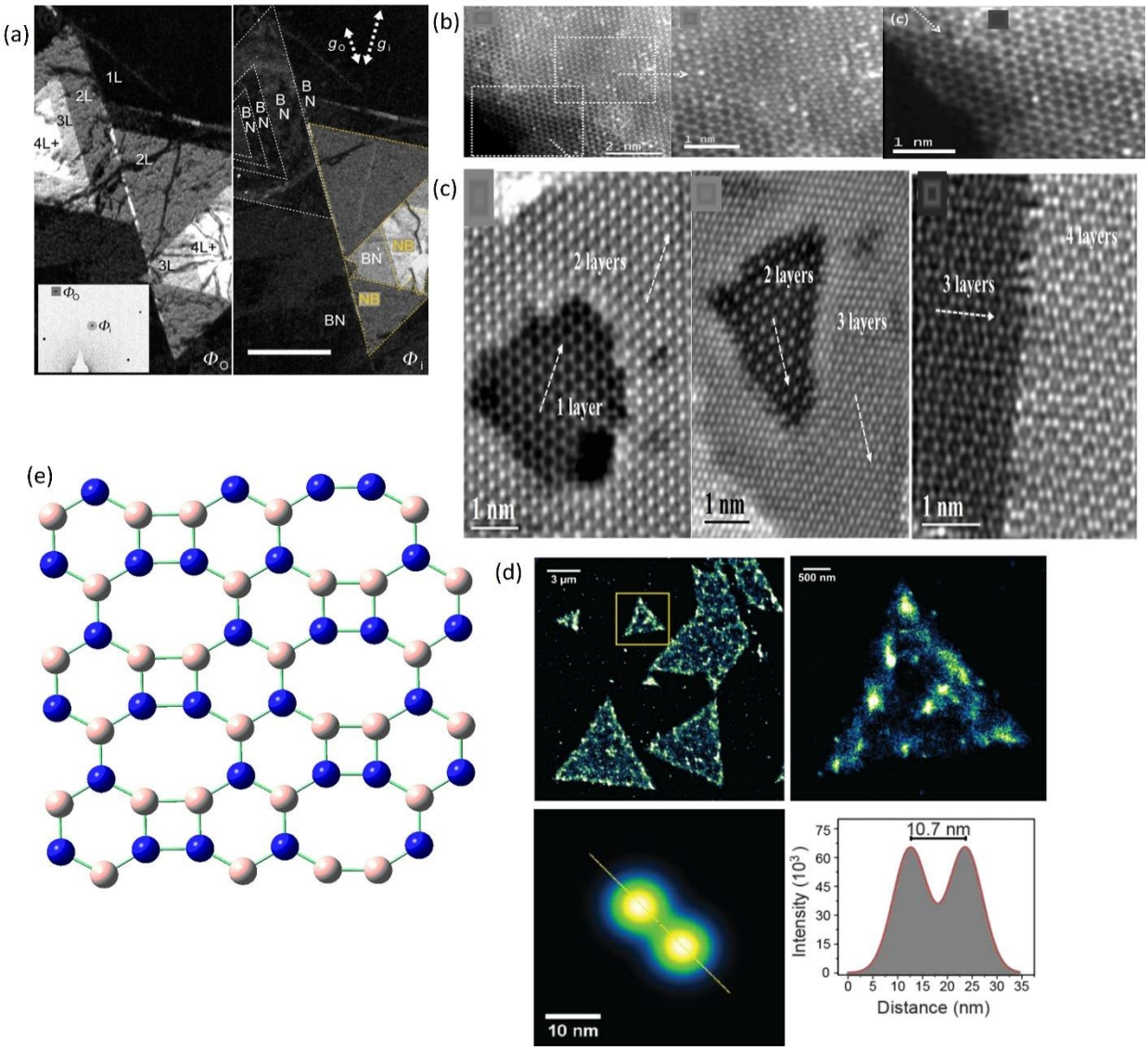

Figure 4: Different stacking configurations in BNNS are illustrated through various imaging techniques. (a) DF-TEM images taken using the w_0 (left) and w_i (right) diffraction spots show AB and AA0 stacking in the left and right triangular domains, respectively. Adapted with permission from Ref.,[77] (b) HAADF-STEM images highlight AB and AA0 stacking in different regions of chemically exfoliated BNNS. Adapted from Ref.,[78] with permission from RSC. (c) Various stacking sequences, AB, ABA, ABAB, AC0, and AC0B, are seen in CVD-grown BNNS via HAADF-STEM. Adapted from Ref.,[79] with RSC permission (d) Reconstructed SMLM imaging reveals defects in h-BN, highlighting a selected region, two distinct nearby emitters, and their distance profile; reproduced with permission from Ref.,[80] Copyright 2018 American Chemical Society

However, this interlayer distance is much shorter for a strong anchoring support between adjacent h-BN monolayers. Thus, recent research focuses on the presence of weak Van der Waals interactive forces between BN layers at much suitable interlayer distance.[81] Figure 5 contain all possible stacking patterns.

Materials Advances Accepted Manuscript

View Article Online
DOI: 10.1039/D5MA01210D

In one of recent report, other stacking patterns for BNNSs are emerged as AB, ABA, AC' and AC'B through the temperature (1000°C) facilitated chemical vapor deposition growth of BN materials on copper substrate.[82] This discussion cleared out as a fact that temperature dictates the assembly of materials through electrostatic forces of interactions and the buildup of ultimate structural configurations into a specific stacking mode. In addition, kinetic energy of the atoms residing in the stack is severely disturbed upon implication of the high temperature conditions which is the determinant of BNNS packing, given in figure 4 (c).[69, 83] Still, there is room for more research and evidence to be collected on the stacking patterns of the hexagonal boron nitride nanosheet growth on transition metals (Ni, Pt, Fe) substrate other than copper and to make a keen comparison with stacks growths on Cu.

Stacking parameters have a prominent impact on the properties (optical/topological) of BNNSs therefore many of research studies oriented towards understanding the impact of stacks on structural properties variations are well documented in the literature.[71] To employ BNNS as a substrate material in the nanoelectronics and optoelectronics, there is a need to provide a detail analysis of the stacking parameters and patterns. Hence, in this regard, more research needs to be carried out.

Open Access Article. Published on 24 June 2026. Downloaded on 6/26/2026 4:24:14 PM.
This article is licensed under a Creative Commons Attribution 3.0 Unported Licence.

Materials Advances Accepted Manuscript

View Article Online
DOI: 10.1039/D5MA01210D

Open Access Article. Published on 24 June 2026. Downloaded on 6/26/2026 4:24:14 PM.
This article is licensed under a Creative Commons Attribution 3.0 Unported Licence.

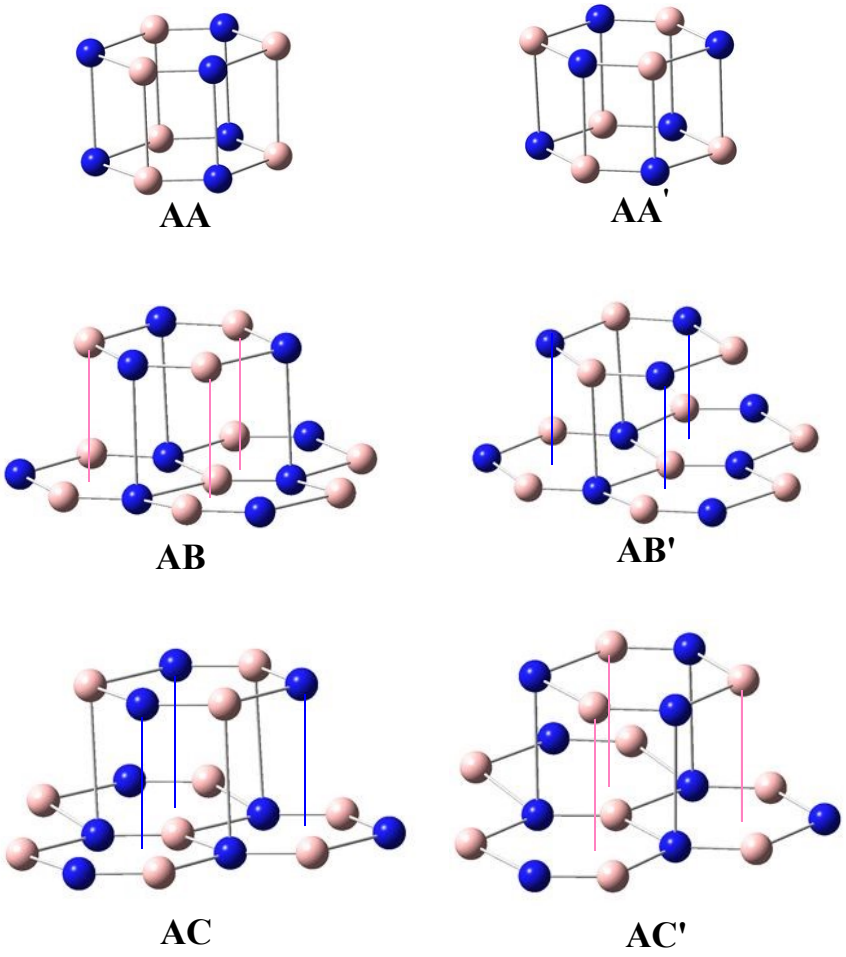

Figure 5: Framework illustration of 6 possible stacking patterns of BN

5. Typical Defect Site Engineering in BNNSs

In accordance with solid state theory, defects are inevitable in two-dimensional hexagonal boron nitride structures. Such defects may involve presence of vacancies site, edges, and dopant either with substitutions or addition and grain boundaries. The emergence of defects can be attributed to the environmental impacts or the synthesis process which seriously alter the performance efficiency, properties and behaviour of materials.[84] These defects might not be prominent in bulk however monolayers are severely affected by it. The reason could be the availability of almost every single atom of the material on the surface where any minute perturbation or disturbance counts. Therefore, defect engineering is a field that needs more attention particularly in the specific tuning and efficient administration of the two-dimensional materials.

For instance, there is a typical Stone-Wales (SW) defect,[85, 86] in BNNSs which is sort of structural modification and imperfection involving pentagon-heptagon pairs (line defect 5/7). This defect

Materials Advances Accepted Manuscript

View Article Online
DOI: 10.1039/D5MA01210D

Open Access Article. Published on 24 June 2026. Downloaded on 6/26/2026 4:24:14 PM.
This article is licensed under a Creative Commons Attribution 3.0 Unported Licence.

can be evident in the band gap reduction.[87] In addition to the effect on band gaps, there is lowering in the modulus of elasticity[88] and bending modulus.[89] This particular defect can be found in C allotropes (graphene) and its effect can be prominent n the conversion of regular hexagonal rings into penta- or heptagon by 90° rotation of bonds making the activation barrier high.[51, 67]

In case of 2D materials mainly mono and few layers the term grain boundary (suited for 3D materials) is replaced with domain boundary. Thus domains (atoms) in poly-layers materials are said to be connected by the domain boundaries (connections). There are two types of topological defects associated with domain boundary termed as disclination and dislocation. SW defects concerning graphene are less favorable than line defect 4/8 because homo atoms are bonding i.e. B-B and N-N are in direct contact.[90, 91] Density functional theory advocates the energetic viability of unpolar (4/8) and polar (5/7) defects in boro-nitrogen nanosheet.[92] In addition, the experimental observations on these defects are confirmed by TEM[88, 93] and STM (Scanning tunnelling microscopy).[87] Atomic level configurations in these domain boundaries and experimental discovery of octagonal square defects[93] are visually represented in Figure 4 (e) while for other type domain boundary defects there needs to be more experimental and theoretical investigational analysis for their confirmation. The nature and type of bonding elements within the defect type domain boundaries are unknown. Therefore, there is need of more research for identification of defect bonding patterns and elements both experimentally and theoretically.

Point defects can be observed in two-dimensional materials as well. These imperfections occur as the presence of the heteroatom in place of the obvious two atoms B and N of nanosheets. The realizations of the point defects can be in terms of B/N vacant sites and the B/N rich sites. In these vacancies new atoms (impurity) can be inserted by bombardment of the high intensity electron beams 74 KeV to 84 KeV[94] to create a triangular hole.[95, 96]

To control the reactivity on defect sites, the computational investigation on BN nanoribbons (BNNRs) simulated that Stone Wales imperfections are more reactive hence confirmed by exothermic nature of reactions as compared to the reactions at center of BNNRs.[97] However, the stabilization of defect presumably depends upon the nature of BN configurations, thus in case of BN nanostructures, defect engineering computational investigation on even pair defects (4/8) is evident that Stone Wales imperfections are energetically unfavorable.[42]

In diamond crystals and other two-dimensional materials, defects are responsible for the optical activity. Defects sites itself are not optically active but behaves like one when strikes with the

Materials Advances Accepted Manuscript

View Article Online
DOI: 10.1039/D5MA01210D

Open Access Article. Published on 24 June 2026. Downloaded on 6/26/2026 4:24:14 PM.
This article is licensed under a Creative Commons Attribution 3.0 Unported Licence.

excitons.[98] In this context, defective sites have applications as single photon emitters and are capable of extracting quantum information of materials at nanoscale level.[99, 100] Although defects are useful as photon emitters only at cryogenic temperatures such as the case of TM dichalcogenides,[98] however h-BN defects are particularly employed as biggest source of high intensity photon emission at room temperature.[101] Quantification of defects is the ultimate necessity, thus Feng and his colleagues reported optical activity dependent defect quantifications in single monolayer boron nitride nanosheets over 10.7 nm distance as shown in Figure 4 (d).[102] Thereby the defect engineering can be modeled in real time calculation, identification and monitoring of fluorescent compounds.

6. Structural and Surface Aspects Regarding h-BN

Most stable configuration of h-BN with advanced properties can be seemingly introduced in h-BNNS whose complete projection reflect the hydrophobic nature due to vertical alignment of interlayer area and horizontal settlement of core morphology. Weitz *et al* addressed this hydrophobicity and argued in experimental settings via droplets hitting method perpendicularly onto BN vertical surface at 150° angle.[103] The vast surface area and porosity ratio discovery in h-BN nanobelts has been carefully analyzed for successful hydrogen storage.[61] In addition the large surface area in BNNS found application as water cleaning agent to selectively adsorb the dirt and oil from an impure water bodies.[104] Different Properties of BN configurations are given in Table 3.

BN specifically portrays the best surface properties among already investigated two dimensional materials perhaps due to low density and large thermal resistance and high deformation index. Furthermore, it reflects high tensile strength and thermal stability against oxidation when exposed in atmosphere or any harsh environmental conditions including attacks in the acidic and basic pools. All of these properties make BN the future asset in the fabrication, modification and utility process while manufacturing electronic devices that operates well in harsh atmospheric conditions.[84] Different Aspects of BN Sheet are visually presented in Figure 6.

Materials Advances Accepted Manuscript

View Article Online
DOI: 10.1039/D5MA01210D

Open Access Article. Published on 24 June 2026. Downloaded on 6/26/2026 4:24:14 PM.
This article is licensed under a Creative Commons Attribution 3.0 Unported Licence.

Table 3: Different properties of BN configurations

BN configurations	Elastic modulus (TPa)	Fracture strength (GPa)	Thermal conductivity (W m^{-1} K^{-1})	Specific surface areas (m^2 g^{-1})
h-BN		Zigzag crack with armchair loading, 81 Armchair crack with zigzag loading, 84[105]	390[106]	1142.9[107]
BN Nano wire				295[108]
h-BNNS				321[109]
BNNS	220-510 Nm-1[110]	172[111]	300-2000 W/mK (theoretical), 300-360 W/mK(experimental)[110]	
Porous BNNSs				606[112]
c-BN	406[113]			
BN chain	1.19 GPa[114]			
p-BN				1062.88[115]
BCN				992.59[116]

6.1 Mechanical Properties

The crystallographic measurements on the mono to few layers' boron nitride nanosheets synthesized by CVD are fewer. Attributing to this, Song et al. provided the first experimental determination of the elastic modulus and fracture strength for CVD-grown h-BN bilayers, reporting values of 0.334 ± 0.024 TPa (112 ± 8 N m^{-1}) and 26.3 GPa (8.8 N m^{-1}), respectively.[89] These values have not been supported by theoretical investigations as value estimation from computational calculations is much smaller. Furthermore, theoretical investigations need a breakthrough in determining the mechanical strength of BN containing few layers. However, monolayer BN computational study reveals the young modulus as 0.716 – 0.977 TPa or 292.1 Nm^{-1} and the breakage strength as 68 – 215 GPa which is a quite wide range of spectrum.[89, 117, 118]

The reduced mechanical properties of CVD-grown bilayer h-BN can be attributed to structural defects, particularly grain boundaries, which disrupt the continuity of the sp^2 bonding network and introduce stress concentration sites.[119] Other experimental analysis calculated young modulus (1.16 ± 0.1 TPa) of 15nm thick BN[120] while the BN thickness can be enhanced to around 50 nm.

Materials Advances Accepted Manuscript

View Article Online
DOI: 10.1039/D5MA01210D

Open Access Article. Published on 24 June 2026. Downloaded on 6/26/2026 4:24:14 PM.
This article is licensed under a Creative Commons Attribution 3.0 Unported Licence.

Materials Advances Accepted Manuscript

There is a lack of proper investigations on the intrinsic properties of thin BN layers of varying thickness which delays the administration of these nanomaterials into useful formulations.

In addition, the simulation of interlayer interactions and their correspondent effect onto the mechanical properties is evident for graphene and multilayer BN.[121] In this regard the keen efforts of Falin *et al* are acknowledged for experimental determination of physical strength regarding ~ 9L BNNS.[122] One layer BN had the experimental value of 0.865 ± 0.073 and 70.5 ± 5.5 GPa for young modulus and breaking strength, respectively. However, the strength few layers BN are comparable to ~ 1L BN.

Herein, graphene and BN has significant differentiation, as in graphene layers increasing thickness translates into lower mechanical strength, mono layer BN in contrast has same mechanical strength as few or many layer BN.[122] This difference in strength occurs for a sole reason that is varying

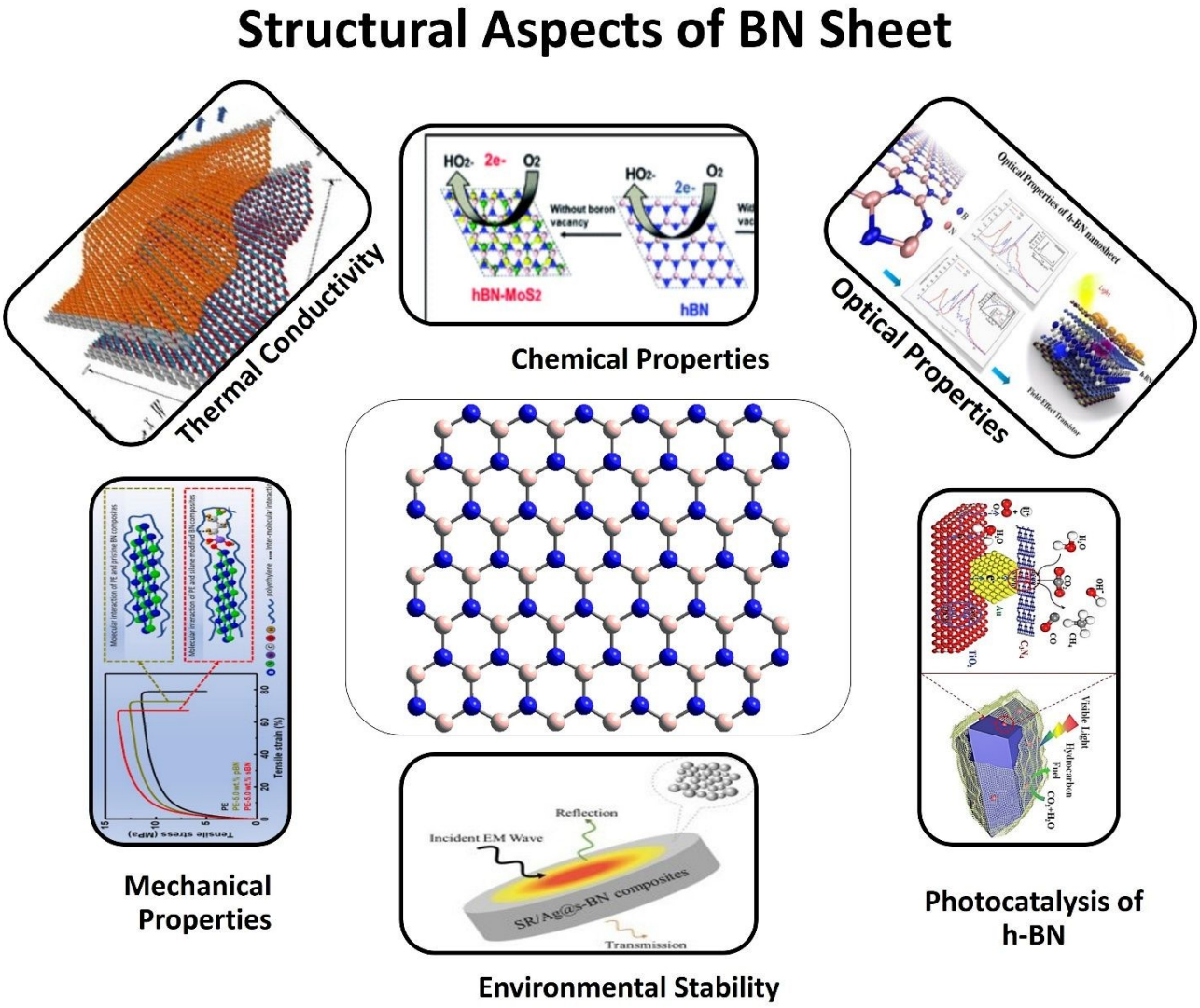

Figure 6: Structural Aspects of BN sheets

View Article Online
DOI: 10.1039/D5MA01210D

Open Access Article. Published on 24 June 2026. Downloaded on 6/26/2026 4:24:14 PM.
This article is licensed under a Creative Commons Attribution 3.0 Unported Licence.

interlayer interactions under strain and compression as conferred by both experimental and theoretical analysis. Thereby the DFT simulations via consideration of van der Waals interactions in 2 layer graphene indicated that sliding is favored energetically near indentation whereas the same 2 layer BN prevents this sliding because of having the higher sliding energy coefficient.[122] The higher sliding energy barrier in h-BN relative to graphene arises not solely from van der Waals dispersion forces but also from an electrostatic interlayer contribution introduced by the partial ionic character of the B-N bond. In graphene, both atoms carry zero net charge, and the interlayer interaction is purely dispersive. In h-BN, the alternating partial positive charge on boron and partial negative charge on nitrogen produce an electrostatic interlayer stabilization energy that raises the energy penalty for relative layer displacement. This electrostatic contribution has direct engineering relevance since the h-BN layers are effectively locked together under compressive and shear loading in a manner that graphene layers are not. Moreover, sandwich beam structure model's statements agree with DFT as layered graphene tend to have sliding effect while in comparison BN interlayers are glued together. Thus a compact statement can be made from these studies that BN has good insulating properties and preferably due to strong adhered layers, it can be well administered in mechanical reinforcement purposes such as mechanical reinforcement fillers in composite materials, while its controlled shear response makes it valuable as a solid-state lubricant in extreme-pressure environments.[122]

6.2 Thermal Conductivity

Hexagonal BN appears to have high thermal conductivity of 400 W m^{-1} K^{-1} which is the highest among same nature of ceramic based nanomaterials. Using suspended microbridge devices, Jo et al. measured the in-plane thermal conductivity of 11-layer h-BN as 360 W m^{-1} K^{-1}, a value closely consistent with the bulk thermal conductivity of 390 W m^{-1} K^{-1}. It shows that phonon transport in this few-layer regime closely approximates bulk behaviour. In the same study, five-layer h-BN yielded a lower conductivity of 250 W m^{-1} K^{-1} at 300 K, an effect attributed to increased surface contamination from polymeric residues.[123] This varying thermal conductivity has been well suited to the varying dimensions of h-BN i.e. high value closer to perpendicular c-axis due to low calculated thermal expansion coefficient ranging between 0 – 2.6×10^{-1} K^{-1} and low thermal conductivity at parallel to c-axis.[124]

The thermal conductivity of h-BN can be affected by density. A study about the thermal conductivity of h-BN presented that the laminate of h-BN has 20 W m^{-1} K^{-1}, performed at room

Materials Advances Accepted Manuscript

View Article Online
DOI: 10.1039/D5MA01210D

Open Access Article. Published on 24 June 2026. Downloaded on 6/26/2026 4:24:14 PM.
This article is licensed under a Creative Commons Attribution 3.0 Unported Licence.

temperature. In this study, it is explored that thermal conductivity is directly related to volumetric density. The experimental study reveals the result is similar to the theoretical calculation to get the dependence of thermal conductivity on density. That ranges from 10^5 W/m^2 K to 10^6 W/m^2 K.[125] Thermal conductivity can also be affected by changing isotopes. A study performed by changing the boron isotopes of ^{10}B and ^{11}B. Both experimental and theoretical study was performed to determine the in-plane and out-of-plane thermal conductivity for h-BN. The study reveals that for pure h-BN in-plane thermal conductivity is measured 200 – 420 Wm^{-1}K^{-1}. In-plane thermal conductivity of ^{10}B h-BN was increased by 585 Wm^{-1}K^{-1} at 300K, while out-of-plane thermal conductivity with the same isotope is 3.5 ± 0.8 Wm^{-1}K^{-1}. For the ^{11}B isotope in-plane thermal conductivity is 408 ± 60 Wm^{-1}K^{-1} while out-of-plane conductivity is 4.5 ± 1.4 Wm^{-1}K^{-1}.[126] The marked enhancement in thermal conductivity that is observed for isotopically pure ^{10}B h-BN (585 Wm^{-1}K^{-1} at 300 K) compared with natural-abundance h-BN (200-420 Wm^{-1}K^{-1}) is mechanistically consistent with the suppression of phonon-isotope scattering. In natural h-BN, the coexistence of ^{10}B (19.9% natural abundance) and ^{11}B (80.1%) introduces mass-disorder at the boron sublattice. This mass-disorder resonantly scatters long-wavelength acoustic phonons, which are the dominant heat carriers in h-BN at room temperature and so it reduce their mean free path and thereby bulk thermal conductivity also get lowered. The isotopic purification eliminates this scattering channel which restore coherent phonon propagation over longer length scales and that also explain the 40-60% increase in conductivity. This isotope effect, analogous to what was observed in isotopically pure diamond and silicon confirms that phonon-isotope scattering is the primary intrinsic thermal resistance mechanism in h-BN at 300 K.[126]

However, the scarcity of detailed computational and MD simulations in determination of thermal resistivity and conductivity for h-BN significantly delays their applications in nanodevices which needs the enhanced thermal properties. Therefore, modulation of thermal conductivity through theoretical investigations demands the extensive research for manufacturing conductive nano oils which contain in-built boron nitride fillers.[127]

6.3 Optical Properties

Typical determination of optical properties concerning h-BN was reported via UV-vis spectroscopy.[128] Experimental and theoretical investigations are in good agreement that there is no absorption peak in visible region of spectrum meanwhile a strong absorption peak is consistently observed in the UV region and that is characteristic of excitonic deep-UV photoluminescence in

Materials Advances Accepted Manuscript

View Article Online
DOI: 10.1039/D5MA01210D

Open Access Article. Published on 24 June 2026. Downloaded on 6/26/2026 4:24:14 PM.
This article is licensed under a Creative Commons Attribution 3.0 Unported Licence.

h-BN.[128] The electronic band gap is the primary determinant of the optical absorption edge and photoluminescence emission energy in two-dimensional h-BN devices, and DFT calculations of the band structure have been used to predict and interpret these optical characteristics. The effective band gap range for optimal performance of h-BN-based optoelectronic devices is from 3.6 eV to 7.1 eV and that depends on structural configuration, as established across the experimental and computational literature.[129]

The experimental UV-vis absorption measurement for optical spectrum aligns with the band gaps 4.94, 4.04, and 3.40 eV in comprehension with the absorption wavelengths at 251, 307 and 365 nm respectively. There is a constant agreement of both experimental and computational analysis for wide band gap nano-material in context with optical character in h-BN.[130] Furthermore, h-BN is inactive in IR and visible range of spectrum but behave peculiarly in UV range with strong absorption (251 nm) and comes with a shoulder excitation peak admitting its role in regulation of optical devices.[131]

A computational study was performed to detect different optical properties of h-BN in the range of 0 – 25 eV energy. It reveals that there is no absorption of light at 4.30 eV in deep UV regions while a high absorption peak is observed at 13.37 eV in extreme UV regions. In the same study, optical reflectivity was observed to be 0.7% in the IR region, 3% in the deep UV region and a maximum reflectivity 10% in the extreme UV region. The dielectric constant value is 1.37 at zero energy decreases in the deep UV region, the highest peak observed at 13.34eV energy range in the extreme UV region.[132]

Another study reveals that for pristine h-BN dielectric tensor is isotropic with a clear single peak at 5.85 eV. This peak is related to the inter-band transition of pz states. That's why halogen bonded on top of h-BN. The refractive index observed at low frequencies is 1.2 while in the UV region reflection peak falls around 208 nm.[133]

In another study when a crystal of few-layers h-BN is grown structural and optical properties increased by the effect of growth temperature primarily when rose above 1000^{o}C, its properties change. The sample was grown at different temperatures and growth rates. Samples with less growth rate have low-intensity spectra due to fewer BN domains taking part in luminescence. This grown h-BN is effectively used in optoelectronic and photonic properties.[134]

The optical properties of h-BN few-layer crystals are grown by the submicron-spacing vapour deposition method. This study explores how poor crystallinity causes a disturbance in their

Materials Advances Accepted Manuscript

View Article Online
DOI: 10.1039/D5MA01210D

properties but as they are grown at high temperatures, a good effect on their properties was observed. The Spectra of the h-BN epilayer show strong peaks at the deep ultraviolet region. So, deep ultraviolet photodetectors based on h-BN have the potential for optoelectronic application.[135] When we take together the computational studies that are discussed above, they provide a consistent and wholistic mechanistic explanation of the optical behaviour of h-BN. The dominant optical transition corresponds to a π-to-π* excitation between nitrogen-derived pz valence states and boron-derived pz conduction states at the K-point of the hexagonal Brillouin zone.[136] The quasiparticle band gap of monolayer h-BN is placed at approximately 7.0 eV by many-body perturbation theory at the GW level.[137] On the other hand, the lowest-energy optical absorption onset is redshifted to approximately 6 eV which is due to a large exciton binding energy and it even exceeds 0.7 eV that is reported to be highest for any two-dimensional material.[137, 138] The absence of both the optical absorption in the visible range and the intense photoluminescence in the deep UV at approximately 215 nm is also explained by this strong excitonic character.[139] The sensitivity of the excitonic transitions to structural perturbations be it through the process of doping, introduction of defects, or the heterostructure formation, all give mechanistic rationale for different optical engineering strategies that are discussed in Sections 7, 8, and 12 of this review.

6.5 Environmental Stability

There is a unique resilience in h-BN for bearing temperature which reflects the environmental, thermal and air stability.[140, 141] Chemically grown BN nano-sheets on metal Ni substrate having thickness of 5 nm have been reported as oxidation resistant under increased temperature condition of 1100 °C and BN Cu grown sheet has the resistivity for 30 minutes under 500 °C.[142]

In contribution to the honeycomb lattice extension in structure, BN is impermeable to the passage of small molecules. Furthermore, it is chemically inert being an insulating material and possesses room temperature environment stability and retention in structural constraints. However, chemical reactions interfaces in nitrogen defects specifically oxygen reduction mechanisms have theoretical prediction at room temperature.[143] Employing BN in environment setting requires the knowledge of structural stability due to presence of defective sites while crystal growth processes. When h-BN is grown as an overlayer to metals their inter-surface stability in the gaseous phase is studied experimentally. In this study, h-BN/Ru (0001) was exposed to atmospheric O_2. The intercalation of O_2 with h-BN overlayers needs a lot of pressure as compared to h-BN monolayer. Intercalation

Open Access Article. Published on 24 June 2026. Downloaded on 6/26/2026 4:24:14 PM.
This article is licensed under a Creative Commons Attribution 3.0 Unported Licence.

Materials Advances Accepted Manuscript

View Article Online
DOI: 10.1039/D5MA01210D

Open Access Article. Published on 24 June 2026. Downloaded on 6/26/2026 4:24:14 PM.
This article is licensed under a Creative Commons Attribution 3.0 Unported Licence.

of the h-BN overlayer happens at room temperature as compared to graphene/Ru (0001) which needs 200°C for O_2 intercalation. The lower activation energy for h-BN makes it potent for manufacturing BN-based devices under suitable conditions.[144]

Due to the potential of BN and its nanostructures in various applications, their chemical and structural stability also matters. To determine this stability in an aqueous environment an experimental study was performed. According to the study, Porous Boron Nitride Fibers (PBNF) can react with water molecules due to their low crystallinity and cause the formation of ammonium borate hydrate. In the same study PBNF was observed with humid air which shows an increase in the mass of the sample with a change in its chemical composition and no change is observed in dry air. Release of ammonia-containing gas was also observed. Humidity affects PBNF's chemical composition mainly. So, to improve the stability of PBNF in an aqueous environment secondary nitriding of BN was done. When these SN-PBNF were exposed to humidity or water, no change was observed.[145]

It is experimentally proved that gas sensors formed by Pt-doped Boron Nitride Nanosheets have good stability and selectivity towards the targeted gas even in harsh environments.[146] The experimental study for the thermal stability of Boron Nitride Nanotubes was performed. It shows that BNNT shows good resistance to oxidation at 900°C but changes into boron oxide at 1100°C.[147] In another experimental study, BNNT had structural and thermal stability up to 850°C in air and the structure degraded at 900°C. This makes its applications in high-temperature conditions.[148]

6.6 Chemical Properties

As per attributes of stabilization merits in BN, there is a strong inertness towards acidic and basic environment. This property enables them to be useful as the coating layer to protect the surface of transition metals against corrosive damage; which serves as the base material in crustal growth of 2D materials. The stability and thickness of the baseline substrate affects the growth process specifically in harsh surrounding.[149] Chemical inertness of h-BN is well adapted to the prevailing thickness of few layers and single atomic layers. This statement has been properly addressed with regard to Ni (111) TM as a substrate surface in propagation of h-BN[150] and the underling influence of TM interactions with BNNSs.[150]

Epitaxial route synthesis of h-BN of varying chemical properties is employed via use of Pd (111), Pt (111), Ru (001), and Rh (111) substrates.[151] Among these synthesized configurations, Ni substrate being magnetic imparts the ultimate spin polarization and compatible crystal growth in

Materials Advances Accepted Manuscript

View Article Online
DOI: 10.1039/D5MA01210D

Open Access Article. Published on 24 June 2026. Downloaded on 6/26/2026 4:24:14 PM.
This article is licensed under a Creative Commons Attribution 3.0 Unported Licence.

h-BN making its applicable as an ideal defect free epitaxial interfacial surface.[150] Furthermore, h-BN is quite inert but TM substrates add extra electronic states in the wide and structure which causes enhanced reactivity due to proper functionalization.

The h-BN has good structural and chemical stability and also has corrosion resistance. This is studied experimentally that when h-BN is grown on copper using CVD, its current density was lower for h-BN/Cu at $(1.22 \pm 0.22) \times 10^{-8}$ A/cm², compared to $(3.08 \pm 0.03) \times 10^{-7}$ A/cm² for bare Cu. This shows that h-BN works as a corrosion inhibitor which may be due to the insulating nature of h-BN.[152] Moreover, the adsorption strength can be increased by lowering the hardness of BN material. A theoretical study was performed by adding dopants to reduce hardness. Pure BN has hardness 0.31020 au and BN model_5C has 0.07399 au. This reduction in the hardness of BN can increase in adsorption strength. In the same study, adsorption energy was calculated by adsorbing dibenzothiophene (DBT) on BN and BN_5C which shows adsorption energy for DBT_BN is −20.12 kcal mol^{-1} and for DBT_BN_5C is −75.70 kcal mol^{-1}. This shows that carbon doping increases the adsorption energy resulting in strong interaction.[153]

Due to the hardness of wurtzite BN, it is assumed that it can be replaced with a diamond as single-phase w-BN formation is much harder. It is the first time experimentally synthesized by using w-BN powder under high temperature and pressure. Vickers hardness of pure polycrystalline w-BN compact was calculated which is 46 GPA means not much harder as diamond but this synthesized material has good thermal stability of 920°C in the air which is much higher than that of diamond.[154] Chemical properties also include oxidation resistance. The oxidation resistance of BN was calculated experimentally which shows that BN nanosheets can resist oxidation at a temperature of 850°C but when temperature increases from 850°C it causes oxidation. The strong oxidation resistance of BN material makes it good for high-temperature applications.[155]

6.7 Sliding Efficiencies

Sandwich beam estimation on geometric parameters covers the sliding tendencies in layered h-BN especially 2L.[122] These experimental estimations explains the interlayer bonding parameters successfully by ruling out the non-liner deformations in structural periphery under indentation.[122] The elaboration extends up to the faces (layers) and core part (weak interlayer interactions). Such assembly fulfills the sandwich concept as the outer layers are much stronger and stiffer than the weak antiplane core area which bears enough shear stress without affecting the bending

Materials Advances Accepted Manuscript

View Article Online
DOI: 10.1039/D5MA01210D

Open Access Article. Published on 24 June 2026. Downloaded on 6/26/2026 4:24:14 PM.
This article is licensed under a Creative Commons Attribution 3.0 Unported Licence.

stiffness.[122] The shear stiffness in this case aligns with the linear approximations in the vdW-DFT calculated sliding energy by comprehensive theoretical computations.[123]

Normal range of shear stiffness was reported to be 2.5 – 9.0 Gpa.[156-158] However, the range can be shifted depending on the external factors such as high pressure where the value can be increased up to 534 GPa[122] but in a case where externalities are omitted the value falls about 6.61 GPa. Generally, shear stiffness in h-BN controls the electronic properties therefore interlayer forces can be modified easily by controlling the compression and shear strain.

Bi-layer h-BN has novel properties by sliding one layer over another, making it potent for slidetronics. A theoretical study was performed to observe the effect of layer arrangement on thermal conductivity. It shows that a strain of -6% can reduce thermal conductivity by 50% while a higher strain of -18% reduces the scattering in layers causing an increase in thermal conductivity.[159] The friction resistance of the material can be affected by the hardness of the material. Polycrystalline c-BN was grown with different sizes and hardness to check the effect of temperature on it. In this experimental study, friction resistance was calculated that friction resistance has a parabolic curve with an increase in hardness from 24.7 to 63.8 GPa along with an increase in grain size.[160]

Optical and electronic properties can be enhanced by changing the stacking pattern of a few-layer 2D material. The theoretical and experimental study was performed to observe the stacking pattern change of bilayer hexagonal boron nitride with the help of a laser. Two stacking configurations of h-BN were made (B over N) AA` and (B over B) AB`. When a laser with a frequency of 4.30 eV is applied dielectric function for AB` is higher than AA`. If strong laser applied stacking becomes more stable for AB`. Dynamic of transition simulated determine that stacking happens in picosecond. When one layer of h-BN has free surface boundary condition Bilayer h-BN can stay in metastable stacking or long time.[161]

BN can be used as a lubricating coating, for this application various studies to determine their thermal stability and friction resistance were performed. According to an experimental study, when fluorinated-based BNNS served as a coating on pure titanium, it had a 15% less coefficient of friction. When the coating was heated at a temperature of above 800^{o}C 87.9% mass retention showed its good thermal stability.[162]

Materials Advances Accepted Manuscript

View Article Online
DOI: 10.1039/D5MA01210D

Open Access Article. Published on 24 June 2026. Downloaded on 6/26/2026 4:24:14 PM.
This article is licensed under a Creative Commons Attribution 3.0 Unported Licence.

7 Impact of Dopants on Structural Properties Variations

Hexagonal boron nitrogen nanosheet contains two major vacancies also known as defect sites where impurities (dopants) are added to impart specific characteristics and modification into the pristine BN to make it a better material. One such vacancy is the boron site or boron vacancy and other is nitrogen vacancy. Dopants can either be fitted in the boron vacancy or nitrogen vacancy depending on the atomic size, electronic configurations and position in the periodic table. Doping is the process that incorporates the heteroatom substituents at atomic level either in place of boron or nitrogen within BN honeycomb framework rather than formation of loop domain which are associated with solo dopants. Variation in band gaps via dopant attachment to either B or N vacancy of BN structure is presented in Figure 7 and simple attachment of dopant to sheet is presented in Figure 8 from reported literature.

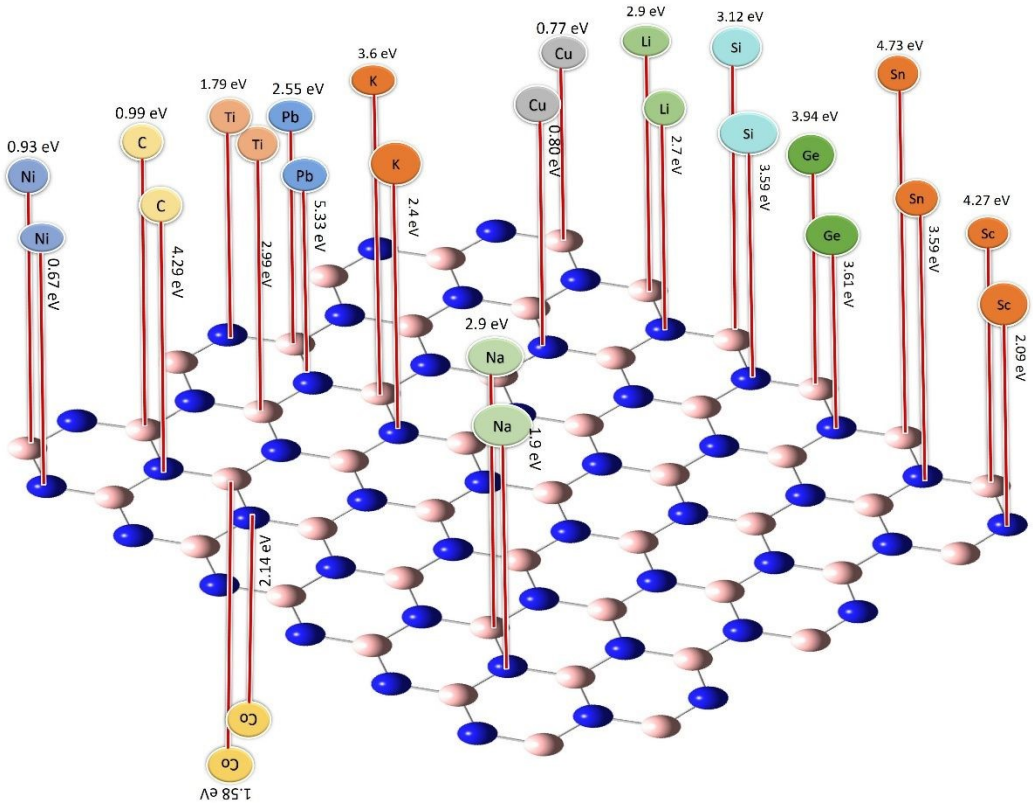

Figure 7: Change in Bandgap by Atoms Placed on "B" or "N" vacancy (Pink for Boron Atoms and Blue for Nitrogen Atoms)

Some property enhancement through doping can be observed in the case of band gaps i.e. BN being an insulator, wide band gap nanomaterials gives a dimension to the research formulation in narrowing down the band gaps while preserving the honeycomb lattice to be utilized in better

Materials Advances Accepted Manuscript

View Article Online
DOI: 10.1039/D5MA01210D

Open Access Article. Published on 24 June 2026. Downloaded on 6/26/2026 4:24:14 PM.
This article is licensed under a Creative Commons Attribution 3.0 Unported Licence.

performance semiconductors. This approach is quite opposite to the homologue graphene and is difficult to execute and find the suitable element from periodic table to make a BN alloy. In this regard, practical and computational chemical doping methods for hexagonal BN (sheets and tubes) demonstrated the tunable band gaps. Role of dopants over the properties of BN structures from reported literature are given in the Table 4.

Table 4 give several overarching structure-property trends that emerge from the collective doping literature. First is that the substitution at boron vacancy (B-site) is preferred energetically for most group III elements (Al, Ga, In, Tl) and noble metal atoms. The reason for this is that these electron-deficient species are complementary to the partial positive charge carried by boron and that minimize local lattice distortion and formation energy. On the other hand though, the electronegative group VI dopants oxygen and sulfur (O, S) and also the halogens preferentially occupy the nitrogen vacancy site, and we can owe that to their similar valence electron counts and electronegativities. Secondly, the magnitude of band gap reduction correlates strongly with the degree to which a dopant perturbs the frontier orbital energies, take the transition metals (Fe, Co, Ni, Cu) for this case where they introduce partially occupied d-states within the pristine h-BN band gap and that produce the largest reductions and even in some cases they drive a semiconductor-to-metallic transition, while main-group p-block substituents (Al, Ga, P) produce more modest band edge shifts through orbital hybridisation. The overwhelming majority of studies that are given in Table 4 are computational in nature, systematic experimental validation particularly for rare earth dopants and heavy transition metals are still a critical research gap. Future experimental programs should prioritize confirmation of DFT-predicted site preferences and band gap values using direct spectroscopic methods such as angle-resolved photoemission spectroscopy (ARPES) and scanning tunnelling spectroscopy (STS).

Table 4: Role of Dopants over the properties of BN Structure

Dopant	BN structure	Amount of dopant	Dopant chemical environment	Dopant role in the study	Nature of Study	Reference
C	Boron Nitride-fullerenes	-------	Replacement of 'N'	Dopants make BNF more reactive and potentially toxic, lowers the gap energy and chemical hardness	Computational	[163]
C	Boron nitride nanosheets	-------	Replacement with 'B' and 'N'	Reduces energy gap CB and CN to 0.99 and 4.29	Computational	[164]

Materials Advances Accepted Manuscript

View Article Online
DOI: 10.1039/D5MA01210D

Open Access Article. Published on 24 June 2026. Downloaded on 6/26/2026 4:24:14 PM.
This article is licensed under a Creative Commons Attribution 3.0 Unported Licence.

				eV, improves its sensing properties, For CB, the Fermi level of h-BN shifts from middle of the energy gap toward the conduction band CN Fermi level from the middle of the band gap toward p-type semiconductor		
C	h-BN	1g	Replacement with 'B' and 'N'	a novel DA sensor was developed, carbon-doping can increase reactive sites,	Experimental	[165]
C	Zigzag BNNT	------	Replacement with 'B' and 'N'	used as a potential material for detecting CF_3CN, Adsorption is stronger for detecting CF_3CN and CF_4, adsorption energy for CB-BNNT is lower than CN-BNNT	Computational	[166]
C	BN nanosheet	3.8mg	Replacement with 'B' and 'N'	the high porosity of BCN endows more active sites, shows high oxidation resistance capability	Experimental	[167]
C	h-BN	6g	On the edge	Promotes the desorption of the intermediates, and brings more basicity leading to good stability	Experimental, Computational	[107]
C	Boron Nitride Nanosheet	------	Replacement with 'N' and 'B'	reduce the energy gap, the C_B sheet adsorbs the O_2 molecule too strongly while C_N sheet adsorbs the O_2 molecule moderately	Computational	[168]
C	BN nanoflakes	-------	On edge	(C_N replacement more favorable) with double doping boosting ORR	Computational	[169]

Materials Advances Accepted Manuscript

View Article Online
DOI: 10.1039/D5MA01210D

Open Access Article. Published on 24 June 2026. Downloaded on 6/26/2026 4:24:14 PM.
This article is licensed under a Creative Commons Attribution 3.0 Unported Licence.

				and single doping facilitating HER		
C	h-BN nanosheets	8.72% to 41.67%	Replacement with 'N' and 'B'	Possess Tune-able band gap, capability for photo catalytic water splitting and CO_2 reduction	Experimental	[170]
C	Triangular Boron Nitride Nanoflakes	-------	In center	Reduces the band gap values, improves the orbital delocalization, high carrier mobilities	Computational	[171]
C	boron nitride nanowire	_____	On edge	CB stable, induce localized edge states Fermi level interaction leads to semiconductor to half-metal transition, Good electronic properties (semiconducting, half-metallicity, nonmagnetic metallic, and ferromagnetic metallic characters)	Computational	[172]
C	h-BN	_____	Replaced with 'B' and 'N'	n-type semiconductor when replaced with B atom while p-type semiconductor when replaced with N atom, adsorption energy decrease, small concentration of C dopant can functionalize large surface area of BN making it catalytic material	computational	[173]
C	boron nitride nanoplate	19%	Replaced with 'B' and 'N'	decreased the chemical hardness of the adsorbent, enhanced the adsorption capacity, and surface interaction	Experimental, computational	[174]
C and O	BN nanoflakes and hybrid	16.61% to 16.68%	Replacement with 'N' and 'B'	hybrid structures change with the length of C and	Experimental	[175]

Materials Advances Accepted Manuscript

View Article Online
DOI: 10.1039/D5MA01210D

Open Access Article. Published on 24 June 2026. Downloaded on 6/26/2026 4:24:14 PM.
This article is licensed under a Creative Commons Attribution 3.0 Unported Licence.

	nanoflake-nanowire			O doped BN nanostructures, increase of the number and length of C and O doped BN nanowires.		
O	BN mesoporous nanowire	_____	Replacement with 'N' and 'B'	enhancement of adsorption desulfurization, surface stability and strong interaction	Experimental	[176]
O	bundle like porous boron nitride	_____	_____	high specific surface area (474.3 m^2/g) and porosity (0.332 cm^3/g) heavy metal pollution control and environmental remediation	Experimental	[177]
Al	Armchair and Zigzag BNNTs	_____	onto the hollow site of a BNNT	High adsorbent capacity, best chemisorption for hydrogen storage	Computational	[178]
Al	boron nitride nanocarriers	_____	Replaced with edged Boron	Adsorption energy values decrease, and the enhancement adsorption process in the water phase is more than that in the gas phase,	Computational	[179]
Al, Ga	h-BNNs	1.40%	Replacement with 'B'	Al-BNNS band gap 3.90 eV, Ga-BNNS 3.64 eV. Good adsorption onto Al-doped BNNs alters the size of the band gap, Al-doped BNNS is better than Ga-doped BNNs in enhancing the adsorption energy, use as biosensors	Computational	[180]
Al, Ga	BN nanosheets	_____	Replacement with 'B' and 'N'	adsorption energies enhanced, HOMO-LUMO energy gaps decrease about 48.28% and 47.95% in gas phase and 42.27% and 38.41%	Computational	[181]

Materials Advances Accepted Manuscript

View Article Online
DOI: 10.1039/D5MA01210D

Open Access Article. Published on 24 June 2026. Downloaded on 6/26/2026 4:24:14 PM.
This article is licensed under a Creative Commons Attribution 3.0 Unported Licence.

				in water media after adsorption on the AlBN and GaBN respectively, both show higher sensitivity and reactivity than the PBN-sheet,		
Al, Ga, In	Boron-Nitride Nanotubes	_____	At the Edge	Improve semiconductor properties, resistant to mechanical change and used in construction of solar panels,	Computational	[182]
Al, Ga, P, As	boron nitride nanosheet	_____	Replacement with 'B' and 'N', in center of hexagonal ring	Al has adsorption energy higher than pristine but lower than Ga, high adsorption energy is when the dopant is replaced with B atom	Computational	[183]
Al, Si	boron nitride nanosheet	_____	Replaced with 'B' and 'N'	sensor devices, Si-doping increases the reactivity but does not increase the sensitivity, The Al-BN is more reactive and sensitive to SO_2 molecules, replacing N atom by Si or Al one is energetically impossible	Computational	[184]
Al, Si	Boron Nitride Nanosheet	_____	Replaced with 'B'	MM can chemically interact with Al- and Si-doped BNNS, Si-doped BNNS is a good sensing device, and Al-doped BNNS is suitable for the decomposition of MM	Computational	[185]
Si	BN nanowires	5%	Replaced with 'B' and 'N'	insulators to semi-conductors, improve the electrical conductivity	Experimental	[186]
Be	hexagonal boron nitride	3.125% to 12.5%	In the plane	Reduction in band gap	Computational	[187]
Fe	boron nitride nanotubes	____	Replacement with 'N' and 'B'	increases their chemical reactivity and stronger	Computational	[188]

Materials Advances Accepted Manuscript

View Article Online
DOI: 10.1039/D5MA01210D

Open Access Article. Published on 24 June 2026. Downloaded on 6/26/2026 4:24:14 PM.
This article is licensed under a Creative Commons Attribution 3.0 Unported Licence.

				chemisorption interactions, HOMO-LUMO energy in Fe_B is lower than Fe_N		
P, S, O, F, Cl	h-BN	_____	Replacement with 'B' and 'N'	Change in conductivity from insulating, P_B added semi-conductive characters to sheets, S and O help to reduce the band gap	Computational	[189]
Bi	BN nanosheets	2.5-10%	Over nanosheets,	bandgap energy decrease, bactericidal activity enhanced the efficiency, nanocatalyst for wastewater, and antimicrobial treatment	computational, Experimental	[190]
Rh	h-BN monolayer	_____	Center of h-BN, top of 'B' and 'N', top of B–N bond bridge site	novel SF_6 decomposed gas sensor, and has ideal adsorption and sensing properties, improved conductivity	Computational	[191]
Be, Mg, Ca, Sr, Ba	monolayer boron nitride	_____	Replacement with 'B' and 'N'	Replaces the N atom, the bond distance increases, Replaces the B atom the bond distance decreases, inducing finite magnetic moments	Computational	[192]
Li	boron nitride nano-cone	_____	Replaced with 'B' and 'N'	large static first hyperpolarizabilities, transition energy becomes smaller after doping, for Li@2N-BNNC, both the LOL and ELF maps indicate the weak coordination electron density localization	Computational	[193]
Li, Na, K	boron nitride nanocages	_____	Replacement with 'N' and 'B'	HOMO-LUMO gap is lowered, has n-type semiconductor properties, TDOS for -	Computational	[194]

Materials Advances Accepted Manuscript

View Article Online
DOI: 10.1039/D5MA01210D

Open Access Article. Published on 24 June 2026. Downloaded on 6/26/2026 4:24:14 PM.
This article is licensed under a Creative Commons Attribution 3.0 Unported Licence.

				8.5 eV, -8.7 eV and -5.7 eV for LiB11N12, NaB11N12 and KB11N12,		
Fe, Co, Ni, Cu, Zn	$B_{12}N_{12}$ nanocage	_____	On the edge	Except for Zn, other TM atoms are adsorbed with strong chemisorption, Ni-BN the most stable nanostructure,	Computational	[195]
Fe, Co, Ni	boron nitride fullerenes	_____	On the edged Boron	Negative values of adsorption energy, in the gas phase the adsorption process is more favourable, adsorption is followed as Ni-BN> Fe-BN> Co-BN> Cu-BN> Zn-BN	Computational	[196]
Co	Boron Nitride Nanosheets	2.5, 5, 7.5, and 10 wt%	_____	exhibit enhanced magnetization and improved catalytic stability,	Experimental	[197]
Ni, Pd, Pt	zigzag single-walled (7, 0) boron nitride nanotubes	_____	Replacement with 'N' and 'B'	increase the adsorption energy, and band gap energy decreased, exhibit better conductive properties, adsorption energy is more negative with B replacement than that N replacement	Computational	[198]
Sc, Ti	armchair and zigzag boron nitride nanotubes	_____	On the edge	Reactivity improved, improving the sensitivity 5FU molecule, Ti_N–aBNNT benefits from a short recovery time	Computational	[199]
Si, O	nanocrystalline hexagonal boron nitride	_____	Nitrogen Vacancy	enhancement of n-type conductivity	Experimental	[200]
Cu	BN nanofibers	0.5 mmol	Replaced to N vacancy	Enhances the CO_2 adsorption capacity of the BN nanofibers, high	Experimental, Computational	[201]

Materials Advances Accepted Manuscript

View Article Online
DOI: 10.1039/D5MA01210D

Open Access Article. Published on 24 June 2026. Downloaded on 6/26/2026 4:24:14 PM.
This article is licensed under a Creative Commons Attribution 3.0 Unported Licence.

				recyclability for repeated uses		
Co Cu, Ni	boron nitride nanotubes	----------	At the central atom	NO_2 adsorption energies in the N-site doped nanotubes are higher than the SO_2, B-site has low adsorption energy	Computational	[202]
Co, Cu, Ni, Zr, and Bi	h-BN nanosheets	5 wt%	Replaced with 'B'	enhances its antibacterial properties, with Bi-doped BN being the most effective, and Cu-BN degrading over 90% of bacteria in just 4 minutes	Computational, Experimental	[203]
Sc, Ti, V, Cr, Mn, Fe, Co, Ni, Cu, Zn	boron nitride nanotubes	_____	In center	semiconductor-to-metallic transition, decreased the band gap	Computational	[204]
Sc, Ti, V, Cr, Mn, Fe, Co, Ni, Cu, Zn	B12N12 nanocage	_____	Replacement with 'N' and 'B'	Sc to Cu tends to chemisorb via covalent interactions, Zn tends to physiosorbed, Decreases HOMO-LUMO band gap and increases metallic character	Computational	[205]
Ge	boron nitride nanotube	_____	_____	observed as a real catalyst for the reduction of N_2O	Computational	[206]
C, Si, Ge, Sn and Pb	boron nitride nanotube	_____	Replaced with 'B' and 'N'	B-site doping is more stable than N-site doping and turns into a p-type semi-conductor except for carbon-doped BNNT at the B-site	Computational	[207]
Ag, Au, Pd, Pt and Ru	boron nitride nanocarrier	_____	_____	bandgap energies decreased except Au and Pd, Ag-doped exhibits reduction in the HOMO-LUMO energy difference	Computational	[208]
F, Cl, Br	BN nanocages	_____	Replacement with 'N' and 'B'	BP nanocages as anode electrodes in M-IBs have higher efficiency than BN nanocages	Computational	[209]

Materials Advances Accepted Manuscript

View Article Online
DOI: 10.1039/D5MA01210D

Open Access Article. Published on 24 June 2026. Downloaded on 6/26/2026 4:24:14 PM.
This article is licensed under a Creative Commons Attribution 3.0 Unported Licence.

Cl, Br, I	hexagonal boron nitride	_____	$edge_B$, $edge_N$, N_v, B_v.	higher adsorptive desulphurisation performance	Computational	[210]
Ru	Porous h-BN	0.58% to 1.13%	B, N, BN, B3N, and BN3 vacancies	exhibit enhanced activity and selectivity toward CH_4	Experimental, Computational	[106]
Mo	boron nitride monolayer	_____	In center	excellent performance for converting CO_2 to CH_4	Computational	[211]
Cr, Mn	BN Nanowires	_____	In center	Mn-doped shows half metallicity, Cr-doped BN nanowire has a semiconductor, decreases the band gaps	Computational	[212]
3d and 5d transition metal	monolayer h-BN	_____	In center	converts insulating h-BN to semiconducting, 3d TM atom substitution introduces larger magnetic moments than 5d TM,	Computational	[213]
Nb	hexagonal bilayer BN	5.5 % to 11.11 %	_____	Turning to ferromagnetic, the energy band gap is reduced	Computational	[214]
Nb, Au	BN nanosheets	75.2%, 55.2%	Replaced with ‘B’	The HOMO-LUMO energy gap decreased, and adsorption over cluster is very strong	Computational	[215]
Y	Open-edge BN	_____	In center	Band gap increased	Computational	[216]
Al, P, Ga, As, In, Sb	BNNT	____	In center	Narrowing of a band gap	Computational	[217]
Cs, Br, Cs-Br	Mono-Layer Hexagonal Boron Nitride	____	Br replaced with ‘N’ and Cs replaced with ‘B’	Bandgap width reduced	Computational	[218]
Dy	h-BNNSs	0.58%		insulators to magnetic semiconductors	Computational	[219]
Al, Ga, In, Tl,	h-BNNSs	_____	Replaced with 'B' and 'N' and also at the centre	prefer to substitute B atoms on BNNSs rather than N atoms, enhanced	Computational	[220]

Materials Advances Accepted Manuscript

View Article Online
DOI: 10.1039/D5MA01210D

Open Access Article. Published on 24 June 2026. Downloaded on 6/26/2026 4:24:14 PM.
This article is licensed under a Creative Commons Attribution 3.0 Unported Licence.

				adsorption capacity for THs, In-atom-based SAAs provide the high adsorption energy		
Te nanobelts	h-BN	50 mg	_____	Te-based field-effect transistors (FETs) exhibit ultrahigh hole mobility up to 1370 $cm^2 V^{-1}s^{-1}$, metal–oxide semiconductor (p-MOS) inverter	Experimental	[221]
Nd	BN compounds	_____	BN@Nd1 - BN@Nd5	lowering the bandgap energies Eg from 6.84 to 0.75 eV and raising the maximum absorption λmax, from 183.25 to 1957.23 nm.	Computational	[222]
Se	h-BN	____	____	Band gap decreased, facile route to synthesize highly efficient Se-doped h-BN photocatalysts	Experimental, Computational	[223]
Sm	BNNT	1%	_____	potential as a nanosized β- emission source for medical therapy, material exhibited a good biocompatibility	Experimental	[224]

7.1 Carbon

BN monolayers preferably the nanosheet configuration can incorporate carbon substitution by applying non-equilibrium environment. Among these structures, boron carbon nitride BCN has thermodynamic stability where graphite (carbon part) and regular hexagon (h-BN part) has phase separation, both configurations alternate and co-exist.[225, 226] Carbon dopants exist in BN lattice either as C_2 or in form of aromatic rings. Throughout the two-dimension X-Y plane, the C_2 can be at one place surround by simple BN alteration rings or scattered in whole structure. The other form with C ring dopants exists symmetrically in centre or edges completed engulfed in BN framework.[227] Betterment in structural constraints is highly signified by doping level. With that C

Materials Advances Accepted Manuscript

View Article Online
DOI: 10.1039/D5MA01210D

Open Access Article. Published on 24 June 2026. Downloaded on 6/26/2026 4:24:14 PM.
This article is licensed under a Creative Commons Attribution 3.0 Unported Licence.

ring domains effectively merged when the doping level is upgraded while C_2 dopants appears in the form stable configuration comprising of alternating BN with C chains and at some points with parallel BN facets, a discovery via first principle theory.[228] The direct attachment in the stable isomer of the carbon to each B and N addressed the structural stress.

Experimental preparation of the BC_2N confirms the stable modalities when rubidium facets are exposed to borazine vapors at controlled condition of temperature.[142] The decoupled BN with C dopant showed alteration in the stable isomeric configurations and the band gap calculated was closer to the theoretical prediction that is 2 eV. There is a significant work on the development of the carbon modified BNNS and BNNT.[226, 229] However, the only lacking element to hinder the synthesis of BCN is the evolved characterization techniques.

An excellent C-doped BN configuration demands the prediction of the bond character and the sufficient knowledge regarding the chemical environment required for crystal growth. Such factors can be overcome by spectroscopic analysis which comprehends the sp^2 hybrid BC or CN bonds. Other challenges can be subdued by the micro analytical techniques which works on elemental and atomic level.

7.2 Oxygen

Doping and impartation of the oxygen in BN framework has been well studied theoretically and there is enough experimental work as well.[230-232] Such incorporation of O is successful by replacement of Nitrogen in nanosheets and nanotubes, the N site because both are electronegative elements and causes less alterations in structure. Although, O can be doped in B site however this placement was predicted to be less effective due to disturbance in configuration.[232] Furthermore, O attachment in place of boron configures the new bonds N-O-N that are linked with enhanced structural deformations.

Somehow, oxygen as dopant atom causes the delocalization in already conjugated π electronic bonds due to injection of the even electrons; this case is quite similar to the bond formation C-N-C in nitrogen doping of graphitic sheets. This is effectively interesting because of the effects on band gap narrowing[232, 233] and the vast amount of applications associated with this oxygen decorations. Some properties can be affected in a good manner that are magnetic or spin manipulations[233] and catalytic efficiency for reduction reactions oxygen and hydrogen evolution.

Teo and colleagues accelerated the work on oxygen modified BN and property enhancements in an experimental analysis which demonstrated the preparation of O-BN via chemical vapor

Materials Advances Accepted Manuscript

View Article Online
DOI: 10.1039/D5MA01210D

depositions, and reported the band gap reduction from typical 6 eV to 4.31 eV;[230] evidenced by theoretical study.[189] The new obtained band gaps increased the conduction in BN a 100 folds. In another experiment regarding cathodoluminescence,[234] oxygen doped BN nanotubes showed radiative electronic transition in UV range if spectrum. This can be applicable in manufacturing of luminescent materials. After that, a work on theoretical first principle simulations founds out the formation of B_3O_6 fragments in BNNT which is responsible for these types of transitions.[235] Hence oxygen modulated boron nitride can be well studied in luminescence spectroscopy for the presence of O defects in BN crystals and related heterostructures.

7.3 Germanium

Boron nitride configurations can fit the Ge atom either in B vacancy or nitrogen vacancy and interestingly there are cases where there is the replacement of BN pair simultaneously with a single Ge atom. Ab initio calculations predict significant band gap modification in BN monolayers upon substitutional incorporation of germanium, with computed reductions of 42% and 81% depending on the substitution site.[236] However, Ge doping process is not smooth and requires the extra energy while the synthesis of BN is in progress. Additionally germanium imparts the significant magnetization character to BN after doping and modifies the optical properties to have a broad range of absorption from visible to UV.[236]

Ge-BNNT consistently provided the modification in the band gaps. Although Ge has equal possibility of addition or replacement with either B or N atom, but B site has more compatibility. This preference of B site in case of Ge dopant is well adapted to the formation energy data and according to first principle calculations, B site corresponds to lower formation energy and hence enhanced structural stability. Ge doping has significant impact such as it is turn the pristine BN into an excellent p type semiconducting material.[207]

Moreover, Ge imparts the specific magnetic properties to boron nitride structures which include magnetism by insertion of dispersionless additional π bands followed by intense structural deformations in the close proximity of Ge atoms.[237]

Experimentally by the use of LP-chemical vapor deposition, n type conduction precisely Ge introduction in hexagonal boron nitride has been made successful via oxygen coupling. For this purpose, h-BN monolayer sequentially utilized the Borazane with GeO_2 powder for the chemical growth alongside employing copper foil as third heating zone following processes of sublimations and transportation of Ge-O to BN monolayers. The appearance of band edges at ~5.93 eV

Open Access Article. Published on 24 June 2026. Downloaded on 6/26/2026 4:24:14 PM.
This article is licensed under a Creative Commons Attribution 3.0 Unported Licence.
Materials Advances Accepted Manuscript

View Article Online
DOI: 10.1039/D5MA01210D

suggested sacrificial impurity coupling and addition of Ge-O is preferably as dopants in BN layers rather than alloy formation.[238] More experimental methods are needed to address the single Ge atom doping rather than coupling interactions and intercalation studies.

7.4 Sulphur

Photo-catalysts for various types of reactions can be synthesized via dopant enhanced BN. Hence for this purpose, synthesis of novel sulfur doped BN was made successful in an experimental and theoretical investigation.[239] In experimental work, sulfur doping in graphene laid the foundation for sulfur impact on two dimensional materials through heat annealing.[240] Similarly, the addition of sulfur through heat treatment in BN contributed efficiently to band gap tuning and additional impartation of semiconductor properties, supported by computational studies.[189, 241]

In particular, sulfur has been found to be enhancing the optical absorption and surface reactivity. Additionally, S doping amount can be varied to achieve the desired properties. Hence d and p orbitals of Sulfur occupied the valence and conduction band to shrink the band gap.[241] But these studies were lacking in precise explanation of fitting S into B or N sites. Attributing to this, Tan et al. (2022) established precise site-selective control over sulfur incorporation into the h-BN lattice. Through their analysis, S has been well adapted to be substituted in N site rather than B site over molten Au in chemical vapor deposition method. The allocation of sulfur in BN monolayer successfully figured out the 1.5 times increased conductivity as compared to pristine BN.[242]

Moreover, enhanced charge mobility of h-BN surface can be a valuable asset for two dimensional semiconductor materials preferably due to S doping sites, evidenced back to visible light response[241] and characterization pattern of XRD. In metal-free catalysis, Sulfur dopant on BN has the excellent surface stability and reactivity for CO oxidation.[243] Furthermore, the precise control on the electronic and optical properties[242] of boron nitride quantum dots has been exhibited by the sulfur dopant in experimental settings.[244]

Although BN quantum dots regulations are still in early stage, but successful modulation can be achieved by the use of the sulfur atom and its varying dopant compositions. However, more theoretical evidence is needed to expand the BN-QDs in displaying optical activity and related electrochemiluminescence properties.[244]

Open Access Article. Published on 24 June 2026. Downloaded on 6/26/2026 4:24:14 PM.
This article is licensed under a Creative Commons Attribution 3.0 Unported Licence.

Materials Advances Accepted Manuscript

View Article Online
DOI: 10.1039/D5MA01210D

Open Access Article. Published on 24 June 2026. Downloaded on 6/26/2026 4:24:14 PM.
This article is licensed under a Creative Commons Attribution 3.0 Unported Licence.

7.5 Bismuth

Bismuth incorporated BN has been prepared by the experimental analysis through liquid phase exfoliation from the bulk material with varying percentage concentrations of the dopant element efficiently with ratio of 2.5, 5, 7.5 and 10.[190] Hydrothermal technique and research findings aligned with the absorption in UV region as an account for the optical properties. Theoretical study modulations successfully determined the alterations in the electronic structure of BN framework particularly the reduced band gap due to induction of additional localized energy states surrounding the Fermi level.[203]

In particular, Bi has the selective potential to enhance the catalytic and bactericidal activities giving BN the edge to be utilized in the biological settings.[203] The dopant concentration has an influence on band gap reduction and increased Bi concentration can comprehend the wide band gaps materials to tuning into efficient semiconductors.[190]

Furthermore, Bi is well adapted in the formulations of the ultra, super and heterostructures composites of BN such as Bi oxides/h-BN complex for adaptations as electrochemical sensors in environmental safety practices.[245] Additionally, bismuth ferrite[246] decorations on hexagonal boron nitride nanosheets in an experimental hydrothermal analysis presumably function well for the stability of epoxy resins due to the surface catalytic activity. More of such bismuth added BN heterostructures are practically available including bismuth phosphate/BN[247] and bismuth sulfide/BN[248] for photocatalytic degradation and electrochemical detection processes respectively. Although bismuth impart excellent electronic characteristics in BN still need research to confirm the preferable substituted positions (B site or N site) to understand the binding orbitals and hybridization mechanism during doping process.

7.6 Gallium

Gallium dopant has better adaptations in BN structure either in B site or N site. However, B site is most suitable attributing to the similar electronic configurations and close proximity of atomic radii. Doping Ga atom on BN surface such as nanosheets, nanotubes or crystals has been well documented in theoretical majorly DFT investigations and is outsized for the surface adsorption of most of the compounds, sugars, pollutants and drug molecules.[180, 249-251] Such impartation significantly alters the planarity of surface and causes changes in the bond lengths, angles to successfully adopt Ga in BN configurations. Thus, the surface distorts and there are variations in the band gaps and other electronic properties. These surface modifications have extended the use

Materials Advances Accepted Manuscript

View Article Online
DOI: 10.1039/D5MA01210D

of gallium dopant in BN structure to perform single atom catalysis for greenhouse gases and other environmental pollutants.[252]

Although computational research is advanced in catering gallium decorated boron nitride-based structure modulations, more experimental studies are necessary to highlight the spectroscopic analysis for determining the optical properties and other characterization techniques to facilitate the reaction chemistry.

7.7 Indium

Indium dopant is equally potable and effective as gallium in the administration of boron nitride complex structures, hence can significantly alter the electronic and structural properties for the better adaptation in the production and assembly of solid-state devices.[253, 254] Among both B and N site for dopant insertion, the boron site has more efficiency to adopt dopant in the structural constraints in such a manner that it has increased chemical reactivity as compared to the pristine BN models.

Apparently, there is an ease of doping process in boron nitride configuration when the dopant is small radii atoms. This preferably makes B site vacancy thermodynamically more stable and favorable for indium insertion rather than N site. Moreover, presence of indium within BN structure can influence the surface reactivity and adsorption capabilities in such an intricate manner that indium can equally adopted in central position surrounded by nitrogen atoms and edge functionalization.[255]

Although central indium is more capable of adsorption process efficiently edge indium has good electronic properties as well. Large atomic radii dopants have greater potential in band gap tuning and engineering for applications in semiconductors devices such as indium and thallium.

Furthermore, vacancy site has the defective states and indium can fit better to influence the electronic properties of BN. Majorly, indium acts as the major heteroatom to build a bridge between electronic systems of nearby nitrogen atoms alongside reestablishments of the geometrical parameters. This makes insertion of indium in BN structure energetically favorable as there can be the modulation of the magnetic properties to expand the range of potential applications.[256, 257]

Computational and DFT modules have been successful in the explanation of indium effect on band gap alterations. Yet more computational studies are needed for the validation of doping process involving indium and BN. There is lack of experimental investigations to provide a solid

Open Access Article. Published on 24 June 2026. Downloaded on 6/26/2026 4:24:14 PM.
This article is licensed under a Creative Commons Attribution 3.0 Unported Licence.

Materials Advances Accepted Manuscript

View Article Online
DOI: 10.1039/D5MA01210D

verification for the synthesis process of indium decorated BN structures and its implications in the nano materials.

7.8 Thallium

Thallium as a dopant has not been much explored for surface level modulations in boron nitride. The reason could be the enhanced toxicity. Therefore, literature is lacking the experimental and theoretical investigations regarding the use of Tl dopants in the different available configurations of BN. However, thallium has been used for selective adsorption process in the hexagonal BN nanosheets as a single metal atom for the desulfurization in Thiophene and related compounds because thallium can directly make a covalent bond with the sulfur atom.[255]

7.9 Aluminium

Use of aluminum atom as a dopant and external impurity in boron nitride configurations has been extensively documented in literature more specifically in regard to first principle DFT investigations.[258, 259] Arm chair and zigzag configurations both are suitable for adaptability however arm chair is employed in most of the computational context all attributing to the better SCF convergence.[260] Al atom anchoring on h-BN is practically important for the surface interactions and adsorption process of the drug fluorouracil,[258] anticancer drugs,[260] and SF_4 gas.[261] Significantly, Al has a replaceable efficiency for settling down in place of the boron, the B site or vacancy. In particular, Al has strong influence on the band gap engineering and modulations of the boron nitride i.e. reductions in the band gaps and transformation of the BN surface into good semiconductors alongside the significant and dedicated enhancements in the adsorption potential.[258, 259, 261]

The involvement of the aluminum atom in BN system can drastically shift the electric properties of its nanotubes, the base effect due to decreased HOMO-LUMO gaps attributing to surge in HOMO energy value. The increased contribution to the metallic character thereby promotes the excessive change in the electronic properties.[259] Additionally, [8, 0] BNNTs having Al as single atom has the potency to be an efficient nanocarrier materials for the cis and neda paltin, making BN a good transport surface for drug delivery in bodies for role in nanomedicine.[260] Still experimental analyses are required to deal with the problems occurring during the synthesis process and the related reaction queries.

Open Access Article. Published on 24 June 2026. Downloaded on 6/26/2026 4:24:14 PM.
This article is licensed under a Creative Commons Attribution 3.0 Unported Licence.
Materials Advances Accepted Manuscript

View Article Online
DOI: 10.1039/D5MA01210D

Open Access Article. Published on 24 June 2026. Downloaded on 6/26/2026 4:24:14 PM.
This article is licensed under a Creative Commons Attribution 3.0 Unported Licence.

7.10 Phosphorus

BN nanosheets and other structures have limited potency and efficacy for employment in the optical devices and electronic field. Therefore, there was a high interest in expanding the absorption range of BN structures in the visible range. Phosphorus doping served that purpose due to ultimate reduction in the band gap from 4.643 eV to 0.824 eV and transforming BN based material into an efficient 2D semiconductor material, as per reported by Zhang *et al.* P addition has a better influence on the visible light driving characteristics of the boron nitride in such a manner that it can behave as a photocatalysts merely due to presence of P in the structural symmetry.[262]

Catalyzation for direct dehydrogenation of ethylbenzene is going to become a challenge in the industry. However, due to excellent catalytic properties, phosphorus-doped boron nitride (PBN) was studied experimentally and theoretically. This study explores the PBN giving 95% styrene selectivity. N_3P–OH sites decrease the energy barriers and deactivate the carbonaceous site for the removal of hydrogen. When PBN is used as a catalyst, the mass effect on the dehydrogenation of ethylbenzene was experimentally studied.[263] In the study, porosity and surface exposure degrees were observed. The pore size depends on the heating rate and increased styrene production to 21.47 $mmol_{ST}\ g^{-1}\ h^{-1}$ and selectivity becomes 98%. The study explores that mass transfer for 2D catalysts was important for chemical reaction.[264] Variation in bandgaps in the BN sheet when dopants attaches to it from literature is shown in Table 5.

The comparison of band gaps across diverse BN structures and dopant types give some clear demarcations about the band gap engineering. There are several trends that emerge from this. First of all, carbon doping achieves the most drastic band gap reductions across all BN configurations, and it achieve values that are as low as 0.34-0.96 eV in BNNTs relative to pristine values of 3.462 eV. This extreme reduction is mechanistically consistent with the introduction of sp^2-hybridised C_B and C_N states that bridge the valence and conduction band edges of pristine h-BN and it creates mid-gap states that enable visible-light absorption. Transition metal dopants (Ni, Pd, Pt) achieve complete band gap closure 0.00 eV in zigzag single-walled (7, 0) BNNTs. It reflect strong d-p hybridisation between the dopant d-states and the nitrogen p-states at the band edges. A finding that has implications for metallic conduction in doped BNNT-based nanoelectronics. At the other end of spectrum, group III dopants Al, Ga, and In produce relatively modest reductions. It is also in line with their weaker perturbation of the frontier orbital energies. Rare earth dopants such as

Materials Advances Accepted Manuscript

View Article Online
DOI: 10.1039/D5MA01210D

Nd have the broadest spectral shift of all and it reduce the band gap from 6.84 eV deep UV absorption to 0.75 eV that is near-infrared active. That is a transformation of potential significance for broadband photodetector applications. All in all, appropriate dopant selection and site engineering give tuneable optical and electronic properties of h-BN from the UV to the near-IR.

Table 5: Variation in band gap in the BN sheet when dopants attach to it

Dopant	BN structure	Pristine BN Band Gap	Doped BN Band Gap	Nature of Study	Reference
C	Boron nitride nanosheets	5.03eV	C_B 0.99 eV C_N 4.29 eV	Computational	[164]
C	Zigzag BNNT	3.462eV	C_B-BNNT is 0.96 eV, C_N-BNNT is 0.342 eV	Computational	[166]
C	Boron Nitride Nanosheet	5.05eV	0.80 eV for the C_B sheet and 0.84 eV for the C_N sheet	Computational	[168]
C	BN nanoflakes	6.3eV	2.9 eV for $1C_N$ and 3.0 eV for $2C_N$, 3.1 eV for $1C_B$ and 2.4 eV for $2C_B$	Computational	[169]
C	Triangular Boron Nitride Nanoflakes	6.44eV	For Ct_{BN} is 0.64 eV, Ct_{NB} is 0.54eV	Computational	[171]
C	boron nitride nanowire	3.7eV	2.0eV for $1C_N$, 1.8eV for $2C_N$	Computational	[172]
Al	boron nitride nanocarriers	9.19eV	6.60eV	Computational	[179]
Al, Ga	h-BNNs	4.24 eV	For Ga 3.64 eV, for Al 3.90eV	Computational	[180]
Al, Ga	BN nanosheets	In gas phase 4.38eV and water media 4.16eV	For Al BNNS in gas phase 4.37eV while in water phase 4.14eV, Ga BNNS in gas phase 4.38eV and water phase 4.14eV	Computational	[181]
Al, Ga, In	Boron-Nitride Nanotubes	0.1564eV	Al BNNT 0.1543eV, Ga BNNT 0.1429eV, In BNNT 0.1521eV	Computational	[182]
Al, Ga, P, As	boron nitride nanosheet	5.751eV	Al BNNS 5.648eV, Ga BNNS 5.672eV, P BNNS 5.144eV, As BNNS 5.031eV	Computational	[183]
Al, Si	boron nitride nanosheet	5.85eV	Al BNNS 5.52eV, Si BNNS 2.91eV	Computational	[184]
Al, Si	Boron Nitride Nanosheet	7.98eV	Al-BNNS 7.70eV, Si-BNNS 6.09eV	Computational	[185]

Open Access Article. Published on 24 June 2026. Downloaded on 6/26/2026 4:24:14 PM.
This article is licensed under a Creative Commons Attribution 3.0 Unported Licence.

Materials Advances Accepted Manuscript

View Article Online
DOI: 10.1039/D5MA01210D

Open Access Article. Published on 24 June 2026. Downloaded on 6/26/2026 4:24:14 PM.
This article is licensed under a Creative Commons Attribution 3.0 Unported Licence.

Si	BN nanowires	7.63eV	Si-BNNW 4.32eV, Si-BNNT 3.76eV	Experimental	[186]
Rh	h-BN monolayer	4.655eV	1.233eV	Computational	[191]
Li, Na, K	boron nitride nanocages	6.8 eV	2.9 eV for NaN 2.4 eV for KN 2.7 eV for LiN 1.9 eV for NaB 2.9 eV for LiB 3.6 eV for KB	Computational	[194]
Fe, Co, Ni, Cu, Zn	$B_{12}N_{12}$ nanocage	4.43eV	1.84 eV for Co-BN 3.77 eV for Zn-BN 2.03 for Cu-BN, 2.94 for Ni-BN, 3.60 eV for Fe-BN,	Computational	[195]
Fe, Co, Ni	boron nitride fullerenes	___	Fe-B 3.69eV, Co-B 3.87eV, Ni-B 2.20eV	Computational	[196]
Ni, Pd, Pt	zigzag single-walled (7, 0) boron nitride nanotubes	3.32eV	0.00eV	Computational	[198]
Sc, Ti	armchair and zigzag boron nitride nanotubes	aBNNT-6.014 eV zBNNT 5.769 eV in gas phase	Sc_N–, Sc_B–, Ti_N–, and Ti_B– aBNNTs in gas phase are found to be 2.095, 4.272, 1.795, and 2.993 eV, Sc_N–, Sc_B–, Ti_N–, and Ti_B– zBNNTs in gas phase are found to be 2.285, 4.408, 1.796, and 2.939 eV	Computational	[199]
Co Cu, Ni	boron nitride nanotubes	___	Co-$_N$ 2.14ev, Co-$_B$ 1.58eV, Ni-$_N$ 0.67eV Ni-$_B$ 0.93eV Cu-$_N$ 0.80, Cu-$_B$ 0.77eV	Computational	[202]
Sc, Ti, V, Cr, Mn, Fe, Co, Ni, Cu, Zn	$B_{12}N_{12}$ nanocage	6.73eV	Zn-BN 5.25eV, Cu-BN 2.00 eV, Ni-BN 3.41eV, Co-BN 3.15eV, Fe-BN 2.68eV, Mn-BN 2.61eV, Cr-BN 2.65eV, V-BN 2.13eV, Ti-BN 2.05eV, Sc-BN 2.20eV	Computational	[205]
C, Si, Ge, Sn and Pb	boron nitride nanotube	5.94eV	C_B 1.64eV_ C_N 4.35eV, Si_B 3.12eV_Si_N 3.59eV,	Computational	[207]

Materials Advances Accepted Manuscript

View Article Online
DOI: 10.1039/D5MA01210D

Open Access Article. Published on 24 June 2026. Downloaded on 6/26/2026 4:24:14 PM.
This article is licensed under a Creative Commons Attribution 3.0 Unported Licence.

			Ge_B 3.94eV_Ge_N 3.61eV Sn_B 4.73eV_Sn_N 3.59eV, Pb_B 5.33eV_Pb_N 2.55eV		
3d and 5d transition metal	monolayer h-BN	5.5eV	Ti 1.8eV, V 2eV, Cr 1.9eV, Fe 2.1eV, Mn 2.2eV, Hf 1.8eV, Ta 1.5eV, W 1.7eV, Re 0.8eV, Os 0.6eV Ir 0.4eV, Pt 0.8eV	Computational	[213]
Nb	hexagonal bilayer BN	5.1eV	3.9eV	Computational	[214]
Nb, Au	BN nanosheets	6.032 eV	NbBN 1.495eV, AuBN 2.701eV	Computational	[215]
Y	Open-edge BN	__	1.66eV	Computational	[216]
Al, P, Ga, As, In, Sb	BNNT	LCAO, LCAW BNNT 7.0, 3.4,	LCAO, LCAW Al_B 6.4, 3.8, Ga_B 5.0, 3.8 In_B 3.5, 3.6 P_N 6.2, 3.2 As_N 5.9, 2.7 Sb_N 5.0, 2.6,	Computational	[217]
Cs, Br, Cs-Br	Mono-Layer Hexagonal Boron Nitride	4.66eV	Br h-BN 4.61eV Cs h-BN 3.52eV	Computational	[218]
Al, Ga, In, Tl,	h-BNNSs	____	Al-BNNS 8.05eV, Ga-BNNS 7.97eV, In-BNNS 6.25eV, TlBNNS5.77eV	Computational	[220]
Sc, Ti, V, Cr, Mn, Fe, Co, Ni, Cu, Zn	boron nitride nanotubes	4.326eV	Ni BNNT 1.115eV Cu BNNT 2.312eV, Zn BNNT 3.455eV.	Computational	[204]
Li	boron nitride nano-cone	7.9eV	Li@2N-BNNC 7.1eV Li@2B-BNNC 4.4eV, Li@BN-BNNC 4.3eV	Computational	[193]
Al	Armchair and Zigzag BNNTs	_____	Al@ BNNT (3,3) 2.448eV, Al@ BNNT (5,0) 1.60 eV	Computational	[178]
Be	hexagonal boron nitride	4.63eV	Concentration ---- bandgap 3.125% ---------- 2.27eV, 6.25%----------1.2eV, 9.37%---------- 1.7eV, 12.5%---------- 1.37eV, 6.25%---------- 1.7eV,	Computational	[187]

Materials Advances Accepted Manuscript

View Article Online
DOI: 10.1039/D5MA01210D

			9.37%---------- 1.46eV, 12.5% ----------0.90eV		
Nd	BN compounds	6.84eV	0.75eV	Computational	[222]

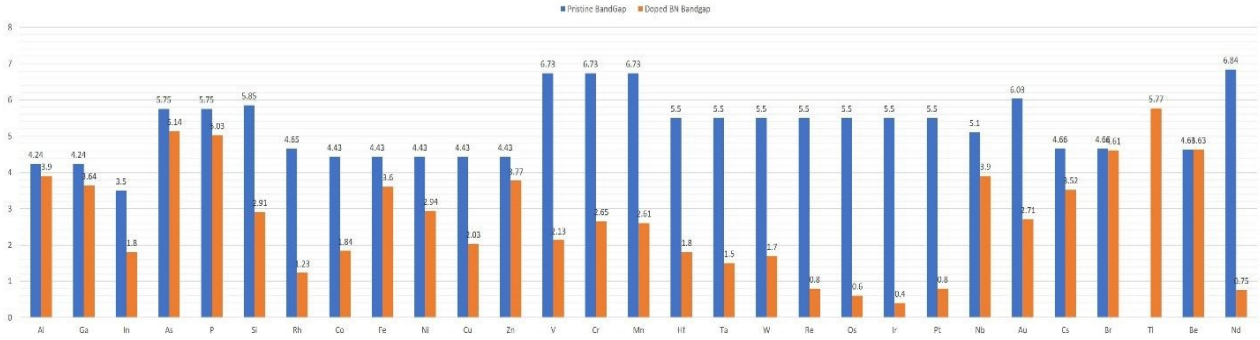

Figure 8: Change in Bandgap when atoms placed on BN structures

8 Surface Modification Via Chemical Functionalization

Although graphene surface suffers from the dangling bonds and interruptions can be well adapted in chemical modifications via functional groups and external moieties. BN and comprehensive nanostructures on the other hand are free from surface dangling; unfortunately, it has not been well researched in term of surface modification in chemical settings both experimentally and theoretically. Perhaps, the use of carbon materials and their counterparts can confer to variety of organic reaction mechanisms while BN needs a breakthrough. A practical strategy is to create reactive surface sites on h-BN through targeted functionalization which enable the same range of organic transformations that have been successfully demonstrated for graphene. This can present challenges however researchers developed some successful chemically modified BNs.

Therefore, functional group exploitations can be adapted to bring the electronic charge stabilizations in the BN, same approach the way graphene is treated. In general, hexagonal BN and graphene surface has made ready for reaction by opening of the polar bonds, the conjugation site on basal ends. This new bonds with added functionality always form at the even number position in reference to graphitic structures. The functionality addition always tends to form a single with two of representative atoms boron or nitrogen hexagonal BN configuration, in turn a compensating group should be attached to unpaired B/N for charge balancing. However, some functional groups come with a bridging effect via opening of double bond mimicking the carbon double bond epoxidations reaction.

Open Access Article. Published on 24 June 2026. Downloaded on 6/26/2026 4:24:14 PM.
This article is licensed under a Creative Commons Attribution 3.0 Unported Licence.

Materials Advances Accepted Manuscript

View Article Online
DOI: 10.1039/D5MA01210D

Open Access Article. Published on 24 June 2026. Downloaded on 6/26/2026 4:24:14 PM.
This article is licensed under a Creative Commons Attribution 3.0 Unported Licence.

Henceforth, functionalized nanostructures of BN always accompany two groups maybe same or different positioning to adjusting a single boron and nitrogen unit. On contrary, functionalized conjugation in carbon allotropes found out in experimental and theoretically setting that two functionalities not necessarily have to be present on neighboring positions instead these can separated in space when system is showing the balanced charge and aromaticity.[265] These settings can be made applicable while functionalizing hexagonal BN. Since BN has two attackable sites refer to N site and B site being susceptible to attack by an electrophile and nucleophlic reagents, respectively, owing to the presence of ionic partially via electronegativity difference in BN. Varieties of functionalized BN structures are presented in Figure 9.

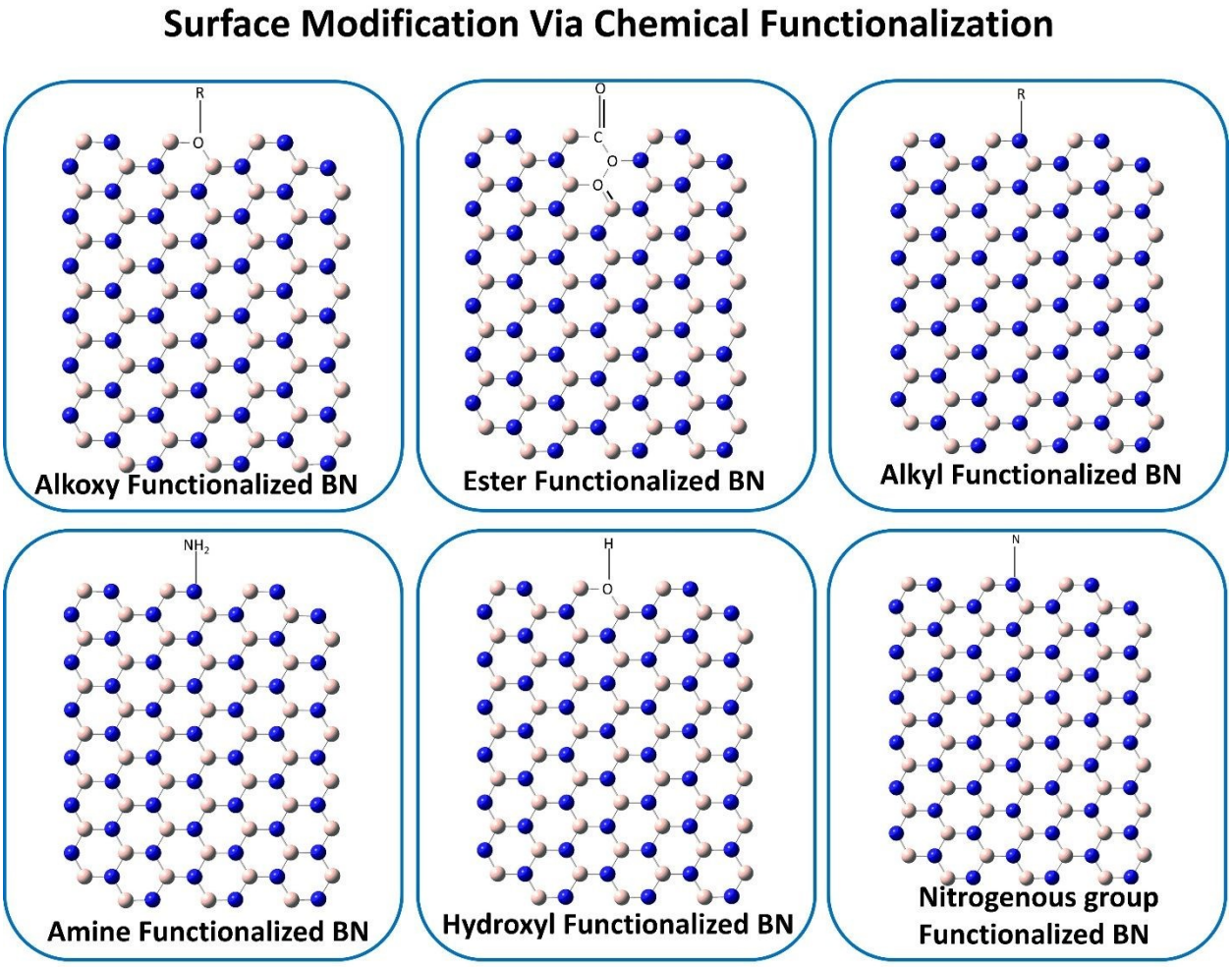

Figure 9: Functionalization of BN sheet

8.1 Alkyl Functionalized BN

Alkylation on BN occurs in a versatile manner. The attachment of alkyl group can either be on B or N site because the carbon chains are equally potent to form bond with boron or nitrogen. The

Materials Advances Accepted Manuscript

View Article Online
DOI: 10.1039/D5MA01210D

Open Access Article. Published on 24 June 2026. Downloaded on 6/26/2026 4:24:14 PM.
This article is licensed under a Creative Commons Attribution 3.0 Unported Licence.

visible links of -R groups can be seen in the forms of bridging bonds or individual bond each lying on B/N atom. Hence, the initial work on BN alkylation was put forward by Sainsbury and colleagues[266] in which alkyl chains were indirectly inserted into the nanosheets based BN framework via attachment of dibromocarbenes and subsequent substitution of bromine atoms by butyl chains, the reaction obtained alkyl functionalized BN nanosheets namely $(n\text{-}C_4H_9)_2C$-BNNSs. This procedure was proved effective via spectroscopic analysis and characterizations of generated product which further enhanced the attraction towards carbene route in synthesis of alkyl modified BN surface.

However, the alkyl chain incorporated BN needed further procedures to make it applicable in natural settings. Such approach was reported in another experiment which is solely based on a reduction reaction after formation of intermediates. In this method, BN nanotubes were employed due to small surface and less disturbing following by the sodium naphthalide treatment in order to establish a concur electron transfers, then reduction takes place in presence of primary bromohexane. This way hexyl functionalized BNNT were successfully produced on which the DFT simulations further revealed that boron site were preferred while attaching the hexyl chain which serves as electron donor into the boron vacancy, particular the empty p orbital.[267] This electron transfer facilitated the formation of covalent bonds making the BN quite stable than the one prepared by carbene route. However, more experimental and computational studies are needed to fully reveal the advantages of alkyl chain incorporation into BN structure.

8.2 Hydroxyl and Alkoxy Functionalized BN

Typically, hydroxyl group can covalently bond with boron electrophilic site via oxygen atom, making it the most effective and ideal functionalities to be mounted on BN hetero structures. OH incorporated BN doesn't need further treatment as the surface itself is ready for several procedures including biological settings, matrix filling and are good precursors for the initiation of reaction that results in formation of complex BN functionalities. Extensive research is there to explain the development of OH based BNNSs and BNNTs. Some of the solid approaches may include plasma treatment, ball milling with sodium hydroxide, and water treatment at high temperature or simply reaction in presence of the reagents that are capable of generating hydroxide radicals.

One such experimental study utilized H_2O_2 for radical production and their reaction with boron nitride nanotubes effectively at 120°C.[268] Chemical bonds between O of hydroxyl group and B of BN structure were confirmed by XPS spectroscopic characterization. The resulting OH/BNNT

Materials Advances Accepted Manuscript

View Article Online
DOI: 10.1039/D5MA01210D

Open Access Article. Published on 24 June 2026. Downloaded on 6/26/2026 4:24:14 PM.
This article is licensed under a Creative Commons Attribution 3.0 Unported Licence.

Materials Advances Accepted Manuscript

was expected to be used in preparation of a stable 1 mL solution with concentration of 0.25g. Later on, a more potent OH functionalisation method was formulated by Lin and his group which used the sonicator to react the water and BN pure powders following the dissolution in sulfuric acid/H_2O_2 to add OH functionality. And recently, air plasma responsible for hydroxyl radical production was use to expose BN structures. Hence, these radicals classify under highly reactive intermediates, reaction can occur rapidly and randomly declaring that OH functionalisation is non-selective. Thus OH has the equally possibility for attachment on the in plane sites as well as the cut edges.[269] Alkoxy functionalized BN structure is presented in Figure 9

In another experimental analysis, Xiao and members applied steam treatment which synergistically involved the exfoliation technique for successful hydroxylation procedure.[270] Additionally a study covered the application selective edge hydroxylation of porous BN nanosheets by use of in-plane inhibitors.[271] Infrared (IR) spectroscopic analysis reported the presence of B-O bond vibrations. Moreover, under visible spectrum the appearance of yellow colour is the ultimate significance for band gap narrowing. Attribution to these experiments, computational investigation has also informed the decrease in HOMO-LUMO gaps when edges are terminated with OH as compared to hydrogen terminated BN analogues.[272] Thereby, the compliance of experimental and theoretical studies on band gap, reduction, modeling and alterations suggested the feasibility of edge functionalized BN for practical response in semiconductors.

Likewise hydroxyl moiety, alkoxy group is another oxygen containing functionality which is preferable for direct attachment on surface of hexagonal BN. Sonicator-assisted alkoxylation reaction on BN nanotubes revealed the conversion of BNNT into nanoribbons due to the wall peel effect in alcohol solutions.[273] The presence of BNNRs was identified by IR spectra that discovered the specific vibrations involving B-O and B-O-C which are not the feature characteristics for BNNT.

8.3 Nitrogenous Group Functionalized BN (NH_2)

Amino and amine groups covered the nitrogenous functionalities which mostly followed the similar synthetic pattern as formulated for -OH group involving the electrophilic attack of nitrogen-based groups on boron sites. The firsthand report on amino functionalized BN synthesis via ammonia plasma treatment was presented in 2007 by keen efforts of Zettl and fellows.[274] This procedure involves the covalent bond formation between the amino groups and BN based nanotubes due to amorphization and breaking of crystal wall in BNNT. For better efficiency, Xie

View Article Online
DOI: 10.1039/D5MA01210D

and colleagues yielded the amino attached BNNT structures which can be converted into stable solutions of particular concentrations.[275] Nitrogenous group functionalized BN structure is presented in Figure 9.

8.4 Covalent Functionalisation in BN

The easy route for the synthesis of BN functionalized ester is the direct attachment of ester into BN structure. Elsewhere, the alternative yet superior approach can be the use of hydroxyl or amine derivative of BN and their modification into esterified BN. Ester incorporation is termed under covalent functionalisation which has the limited proficiency and applications due to structural inertness However, in a recent study,[276] BN reductive functionalisation was successfully reported by the use of unsaturated ester (methyl methacrylate). For this purpose, BNNSs were subjected to an electron pool for generations of reduced BN having negative charged boron site followed by polymerization reactions to prepare polymethyl methacrylate boron nitride nanosheets PMMA/BN.[276] Under spectroscopic analysis via FTIR/XPS, B-C bonds were found to be the basis for functionalization. In addition, reduction by charge applications can be scaled to the development of new sensors, coating materials, drug delivery systems and catalysts.[276]

Other functional groups such as amides and acyl can be introduced into BN. Amine functionalized BN structure is presented in Figure 9. The route can be quite similar to esterification. The initial covalent functionalized BN were obtained by refluxing BN nanotubes with acyl and amino groups.[277, 278] However, this procedure is difficult to approach and there are only few studies directing to these particular functionalities. These modifications provide a great variety of dispersibility over solvents particularly acetone and ethanol; owing to the excellent fabrications in nano composites.

The precursor can always be hydroxyl/amino BN through which synthetic routes were leading to complex functionalities. One such method involved the esterification of hydroxyl functionality in nanotubes and BN nanosheets by perfluorobutyric or thioglycolic acid, further isocyanates could have been used for functionality adoption.[268] Henceforth, dielectric modification of BN nanotubes via potentially polyhedral oligosilsesquioxane structures was revoked by a multi-step synthesis.[279] In this study, oxosilane was reacted with hydroxyl part then coupled by POSS derivatives for successful modification. Likewise, in place of hydroxyl functionality amino groups can be successfully acylated. These procedures enabled the grafting modulation of BN and their respective heterostructures immensely contributed to the development of effective chemical

Open Access Article. Published on 24 June 2026. Downloaded on 6/26/2026 4:24:14 PM.
This article is licensed under a Creative Commons Attribution 3.0 Unported Licence.
Materials Advances Accepted Manuscript

View Article Online
DOI: 10.1039/D5MA01210D

functionalisation procedures and more specifically the design of modeled BN nanofillers for their use in composites.

The covalent functionalized BN gives a simplest alternative that is hydrogen based BNNS. This addition proved useful via first principle investigation because band gaps narrowing were observed with the value of 3 eV[280] when compared with non-functionalized hexagonal boron nitride. Additionally, if hydrogen were to be incorporated on half of BN, majorly the boron sites, there were exceptional decrease in the band gaps and new value obtained was 2.2 eV[281] a theoretical investigation by Yang and colleagues. Hence, this band gap range showed the correspondence to yellow-green absorption spectrum under visible light. The energetic favorably hydrogen incorporated BN is supported because hydrogen is chemically adsorbed on BN given the energy of adsorption as -0.3 eV. Simultaneously, single hydrogen reduction and water oxidation reactions were complying the predicted band gap range of half H functionalized BNNS, demonstrating the water splitting under photo catalysis.[281]

Fluorine could also bring possible changes in BN structures as nanotubes functionalized by Fl atom were obtained by reaction of BNNT and BF_3.[282] Although non-functionalized BNNTs are insulators but the fluorine (~4 % concentrated) incorporation made it useful for semiconductors as there was three time increase in conductivity. From the perspective of theoretical investigations the fully occupied fluorination of BN demonstrates the reduced band gaps 3.2 eV than h-BN,[280] approximately equal to H-BNNS. The experimental analysis complies with the theoretical result calculations for band gaps.

In addition some other functional groups including methyl, cyano and aldehydes are useful for BN functionalisation as per the computational investigation of Bhattacharya's group on the respective band structures. These functionalities brought about the varying band gap range presumably 0.3 to 3.0 eV in BN heterostructures.[280] Hence, many of the functional groups are responsible for the insertion of direct band gaps in the semiconducting materials. As far as the stability of these chemical functionalities in BN is concerned, the vibrational modules for frequency calculations can be used for prediction of the structural integrity and stability for versatile purposes.

9 BN as Catalyst Support for Reactive Investigations

Boron nitride, its analogous structures and regarding materials specifically the nanosheets are the perfunctory configurations modeled as the mitigation processes in reduction of environmental

Open Access Article. Published on 24 June 2026. Downloaded on 6/26/2026 4:24:14 PM.
This article is licensed under a Creative Commons Attribution 3.0 Unported Licence.
Materials Advances Accepted Manuscript

View Article Online
DOI: 10.1039/D5MA01210D

Open Access Article. Published on 24 June 2026. Downloaded on 6/26/2026 4:24:14 PM.
This article is licensed under a Creative Commons Attribution 3.0 Unported Licence.

pollutants and other toxic gases. However, boron nitride is not the first nanomaterial to employ as the catalytic support or a surface adsorbent to capture these toxic substances and the gases. Many other nanomaterials have the vast range of application in the use of the surface adhesion and adsorption influence such as metallic oxide including ZnO, TiO_2, WO_3 and In_2O_3 and of course the carbon materials. Somehow these materials could not meet the standard criteria because of inefficiency to give better results, low surface sensitivity, slow response time in mechanistic investigations, poor gas selectivity during surface interactions and slower recovery time in regeneration steps, these turned out to be an ineffective choice as a candidate for good gas sensors. Boron nitride prolonged use in the surface reactivity facilitates the adsorption procedures of various different compounds. The interaction of many of compounds with h-BN leads to notable structural changes at the atomic level. For instance, upon adsorption, there may be slight distortions in the bond angles and lengths within the h-BN lattice due to strain induced by gas molecules. These changes can alter the electronic properties of h-BN, affecting its band gap and conductivity. Boron nitride can increase the activation of C-H bonds in methane to facilitate its conversion into CO or CO_2. Likewise, it can improve the reduction pathways of sulphur oxides leading to elemental sulfur or sulfate formation. Also, BN provides excellent catalytic pathways enable conversion of nitrogen oxides into N_2. Similarly, BN benefits electrochemical reduction processes to yield CO or hydrocarbons.

To give an edge in the environmental analysis, Boron nitride has been proved to be selective, efficient and effective choice for interactions with pollutants both in the experimental and theoretical settings. Therefore, early investigation based on boron nitride nanotubes unsuccessfully demonstrated the gas sensitivity activity, all attributing to the very small extension of the surface in space which reduced the efficiency to detect small gas molecules. This fault stipulates the modern investigation on extension of this concept and employment of two dimensional nanosheets as the surface support in experimental investigation which proved to be successful because of the large surface area covers the possibility of gas molecules to capture any sort of point where gas is tend to be adhering to the surface.

In addition, boron nitrogen nanosheets demonstrated the excellent surface functionalities where most of the nanomaterials fail to adapt in the setting to capture bit of molecules. Although optical and electrochemical sensors are available but BN has a satisfactory edge on them because of the semiconducting nature therefore termed under next generation semiconductor-based sensors.

Materials Advances Accepted Manuscript

View Article Online
DOI: 10.1039/D5MA01210D

Open Access Article. Published on 24 June 2026. Downloaded on 6/26/2026 4:24:14 PM.
This article is licensed under a Creative Commons Attribution 3.0 Unported Licence.

Highlighted properties of boron nitrogen-based gas sensors include long term surface stability, high surface to volume ratio, better gas selectivity and sensitivity, auto heating capacity, and can operate in harsh environmental conditions as well. Moreover, these sensors provide the cost-effective operational procedures in the manufacture and other treatments. The estimated interaction of gases with h-BN surfaces is primarily governed by adsorption energy and the adsorption sites available on the material. Computational studies using Density Functional Theory (DFT) have shown that the adsorption energies for various gases can vary significantly based on the functional used and the specific site of adsorption. For instance, studies indicate that the adsorption energy for carbon containing gases on pristine h-BN is relatively low, suggesting weak physisorption, while modifications such as doping with metals can enhance these interactions dramatically.

This section discusses the reaction potential of h-BN and its derivatives, focusing on the adsorption characteristics and reduction mechanisms of various substances.

Investigation on methane in regard to the theoretical DFT approach predicted the efficiency of the boron nitride and its aligned configurations in term of ease of the adsorption potential which translates as better sensitivity. The underlying mechanism is the donation of few of the electrons from the gas to the substrate structure (BNNS) which is presumably responsible for the alteration in the electrical attributes of the nanosheets, brought out the tuning of band gaps to fit the semiconductor properties.

Although BNNT can be a good sensor however the underlying issues was the invalidity of a reasonable chemical or physical absorption mechanisms invalidates the use as sensor. Therefore, the investigation shifted towards the use of boron nitride nanosheets with applications of GGA approximations.

Boron Nitride Nanosheets' properties are rare and can be utilized to increase the reaction rate. h-BN was used by Wenliang Sen *et al* in experimental study, it was found that h-BN increased the reaction rate by 20% and Pd doping increases the catalytic activity of BNNS.[283] The metal-free catalysis and stability of BN structures are proposed in different chemical reactions to increase their yield. Another experimental and theoretical study was performed to increase the yield of propene production when catalyzed with h-BN and BNNTs. Oxidative dehydrogenation of propane by using a BN catalyst causes the propane conversion to about 14% and selectivity to 91% which is much less by using any other catalyst. The rate of conversion is higher with BNNTs due

Materials Advances Accepted Manuscript

View Article Online
DOI: 10.1039/D5MA01210D

Open Access Article. Published on 24 June 2026. Downloaded on 6/26/2026 4:24:14 PM.
This article is licensed under a Creative Commons Attribution 3.0 Unported Licence.

to their large surface area. The catalytic activity explores that oxygen functionalizes on BN structure's surfaces and this functionalization is high in the presence of hydrocarbons. The oxygen breaks the BN bond and bonds like >-O-O-N<. This works as an active site and causes the removal of the H atom from the secondary carbon of propane. This removal also breaks the O – O bond and forms B – OH and nitroxyl radicals. This radical reacts with propyl radical to form a surface-stabilized reaction as represented in Figure 10 (a). Due to its stabilization high olefin selectivity was also observed. Desorption of propene causes the production of a water molecule which when desorbed, its active site again formed.[284]

Another study for oxidative hydrogenation from CO_2 was performed by using porous BN (PBN) as a catalyst is visually represented in Figure 10 (d). The experimental study explores how that increase in synthetic temperature affects the surface area and pore size of PBN inversely. Pore size and total pore volume at a temperature of 900°C are 747 $m^2\ g^{-1}$ and 1.06 cm^3/g^{-1}, at 1000°C 657 $m^2\ g^{-1}$ and 1.07 $cm^3 g^{-1}$ and at 1100°C 657 $m^2\ g^{-1}$ and 0.98 cm^3/g^{-1} respectively. XRD shows that temperature increase also affects the d-spacing plane inversely. The study explores that when CO_2 is used for oxidative dehydrogenation the increase in temperature changes the degree of the active site edge – BOx resulting in a decreased conversion rate. The temperatures 900°C, 1000°C and 1100°C were used for the reaction giving the rate of conversion 15.7 %, 10.9%, and 5.5% respectively. Order of activity was 21% > 16% > 9% for temperatures 900°C, 1000°C and 1100°C.[285]

h-BN provides an enhancement to the selectivity and stability of the catalyst when supported on the surface of it. An experimental study was performed for propane dehydrogenation (PDH) as shown in Figure 10 (c). The study explores that Pt/BN is more stable and appropriate as compared to Pt/Al_2O_3. Propane conversion decreases slowly on Pt/BN as compared to Pt/Al_2O_3. Coke accumulation shows the deactivation of the catalyst which is a quarterly low for Pt/BN (0.45%) as compared to (1.73%) Pt/Al_2O_3. The acidity of support also makes the coke hydrogen deficient as Pt/Al_2O_3 has a H/C ratio of 1.04 while for Pt/BN it was 1.33. This is due to acidity suppressing the active site, and lead it to coke formation. Pt/BN also have efficiency in selectivity as it shows 98% selectivity initially also increases to more than 99% when the reaction proceeds. While Pt/Al_2O_3 shows a selectivity of 90% initially and increases slowly when the reaction proceeds. This high activity of the catalyst is due to proper calcination and reduction at specified temperatures. Further

Materials Advances Accepted Manuscript

View Article Online
DOI: 10.1039/D5MA01210D

increases in temperature cause a decline in catalytic activity and low propane conversion. Catalyst performs with excellence when calcinated at 600°C and reduced at 550.[286]

Another experimental study investigated that h-BN has catalytic properties with acid as well as base functionalities. The study explores that ball-milled h-BN has a high surface area due to distorted structures. Milling converts the BN bond to amino and hydroxyl groups which then can be reacted as acidic and basic sites. This structure also has weak acid sites but moderate basic sites when compared with hy zeolite and ky zeolite respectively. Its high sensitivity towards b nitro alkene while not any activity shown by nontreated h-BN. In nitroaldol reaction, its 77% high activity shows the formation of reaction sites which improve its catalytical activities.[287]

Nitrogen fixation is an important step for the synthesis of Ammonia but also a bit difficult step. So, a computational study was performed to introduce a novel metal-free catalyst for the conversion of N_2 to NH_3. This method is also cheap and effective for NH_3 production. The adsorption and desorption of N_2 on the surface of a pristine zigzag edge and different metals were calculated. The adsorption energy of N_2 and NH_3 on pristine is – 3.02 eV and – 1.45 eV. This shows the strong interaction of N_2 which causes the problem in reaction.

For boron-doped BN the adsorption energy becomes -1.25 eV for end-on configuration and it also becomes decrease to -0.68 eV for side-on configuration. Side-on configuration also proved unsuitable for adsorption due to less value of Bader charge analysis. Its catalytic activity shows that the reduction of N_2 happens by two different methods. In one method, the proton-electron pair bonded with both at one time making one nitrogen atom free and reducing it, then the second bonded atom reduces and causes the formation of NH_3. While in others, N-atoms reduce alternatively. Also, the desorption of NH_3 from B-doped zigzag BN calculated from Gibbs free energy is 0.35 eV which is very low to reported values. These all properties make it a novel catalyst for N_2 fixation to NH_3.[288]

Open Access Article. Published on 24 June 2026. Downloaded on 6/26/2026 4:24:14 PM.
This article is licensed under a Creative Commons Attribution 3.0 Unported Licence.

Materials Advances Accepted Manuscript

View Article Online
DOI: 10.1039/D5MA01210D

Open Access Article. Published on 24 June 2026. Downloaded on 6/26/2026 4:24:14 PM.
This article is licensed under a Creative Commons Attribution 3.0 Unported Licence.

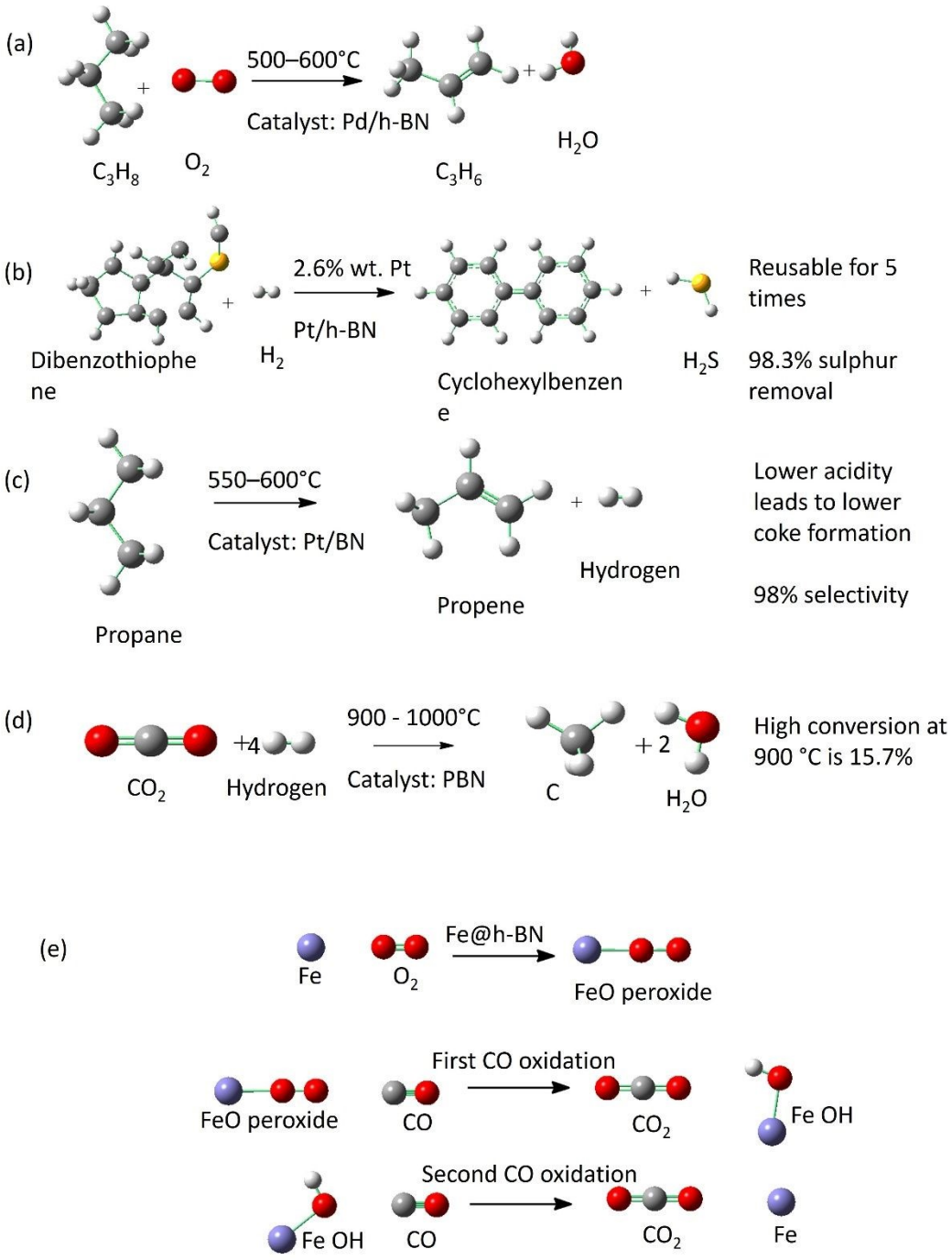

Figure 10: Reaction summary of BN sheet as catalyst support

However, another study for N_2 reduction was performed by using a catalyst of Transition Metal doped BNNT. This theoretical study explores that from other transition metals Fe, Mn and Pd doped structures have good catalytic properties for N_2 reduction. When TMs are doped to BNNT, their negative binding energy shows their stability. But electrochemical stability of all TMs is also

Materials Advances Accepted Manuscript

View Article Online
DOI: 10.1039/D5MA01210D

Open Access Article. Published on 24 June 2026. Downloaded on 6/26/2026 4:24:14 PM.
This article is licensed under a Creative Commons Attribution 3.0 Unported Licence.

less than zero making them less stable instead of Fe, Mn and Pd. It is observed that all other TMs have adsorbed less N_2 as compared to selected TMs, and also have negative Gibbs Free energy. The selected metal has less but positive Gibbs-free energy. The addition of TMs makes BNNT more conductive due to band gap reduction. N_2 adsorb on end-on mode and the one reaction mechanism shows that the reaction with Fe is exothermic and for the other it was endothermic. The mechanism explains that N_2 is adsorbed on the catalyst surface. Hydrogenation happened and Pd-doped BNNT showed good electrocatalytic activity. Their catalytic properties even further improved the dual atom catalyst formed.[289]

At the industrial level, the reduction of N_2 takes a lot of energy and causes the formation of side products. So, to increase the efficiency of the reaction h-BNNS and h-BN were used as catalysts by Ya Zhang et al. in an experimental and theoretical study. Experimentally the study was carried out by using these catalysts deposited on a carbon paper (CP) surface. The reaction proceeds by using two control experiments, immersing the sample in N_2 saturated solution with no voltage and Ar saturated solution with a voltage of -0.75 V for 2h. UV detection explores the NH_3 formation but NMR detection reveals that NH^{4+} forms.

When the reaction proceeds on carbon paper no reaction happens. But using h-BN/CP NH3 yield became 5.7 $\mu g \cdot h^{-1} \cdot mg^{-1}_{cat}$ and this also increased by using h-BNNS/CP 22.4 $\mu g \cdot h^{-1} \cdot mg^{-1}_{cat}$. The high charge transfer rate in h-BNNS and CP makes it more active for high-yield production. Stability in morphology and yield production after 6 recycles makes it more active in applications of electrosynthesis. The theoretical study explores that when N_2 moves towards h-BNNS, it approaches edge boron atoms. The boron atom becomes electron deficient due to the accumulation of electrons towards N_2. Therefore, when the electron from the nitrogen π-orbital accepted by the boron valance shell, it forms chemical adsorption with an inert molecule. The reduction potential was also calculated theoretically at -0.60 eV similar to the experimental value.[290]

Removal of Sulphur by aerobic oxidation can't be an easy process without a catalyst. However, a study investigated its 100% removal by the addition of catalyst C incorporated into BN (BCN). This study was performed by using Dibenzothiophenol (DBT) from which Sulphur was to be removed reaction available in Figure 10 (b). When DBT reacted with BCN Sulphur removal was 15% with N_2 oxidant but 100% with air as oxidant. This removal is also affected by the change in temperature as at 150°C the removal is 100% but when the temperature lowers its removal also lowers with an increase in the time of reaction completion. When the same reaction was performed

Materials Advances Accepted Manuscript

View Article Online
DOI: 10.1039/D5MA01210D

Open Access Article. Published on 24 June 2026. Downloaded on 6/26/2026 4:24:14 PM.
This article is licensed under a Creative Commons Attribution 3.0 Unported Licence.

to other Sulphur-containing compounds it removed Sulphur efficiently. After desorption, the catalyst was also regenerated.[291]

Another experimental study was performed to observe Sulphur removal. Pt Nanoparticles dispersed on the h-BN metallic surface to increase its catalytic activity. The study explores that 98.3% of Sulphur can be removed from DBT. It shows less production of aromatic hydrocarbons. This dispersion on the surface makes catalytic stability and work without any reduction in activity 5 times. A significant charge transfer between Pt and h-BN makes it a strong catalyst but shows no charge transfer when Pt is supported to SiO_2 or C. Sulphur removal with Pt/SiO_2 was 81.6% and with Pt/C it reduced by 80.3%. Catalytic performance is affected by concentration increases. When the concentration reaches weight % 2.6 catalytic activities becomes a maximum, and further increase in concentration makes decreases the performance. The mechanistic reaction shows that when electron transfer happens from Pt to h-BN. The Pt surface has electron deficiency. This is fulfilled by the adsorption of Sulphur compounds that have unpaired electrons.[292]

Another experimental and theoretical study was performed having the use of BCN as a catalyst for the condensation of benzaldehyde. BCN has a higher specific surface area than h-BN and graphene also shows a high conversion rate of 81.9% in 15 minutes. Also, have high stability even after 5 cycles of reaction. Its basicity was evaluated by desorption of CO_2. For graphene, it desorbed at 89 °C and for h-BN and BCN it desorbed by an increase in temperature of 43 ^oC more than it. This explores that BCN and h-BN have strong basicity. This basicity also improves the catalytic properties.

To observe the mechanism DFT study was performed. According to this, the active site is formed for the reaction at which oxygen attaches to the carbon edge of BCN. The first step is the adsorption of O at B^V-BCN via adsorption energy of -0.59eV and at N^V-BCN via energy of +0.95eV. Strong bonding of O_2 causes the breakage of the O – O bond and forms an active site for reaction. Then the malononitrile molecule adsorbs to the O active site and forms an intermediate while reacting with benzaldehyde. The formation of benzylidene malononitrile causes the release of water. The study reveals the catalyst BCN for Knoevenagel condensation reaction that is efficient as compared to graphene and h-BN.[107]

The catalyst used is Ni supported over h-BN and B defect h-BN (B-D-h-BN). Introducing B defect in h-BN makes a strong interaction between Ni and support due to high charge transfer. This charge transfer for Ni-h-BN is 0.18 – 0.24 electrons while for B-D-h-BN is 0.44 – 1.62 electrons. The

Materials Advances Accepted Manuscript

View Article Online
DOI: 10.1039/D5MA01210D

Open Access Article. Published on 24 June 2026. Downloaded on 6/26/2026 4:24:14 PM.
This article is licensed under a Creative Commons Attribution 3.0 Unported Licence.

adsorption energy for Ni over h-BN is –4.28 eV while for B-D-h-BN it becomes –8.70 eV. It increases the stability of the catalyst. The high magnetic moment of Ni over h-BN as compared to B-D-h-BN shows strong metallic interaction of Ni_2.

The mechanism involves the first activation of CH_4 and CO_2 at a temperature of 973.15K. The energy barrier for dissociation of CH_4 over Ni\h-BN and Ni\B-D-h-BN is 0.11 eV and 0.36 eV. So due to less energy barrier CH_3* and H* are more stable with Ni/h-BN. While the dissociation energy is also low in Ni\h-BN is 0.39 eV and for Ni/B-D-h-BN is 0.50 eV. The CO_2 activation is followed by two methods. The first method of direct decomposition has an energy barrier of 1.68 eV and 1.31 eV for Ni/B-D-h-BN and Ni\h-BN respectively. While the second method is activation with hydrogen and forms a COOH intermediate. The main reaction is the reaction of CH_3 and O* forming CH_3O. The increased amount of Ni and B-D-h-B as support improves the carbon deposition by increasing the active sites. Introducing defects in h-BN increases its selectivity and sensitivity.[293]

Another study was proposed experimentally for the observation of BN activity as a catalyst in the dry reforming of methane. The Rh-doped BN was used as a catalyst in the study, formed by wet chemical method. The catalytic activity increased with the increase in temperature. Initially, the conversion rate at 600^{o}C is 59.9% while at 750^{o}C it increases to 100%. However, the reaction for a long time decreases the conversion rate due to the formation of boron species (BOx), which can be overcome with high temperatures. Ar and water are also used to overcome the problem of overlayer but the use of Ar affects the regeneration of the catalyst. O* from H_2O helps in the decomposition of CH_4 into CH_3* and H*. The adsorption capacity of CO on Rh-BN and CO_2-treated Rh-BN is 2.69×10^{-2} and 1.45×10^{-2}. As the simple method conversion rate of CH_4 is 1 molCO_2 molCH_4^{-1} while using CO_2 it increases to 2.1 molCO_2 molCH_4^{-1}. The study explores the efficient reactivity of catalyst Rh/BN via using CO_2 partial pressure.[294]

BN is mostly used as a single-atom catalyst in reactions. When oxidation of CO is carried out by Fe-doped h-BN, Fe increases the active site for capturing O_2 and prefers to adsorb on N-vacancy as visually represented in Figure 10 (e). Fe adsorption causes the formation of four forms out of which sextet is used for further study. The HOMO/LUMO energy difference decreases from 6.58 eV for h-BN to 3.88 eV for N-vacancy and 3.59 eV for B-vacancy. h-BN have low binding energy with CO and O_2 at 0.02 eV and 0.10 eV respectively. In the case of B-vacancy, it becomes 0.72 eV and 1.03 eV while for N-vacancy it increases to 1.71 eV and 2.69 eV. Firstly, O_2 binds with Fe

Materials Advances Accepted Manuscript

View Article Online
DOI: 10.1039/D5MA01210D

Open Access Article. Published on 24 June 2026. Downloaded on 6/26/2026 4:24:14 PM.
This article is licensed under a Creative Commons Attribution 3.0 Unported Licence.

molecules in the form of peroxides. Then CO molecule comes and attaches with 1 peroxide and causes the formation of a CO_2 molecule. The remaining peroxide again attaches the CO molecule and forms CO_2. CO_2 has less binding energy with the dopant making the regeneration of the catalyst easy. The energy barrier for oxidation of CO with N-vacancy is 1.18eV and with B-vacancy is 1.88eV. So, less energy barrier for N-vacancy makes it a suitable catalyst for the oxidation of CO.[295]

However, theoretical study performed for the oxidation of CO uses Ag as a dopant over B-vacancy. The study explores that the binding and adsorption energy for Ag dopant and B-vacancy is suitable as compared to N-vacancy. The high charge transfers due to the positively charged Ag atom (0.52eV) and negatively charged O_2 atom (0.30eV) make the adsorption stable with E_{ads} of 0.86eV. While the E_{ads} for CO is 1.04 eV. Two ways are there for the oxidation of CO. Both are studied computationally in this study. In the first Eley–Rideal (ER) mechanism, the O_2 molecule adsorbed over the Ag. CO directly bonded with this O bond causes the formation of CO_3 with an energy barrier of 1.80 eV. Then CO_2 was produced with a reaction energy of 2.20eV.[296]

The second Langmuir–Hinshelwood (LH) mechanism involves the reaction mechanism started by the co-adsorption of CO + O_2 due to low co-adsorption energy as compared to individually adsorbed. Then a reaction happens and CO_2 is produced with the energy of 1.89eV. The CO_2 molecule has adsorption energy of 0.26eV and it can easily desorb. The catalyst also regenerated when 2nd CO_2 formed with energy of 0.17eV and this energy was easily gained as the reaction is exothermic. Another reaction mechanism studied is termolecular Eley−Rideal mechanism (TER). In this mechanism the O_2 bonds with Ag by making an Ag–O bond. The CO adsorbed and desorbed 2 CO_2 molecules at a time with a reaction barrier of 0.33eV and it could be overcome as the reaction was exothermic (4.63eV). The calculated activation barrier of 0.33 eV for the TER mechanism over Ag-doped h-BN is accessible by providing heat at moderate temperatures, since the thermal energy k_BT at 100 degrees C (approximately 0.032 eV) provides sufficient activation for crossing of the barrier at reaction rates that are experimentally relevant via an Arrhenius-type kinetic process. This barrier compares favourably with values of 0.4-0.6 eV for CO oxidation over Au/TiO_2 and 0.6-0.9 eV over Pt/Al_2O_3. That means Ag-doped h-BN could achieve competitive catalytic activity at significantly lower operating temperatures. This is a practically important advantage for room-temperature air purification and automotive emission control applications where catalyst bed temperature is constrained. Further the strongly exothermic total reaction

Materials Advances Accepted Manuscript

View Article Online
DOI: 10.1039/D5MA01210D

Open Access Article. Published on 24 June 2026. Downloaded on 6/26/2026 4:24:14 PM.
This article is licensed under a Creative Commons Attribution 3.0 Unported Licence.

energy of 4.63 eV per catalytic cycle confirms that the overall process is thermodynamically irreversible under practical conditions and that ensures the high selectivity for CO_2 over undesired partial oxidation products. Ag is also suitable for the oxidation of CO due to its low reaction energy barrier as compared to all other noble metals previously studied as single-atom catalysts.[296]

O – O bond activation over a single atom catalyst enhances the CO oxidation. A computational study was performed to understand the O – O bond activation. The study explores that metals (Co, Ni, and Cu) have weak interactions with pristine h-BNNS while creating vacancy increases the stability. Adsorption of metal on B-vacancy is stable due to high adsorption energy as compared to adsorption on N-vacancy. For Co, it is -9.92 eV at B-vacancy and -7.25 eV at N-vacancy which is higher than other metals respectively showing Co is highly stable at BN vacancy. The charge transfer for Co, Ni and Cu is 1.042e, 1.063e, and 0.933e at B-vacancy and 0.084e, 0.321e, and 0.062e at N-vacancy respectively. The interaction of these metals to B-vacancy shows the increase in fermi-level.

With Co, O_2 only attach in parallel to the BN sheet. But other metals can attach to both parallel and perpendicular. The adsorption energy for O_2 on Co is -1.31 eV, while for Ni and Cu the adsorption energy of O_2 is -1.1 eV and -0.41 eV. The metal adsorption especially Cu on N-vacancy is weaker as compared to B-vacancy. This weak interaction at N-vacancy extends the O – O bonds more than the adsorption on B- vacancy. Due to this less charge transfer from metal to sheet happened in N-vacancy, and more charge available at metal more activates the O – O bond.

For CO oxidation, CO prefers to attach on a perpendicular site and the adsorption energy is -1.46eV. This binds with O_2 and CO_2 formation happen, its desorption is also a fast step. So, Cu@ N-vacancy of BN highly activates O – O for CO oxidation.[297]

Single-atom catalysts can used to study hydrogen evolution reactions (HER). A DFT study was performed by using a def2-TZVPP basis set for HER with metal-adsorbed defected Graphene and h-BN. About 9 transition metals (Fe, Ru, Os, Co, Rh, Ir, Ni, Pd, Pt) are taken from 3d to 5d for the study. The binding energy increases due to an increase in charge transfer from 3d to 5d metals. The adsorption energy of Fe is high and lower downward to Pt for graphene and C-defected graphene is low for Fe but higher downward to Pt. This also happens in the case of h-BN and B-defected h-BN where adsorption energy is high for Fe and lowers downward to Pt. But for N-defected h-BN, the adsorption energy becomes low for Fe and high moving downward to Pt.

Materials Advances Accepted Manuscript

View Article Online
DOI: 10.1039/D5MA01210D

Open Access Article. Published on 24 June 2026. Downloaded on 6/26/2026 4:24:14 PM.
This article is licensed under a Creative Commons Attribution 3.0 Unported Licence.

Fe is considered the most stable catalyst due to its high adsorption energy. The H-adsorption at C-vacancy and B-vacancy is weak. But at N-vacancy, adsorption energy is good and is more reactive due to low binding energy as compared to other vacancies that have high binding energy. The co-adsorption of two H on the metal surface is only possible in Os attached to N-vacancy. On the other, both H atoms attach to B next to metal making their recombination more difficult. Metal atoms have larger band gaps and can't bond with the H atoms strongly. The band gap of Fe to Pt at N-vacancy ranges from 2.1 eV to 3.3 eV and can bind one H atom strongly but the 2nd can't adsorb strongly due to an increase in their bandgap. In the case of Rh and Ir dopants have large bandgaps so they can't adsorb the first H atom easily but this adsorption causes a decrease in the bandgap making the 2nd adsorption stronger. For recombination of H_2, Os at N-vacancy has an energy barrier of 0.11 eV, for Ni at N-vacancy energy barrier is 0.16 eV and for Ru at N-vacancy it is 0.43 eV. For all other atoms, this energy is much higher to overcome. So, h-BN with adsorbed Os, Ni and Ru at N-vacancy makes the HER reaction fast and the catalyst is also cost-effective, as compared to all other metals and vacancies created at h-BN and Graphene.[298]

Haber's process for the reduction of N_2 causes economic loss. To replace this electrocatalytic reduction is a suitable process to produce it. A DFT study was performed to observe the suitability of a defected BN catalyst for the reduction of N_2. In this study 18 Transition metals are selected to observe their potential over h-BN. TM adsorption over defective BN has negative values making the catalyst stable. Ta, Nb and V have relatively high charge transfer and adsorption energies as compared to all other metals. Side-on configurations have longer bonds as compared to end-on configurations due to high charge transfer causing repulsion in N – N bonds. Tc and V have an energy barrier of 0.59 and o.41 eV respectively which is much less as compared to other metals and pristine h-BN. So, V and Tc are selected for further reaction.

The first protonation of N_2 happens at 0.31 eV and 0.56 eV to make N_2H respectively for Tc and V. Then 2nd protonation happens to make HN – NH at 0.15 eV and 0.01 eV. One NH_3 is released when the fifth H attacks at 2HN – NH_2. This release is an exothermic process with a release of 0.5 eV and 0.63 eV of energy respectively. Then last proton attacks on remaining *NH_2 and is the rate-limiting step. This protonation and NH_3 release are endothermic with an energy of 0.41 eV. Adsorption of H on active sites blocks them. Due to this ability, the HER energy barrier was also studied for these two metals.

Materials Advances Accepted Manuscript

View Article Online
DOI: 10.1039/D5MA01210D

Open Access Article. Published on 24 June 2026. Downloaded on 6/26/2026 4:24:14 PM.
This article is licensed under a Creative Commons Attribution 3.0 Unported Licence.

For Tc, the energy barrier was 0.54 eV and for V, it was 0.49 eV, which is high as compared to the N_2 reduction reaction. Tc has good selectivity for HER due to less energy barrier as compared to the N_2 reaction. But V has good sensitivity for N_2 reduction reaction with less energy barrier. V adsorption makes the BN sheet a good conductor for NRR due to high charge transfer. For N_2 adsorbed on V-BN surface the charge transfer is 0.41e but the charge transfer from V is 1.75e so this shows that the charge also comes from the BN sheet. The study provides a single-atom catalyst with good conducting properties for N_2 reduction reaction.[299]

A potential novel catalyst for Oxygen Reduction Reaction (ORR) designed by a computational study using Single Atom Catalyst. The Co adsorbed at B defected BN with adsorption energy of -10.19 eV and 0.31e charge transfer. Co at B-defect of BN enhances the electronic properties by reducing the bandgap to 2.00 eV. This structure has stability at 1000K and has an energy barrier of 5.87eV for the reaction of Co transfer from defected BN to B3N3. The O_2 molecule adsorbs over Co/BN with adsorption energy of -0.9 eV and charge transfer of 0.2e. While the adsorption energy for a few intermediates of Oxygen OOH, O, OH, and HOOH adsorb with the energy of –2.00, –4.52, –3.13, and –5.14 eV respectively. The reaction process is after the adsorption of O_2 over the catalyst surface.

The reaction explores that addition of one hydrogen to form OOH takes less energy barrier (0.30) and is exothermic (-0.49) while the formation of 2O molecules needs more energy barrier (1.39) and the reaction is endothermic (+0.41). Then in the next step formation of O and OH has a high energy barrier (0.54) with energy release (-0.18). While addition of one electron with hydrogen has an energy barrier (0.08) and energy release (-1.83) which is favorable. This addition causes the formation of H_2O and O, which next addition of one electron with hydrogen forms OH with an energy barrier (0.14) and release of energy (-1.24) which further addition of one hydrogen and electron forms H_2O. Ultimately, the reaction proceeds at Co-doped graphene and Pt catalyst, the energy barrier for rate-determining step 0.38eV and 0.79eV respectively is high as compared to the energy barrier for Co/BN 0.30eV. The Co/BN has low overpotential making it a stable catalyst as compared to Bn Co/Graphene and Pt catalysts. This study shows that Co incorportated BN is a stable and promising electro-catalyst for ORR reaction.[300] Thus BN can be used as a support in many of the reactive investigations.

Materials Advances Accepted Manuscript

View Article Online
DOI: 10.1039/D5MA01210D

Open Access Article. Published on 24 June 2026. Downloaded on 6/26/2026 4:24:14 PM.
This article is licensed under a Creative Commons Attribution 3.0 Unported Licence.

10 BN as Drug Delivery System

Nanomaterials involving the low dimensional structures are the drug carrier support surfaces for the successful administration of the chemotherapeutic agents. Earlier investigation on the Graphene oxide nanostructure demonstrated that these are well known for their role in the delivery of drugs in vivo. However, boron nitrides are rather economical options as the surface has a considerable distribution of the boron and nitrogen which makes it effective sites for the interaction of the drug molecules and enhanced the capability of anchoring drugs. Recent investigation favored the administration of hexagonal boron nitrogen in biomedical fields as nanotransducer and carrier materials.[301]

Controlled and safe drug delivery system comprises boron nitride systems specifically in the management of cancer related medicines. The physicochemical attributes in the surface of the two-dimensional hexagonal boron nitride nanosheets can be easily conceptualized while formation of a BN based drug delivery system. Furthermore, BN functionalization routes have a potential to enhance the drug efficacy triggering the safe delivery hence finally applicable in the biological environments for the therapeutic applications. Biocompatible nature of BN provides the usefulness of those BNNSs in tissue culture engineering, biomolecule sensors and nanocarrier for significant drugs.

Biocompatibility determines the modulation of drug delivery as a safe practice and it is dependent on the several factors such as size, shape, nature, arrangement of structure and surface reactivity status of BN.[302] Although the in vitro investigations of micro size BNNS has been found to be highly compatible for the screening of the osteoblast and related cellular structures. In contrast the BN nanosheets with a size any less that one micrometer alongside the 100 nanometer depth criteria unfortunately failed to address the biocompatibility.[301] The particular reason behind it resides in the generation of the boron radicals on the surface especially the edges of nanosheets, and ultimately leading cause of cellular destruction.

Materials Advances Accepted Manuscript

View Article Online
DOI: 10.1039/D5MA01210D

Open Access Article. Published on 24 June 2026. Downloaded on 6/26/2026 4:24:14 PM.
This article is licensed under a Creative Commons Attribution 3.0 Unported Licence.

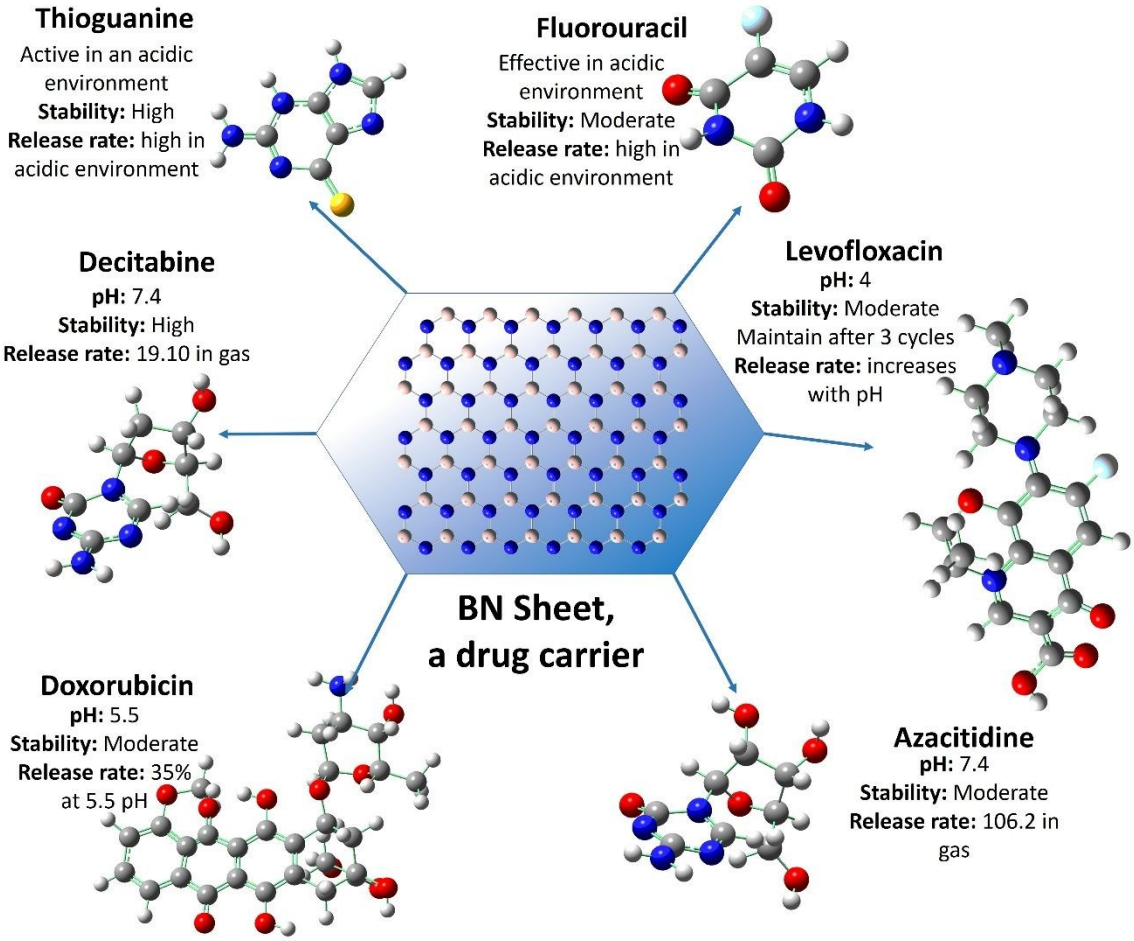

Figure 11: Stability, Release rate and pH of different drugs on BN sheet

As far as the in vivo bioavailability and biocompatibility investigations on boron nitride nanosheets are concerned, research is limited. However, an initiative approach on investigating the pharmacokinetics of this nanomaterial proved the distribution mechanism of BNNS in vivo. This unfolded in vivo analysis on the possibility that BNNSs prefer not to be cytotoxic although the assimilation of BN and its protection with a coating layer can significantly reduce the cytotoxicity. Still critical investigation is much needed in the in vivo screening to guide the biocompatibility of this material in the transport of the useful drugs and other molecules for the curing potential against diseases, preventing the acute impacts and chronic as well.

Attribution to the excellent mechanical properties and piezoelectric characteristics, BNNTs as per the ab initio approach produce the larger response in terms of surface sensitivity and its almost comparative to semiconductors preferably in wurtzite classifications.[303]

Materials Advances Accepted Manuscript

View Article Online
DOI: 10.1039/D5MA01210D

Open Access Article. Published on 24 June 2026. Downloaded on 6/26/2026 4:24:14 PM.
This article is licensed under a Creative Commons Attribution 3.0 Unported Licence.

Advanced attributes in the precious nanostructure of boron nitride contributes to the stronger interaction with the drugs. In particular a DFT investigation on the anchoring of 5-fluorouracil which is basically a drug modeled for the anticancer effects in human body catered to adsorption on the fullerenes tested out be of bad performance in terms of the lowest possible adsorption energy calculated as -3.2 kcal/mol. Structure of Fluorouracil is presented in figure 11. This demonstrated the least effective interaction and unsuitability of fullerene as a nanocarrier for drugs. In contrast, the replacement of one of the carbon atom with boron increased the adsorption energy -24 kcal/mol in the original value.[304] Hence it was formulated that the presence of the boron dopant in the structural configuration uplifted the electronic properties which resulted in the enhanced adsorption potential of the nanomaterial.

The doped analogue of boron carbon nitride nanotubes were successfully employed in the administration of particular drug substance namely CT via investigative density functional theory simulations. The presence of active amino group on the CT tends to do the attachment onto the nanotube carrying the dopants like silicon and aluminium. Hence, the adsorption energy data comprehended the effectiveness of silicon based BCN structures concerning the shorter recovery times and highly sensitive interactions.[305] Hence, boron nitrogen nanostructures are highly capable of producing good results in the synthesis and delivery of the regular and new drug testing.

Another investigation on the cathinone drug uses the various nanostructure of the boron nitrogen nanomaterial. Among that structure the superior were nanosheet, nanotube and nanocage.[306] Based on the interaction efficacy the drug tends to adhere to the boron atom of the nanostructure while modeling of DFT calculations. The data of the Adsorption interaction in terms of energy was calculated to be for drug as 16.1, 14.0 and −5.0 kcal/mol, for respective configuration of cage, tube, and sheet, respectively. Cage was more sensitive and can transform into the electrical sensors due to presence of the conductivity index. $B_{12}N_{12}$ cage configuration complied with the shortest recovery time and zero to none structural altercations while drug modeling.[306]

A theoretical and experimental study was performed to discover drug carriers for the treatment of cancer. A chemical vapour deposition process was used to obtain Boron nitride nanoparticles. The loading of drugs was studied by using Doxorubicin (DOX) gives 98% saturation at a pH of 8.4. Structure of DOX presented in figure 11. DOX is hydrophilic at low pH by forming NH^{3+} ions while at high pH NH_2 ions form and the interaction of DOX is good with BNNP due to less solubility with water. It is revealed theoretically that the presence of O in BNNP due to its

Materials Advances Accepted Manuscript

View Article Online
DOI: 10.1039/D5MA01210D

formation from B_2O_3, a high concentration of O makes good bonding of DOX to the surface of BNNP. Neutral DOX have high binding energy as compared to protonated DOX, as protonated DOX less stabilize the system by having a negative charge density. It gives beneficial results for drug carriers due to its strong adsorption with drugs and anti-cancer and anti-infectious properties.[307]

Another experimental study for BNNP as a carrier of Doxorubicin (DOX) validates that Liquid exfoliation uses bulk h-BN for the production of BNNP. For the study inquiry, cancerous cells were grown and observed that BNNP penetrates cell membranes very fast. 2D-BNNP increases the intensity of the Raman band spectrum about 2-5 times by reflection while passing through organelles. This also helps to identify the location of BNNP in cells. Due to the drug release in the acidic environment, the DOX can't affect the normal cell when incorporated in the cell with the BN carrier and only affects the cancer cell which generally has an acidic environment.[308, 309]

The experimental and theoretical study was performed to observe the drug delivery system of porous BN. Novel Hydroxylated and porous BN was prepared for delivery of the Doxorubicin drug. The prepared P-BN at 800°C for 1h gives a high loading capacity for DOX. The loading capacity also increases as the DOX concentration increases by the mass ratio of 5:1 of DOX: P-BN. The release of the drug from the carrier was at different pH using a buffer solution. This shows that the DOX/PBN releases 53% at pH 5.5 while the release rate decreases from acidic to neutral pH in the buffer. At 6.2 pH, the release rate for the drug becomes 43% which further decreases to 21% at 7.4 pH in 1h. While the release rate at 7.4 pH for 24h becomes 36%. The in-vitro observation of the effect of the carrier to cell performed, which explores that 92% of cells can survive shows low toxicity of BN to cells. A high concentration of loaded DOX 67 – 79% can easily reduce the cell viability of cancerous cells to 18 – 21% as compared to only DOX. Also, the BN-covered DOX can enter through the process of endocytosis and release due to an acidic environment in the cell at low or 5.5 pH. This novel BN carrier due to its high loaded and release rates shows potent applications in the medical field.[310]

To observe the interaction between anti-cancerous drugs and h-BN nanosheets, a computational study was performed. The study reveals that the binding energy of h-BN with 5-fluorouracil (FU), 6-mercaptopurine (MP) and 6-thioguanine (TG) is – 19.92 eV, – 20.66 eV and – 22.07 eV respectively. The strucutre of thioguanine is presented in figure 11. The Gibbs free energy or adsorption is also high for TG (- 8.67) as compared to MP (- 7.30) and FU (- 6.63). The binding

Open Access Article. Published on 24 June 2026. Downloaded on 6/26/2026 4:24:14 PM.
This article is licensed under a Creative Commons Attribution 3.0 Unported Licence.
Materials Advances Accepted Manuscript

View Article Online
DOI: 10.1039/D5MA01210D

Open Access Article. Published on 24 June 2026. Downloaded on 6/26/2026 4:24:14 PM.
This article is licensed under a Creative Commons Attribution 3.0 Unported Licence.

energy gap is also less for TG as compared to other studied drugs. The chemical reactivity and hardness of BN with drugs are high for TG and then reduced for MP and FU, this shows the stability of the structure. Due to the acidic environment formed by cancerous cells, drug release is observed in acidic situations. It is calculated that the release rate is also high in an acidic environment as compared to a neutral one as the interaction of the drug with the BN sheet becomes weak. The study provides the drug carrier that provides exothermic adsorption and a high release rate of anti-cancerous drugs.[309]

For the delivery of the chemotherapy drug DOX, the BNNP is also used as an effective carrier. The BNNPs were made experimentally which reveals that loading of DOX to BNNP decreases with an increase in pH, and efficient loading happened at a pH of 8.4 to 9.4. The drug release also depends on pH, when investigated in an acidic buffer solution with pH from 4.4 to 5.4, the release rate was 15 – 20% in 24h. The concentration of DOX/BNNP in cell nuclei was retained for more time as compared to the concentration of free DOX. The DOX/BNNP enters the cell via endocytosis and releases the drug into a lysosome with an acidic pH. Drug resistivity is also reduced by the use of BNNP for delivery. DOX/BNNP shows high sensitivity for leukemia cells as more DOX molecules can be stably present, which explores the BN-based Nano-vehicles for efficient treatment of Leukemia.[311]

A study for adsorption and carrier of drugs Levofloxacin, Tetracycline and curcumin was performed. The experimental and theoretical study reveals that from 10mg/L Levofloxacin the adsorbed is 96.4% to PBN and 94.1 to BNNS at a pH of 4, while from 50mg/L Tetracycline the adsorbed is 84.2% to PBN and 82.7% to BNNS with pH of 6. The structure of levofloxacin is presented in figure 11. The drug release was observed at different pH explores the release rate for levofloxacin at 2 pH was 19% in 48 h which further increased to 35% and 62% for a pH of 7.4. The release from PBN is very efficient due to electrostatic interaction change between them. The theoretical studies explore that the adsorption energies for Levofloxacin, Tetracycline and curcumin were – 0.76 eV, - 0.79 eV and – 0.60 eV respectively. The adsorption is favourable due to the interaction between H of drugs and N from BN also the electronegative part with B. The drug has an efficient recyclability for 3 cycles without any effect while it has little adsorption ability effect at the fourth cycle. This makes it potent and sustainable for drug delivery.[312]

A theoretical study was performed to investigate the drug carriers in the gas and solvent phase. The study explores BNNT as an efficient carrier for anti-cancerous drugs Azacitidine (Aza) and

Materials Advances Accepted Manuscript

View Article Online
DOI: 10.1039/D5MA01210D

Open Access Article. Published on 24 June 2026. Downloaded on 6/26/2026 4:24:14 PM.
This article is licensed under a Creative Commons Attribution 3.0 Unported Licence.

Decitabine (Dac), structures of Aza and Dac are visually represented in Figure 11. The adsorption of Aza to BNNT is stable when the base ring of Aza is parallel to the BNNT surface, with adsorption energy of – 80.2 eV. While in the case of Dac, the adsorption is also highly stable for parallel ring structure with adsorption energy of – 75.81 eV. The stronger hydrogen bonding in Aza makes its structure shorter, hence its polarity increases making it soluble in polar solvents.

The release time is also high for the complexes with high adsorption energies. For Aza, the release time is 106.2 and for Dac, it is 19.10. For the solvent phase, the adsorption energies decrease to – 58.12 eV for Aza and – 60.32 eV for Dac, while stability is the same for the gas phase. The calculated recovery times in the solvent phase are 0.015 for Aza and 0.037 for Dac, which is less as compared to the gas phase. The energy gap for Aza/BNNT is – 8.944 eV and for Dac/BNNT is – 8.1312 eV, showing that Aza/BNNT is stable and hard as compared to Dac/BNNT. Short recovery time and high stability of BNNT with drugs make it an efficient drug carrier.[313]

A chemical vapour deposition process was used to form a BNNP nanocarrier for drug delivery in cancerous cells. The study explores that the maximum drug loading on BNNP was 0.055 mg per NP's mg. The drug is released in an acidic pH of 4.5 – 5.5 while becoming stable in a neutral pH of 7.4. The cell viability decreases with an increase in the concentration of BNNP. Free drugs face resistivity as compared to BN-loaded drugs, while the entry method was endocytosis through its needle-like surface. When the drug enters the cell, it accumulates the nuclei and cytoplasm, and the drug shows its effect and causes the death of the cell.[314]

11 BN as Precursor and Sensors in Environmental Toxicology Analysis

Two-dimensional materials are well adapted to dealing with environmental toxic agents. Specifically, carbon-based substances are highly potent in the detection and sensing of the elements and substances adding toxicity to the atmosphere. Therefore, such carbon analogues are researched experimentally and computationally. Sensing properties mainly include the charge transfer and adsorption of pollutants to the surface of nanomaterial. Graphene exhibits good electrical properties like charge transfer, but these properties are affected by the size, shape and quality production rate. A major property that makes BN a more prominent sensor instead of graphene is that graphene faces the challenge of a zero-band gap which makes it less sensitive and selective towards pollutants.

Materials Advances Accepted Manuscript

View Article Online
DOI: 10.1039/D5MA01210D

Open Access Article. Published on 24 June 2026. Downloaded on 6/26/2026 4:24:14 PM.
This article is licensed under a Creative Commons Attribution 3.0 Unported Licence.

Conversely, h-BN has excellent dielectric properties like a wide band gap, good adsorption property, more charge transfer ability, and chemical interaction with pollutants increases the sensing and selecting ability of BN making it a good precursor material in forming nanoelectronics devices. Interaction of pollutants with BN is analyzed through adsorption energy, energy gap variation and electron density, but mainly adsorption ability detected by adsorption energy and these all play important roles in determining sensing properties of a nanomaterial. The electron transfer in h-BN is much higher than in graphene due to the polar nature of bonds between B–N, which also makes it good selective for detecting environmental pollutants.[315]

So, due to these properties, Boron Nitride and its nanostructures are used in sensors to improve their selectivity and sensitivity for the detection of environmental toxicity. Rather than traditional sensors, BN sensors show exceptional properties to detect or adsorb any environmental toxicity-causing pollutants in a very short time, making their excellent applications in nanomaterials used as environmental sensors. These properties can also be enhanced by creating defects in nanomaterials or by adding any impurities to them this will enhance the band gap, adsorption energy and charge transfer according to the increase in the detecting ability of the nanomaterial.[316]

11.1 Analysis of Heavy Metals

Naturally existing metals in trace amounts are important for a few living creatures in their metabolic activity, but their high concentration becomes toxic to them because they start to combine with proteins and DNA structure destroying them and making them bio-toxic compounds and these molecules can't function normally.[317] As, Cd, Cr (VI), Hg, and Pb are toxic at even low concentrations, causing serious health issues to humans and worse effects on plants and animals, mostly aquatic life as these metals are easily soluble in water.[318] A lot of traditional sensors are used for the detection of heavy metal ions including graphene, its composite, carbon nanotubes, phosphorenes (BP), and Transition Metal Dichalcogenides (TMDCs), for their peak achievement in electrically transduced chemical sensing applications.[319]

There are generally different methods to detect different heavy metal ions, like for the detection of Fe^{3+}, quantum dots are a good method but g-C_3N_4 or its chemically broken parts are excellent detectors.[320] Hence, graphite oxide was synthesized by the hummer's method to obtain Graphitic Quantum Dots (GQDs) solution which was later used to synthesize of graphitic quantum electrode.

Materials Advances Accepted Manuscript

View Article Online
DOI: 10.1039/D5MA01210D

Open Access Article. Published on 24 June 2026. Downloaded on 6/26/2026 4:24:14 PM.
This article is licensed under a Creative Commons Attribution 3.0 Unported Licence.

The glass carbon electrode was obtained by sonicating the glass carbon electrode in ethanol and then coated with GQDs which were dispersed in water earlier and dried at room temperature. This electrode was used for the detection of heavy metal ions to determine the Pb^{2+} ions in solution it takes 60 second deposition time by Pb^{2+} ion when - 1.0 constant potential was applied.[321] In another study, silver nanoparticles doped Reduced Graphene Oxide (RGO) were synthesized by using RGO solution (prepared by Natural Graphite) with dispersed solution of $AgNO_3$ with different ratios at 60°C for 2h. For the detection of heavy metal ions RGO suspension with alcohol is spread to a Magnetic Glass Carbon Electrode (MGCE) to experiment, this electrode was dipped in a solution of the metal mixture and heavy metals started to deposit on the surface of the working electrode at the potential of -1.5V.[322]

Now with proper conjunction BN has much more efficacy in detection of heavy metal ions. In this regard, a DFT study to determine the sensitivity of heavy metal ions Fe^{2+}, Cr^{2+}, Mn^{2+} Au^{+}, Cu^{+} and Ag^{+} by BNNT shows that divalent ions have higher adsorption energy than monovalent ions making a stable interaction with the chemisorption process having the highest adsorption energy for Fe^{2+}, -1474.30 KJ/mol and lowest adsorption energy for Ag^{+} -173.25 KJ/mol. Adsorption of these metals causes changes in the band-gap with the lowest value of band-gap energy for divalent showing that BNNTs are more receptive towards divalent ions as compared to monovalent ions. This shows that BNNT is more sensitive towards ions, especially divalent ions.[323]

Another DFT study observed exploring the detection of heavy metals, As, Hg and Pb, by 2D allotropes of BN. This study shows that the adsorption of heavy metals on allotropes of BN is a thermodynamically stable process due to an increase in values of adsorption energy. Charge transfer and adsorption energy in the case of As is high as compared to other heavy metals indicating high chemical interaction of As with allotropes of BN. This chemical interaction shows the high selectivity and sensitivity of BN allotropes towards heavy metal detection.[324]

By creating defects or adding impurities can enhance the detection ability of BN as compared to pristine. So, to detect heavy metals like Cd (II) and Pb (II) which are causing serious health issues to humans, BCN-modified electrodes were made that show excellent sensation for these heavy metal ions with a limit of detection of 0.41 and 0.39 μg/L respectively. This electrode due to its high specific surface area and porous surface had good adsorption for heavy metals. This method has great sensitivity for different complex ionic samples.[116]

Materials Advances Accepted Manuscript

View Article Online
DOI: 10.1039/D5MA01210D

Open Access Article. Published on 24 June 2026. Downloaded on 6/26/2026 4:24:14 PM.
This article is licensed under a Creative Commons Attribution 3.0 Unported Licence.

11.2 Analysis of Toxic Gases

h-BN-based sensors used for the detection of environmental toxic gases like NO_2, SO_2, H_2S, $COCl_2$, HX, NO, NH_3 and HCN. A novel metal-free cataluminescence gas sensor was made of metal-free material, porous boron nitride (p-BN) using Zn salt as a co-reagent. Due to the high specific surface area and pores (B-vacancy) present in it, it shows highly efficient sensitivity towards H_2S gas ranging from 2.79 to 178.6 μg mL^{-1} with low limit detection of 0.52 μg mL^{-1}.[325]

A DFT study was performed to investigate the sensing ability of Armchair Boron Nitride Nanoribbon (ABNNR) towards COCl2, revealing that the adsorption of $COCL_2$ occurs through O atom and was more favored to open-edge ABNNR as compared to close-edge ABNNR with adsorption values -3.085 eV and -1.058 eV respectively. Changes in its electronic properties due to adsorption like band gap and electron transport make it potential for sensing toxic gases.[322] Another DFT study was performed to investigate the detection of HX environmental pollutants demonstrating that the HX detection ability of BNNT as a gas sensor depends upon its electrical response and that strong interaction between electron donor and acceptor shows good stabilization energy like for HF stabilization energy is much larger than all other HXs, sensing behaviour based on conductance change due to BNNT band gap difference having sensitivity order HCl > HF > HBr.[326]

The theoretical study on pristine and single vacancy graphene doped with Co for investigation of NO, SO_2, NH_3, CN and HCN sensing properties explores that weak interaction between Co and pristine graphene causes more charge transfer from Co-pristine graphene to adsorbed gases, so more stable adsorption occurs between them. This demonstrates that a doped pristine graphene sheet is suitable for sensing devices.[327] A computational study explores that a Nano sensor of 2D CoOOH has good sensitivity for toxicity analysis of HF and HCN H_2S. CoOOH makes a physical interaction with gases with adsorption energy -0.58, -0.80, and -0.43 respectively, this makes good selectivity for gas molecules. Adsorption reduces the band gap of a sheet which also makes it a good candidate for sensing device.[328]

Pure nanostructure of BN has good sensing ability but when they are doped with any metal or compounds their sensing behaviour becomes enhanced due to changes in their band gap and conducting properties. Low chemical reactivity makes h-BNNSs a challenging material towards

Materials Advances Accepted Manuscript

View Article Online
DOI: 10.1039/D5MA01210D

its application for detection and selective sensation. For improvement, Sulphur-BNNSs are modified which becomes an experimentally proven excellent NO_2 sensor with low-limit detection of 20 ppb. Hence it was theoretically proved that its surface adsorption capacity enhanced making it a good sensor for NO_2.[329]

Another DFT study for the detection of SO_2 by Ni-BNNT explores that when Ni doped to BNNT, its electronic behaviour deformed by reducing the band gap and enhancing its adsorption ability, strong electron hybridization in SO_2 system makes it a potential sensor for SO_2 and SF_6.[330] While when Mn doped to BNNT, the best site for SO_2 adsorption is MnN due to the large magnetic moment, Mn-BNNT shows high reactivity towards SO_2 and analysis shows that SO_2 and Mn have covalent interaction, so it can be used as a potential raw material manufacturing for SO_2 gas sensor.[331]

Here's a DFT study that explored the investigation of pure BNNT and doped with Al and Ga for the synthesis of CNCl sensors. Study shows that the band gap decreases with Ga doping and increases in adsorption energy than Al-doping, but when CNCl adsorb to doped BNNT, the band gap reduces for Al than Ga with values 1.762 eV and 2.503 eV which makes Al-BNNT more sensitive to CNCl than Ga-BNNT.[332]

11.3 Analysis of Aqueous Pollutants

There are a lot of techniques being studied to get sensors to detect toxic materials in water reservoirs. An approach towards BNQDs to make toxicity sensors is through hydrothermal experiments using a mixture of boric acid and melamine. Dispersion of BNDQs in an aqueous solution is easy and becomes selective and sensitive towards Fe^{3+} ions present in water with a limit detection of 0.3 μM.[333] For the detection of toxicity caused by zinc metals (Zn^{2+}), the computational investigation was successful in employing Graphene nanosheet and BNNS as a sensor material in aquatic environments. In this method, the adherence of zinc ions occurs more likely to BNNS due to its surface-level porosity. For good performance, these are centrally functionalized with suitable atoms, but in comparison to graphene sheets BNNS are more proficient in the detection or removal of Zinc ions because Zn^{2+} ions graphene sheets have an energy barrier. With increasing applied voltage, more ions pass through the sheet but their residence time also decreases.[334]

Open Access Article. Published on 24 June 2026. Downloaded on 6/26/2026 4:24:14 PM.
This article is licensed under a Creative Commons Attribution 3.0 Unported Licence.
Materials Advances Accepted Manuscript

View Article Online
DOI: 10.1039/D5MA01210D

Open Access Article. Published on 24 June 2026. Downloaded on 6/26/2026 4:24:14 PM.
This article is licensed under a Creative Commons Attribution 3.0 Unported Licence.

Water pollution due to pesticides and bacteria is also a vital issue to human health. A DFT study of pristine and Ag-doped BN allotropes was used for the detection of bacteria through the amino acid present in their wall in the gas and solvent phase. Haeck-BN and Twin-BN sheets were used to study three amino acids, Histidine, Phenylalanine and tyrosine. The study explores that Histidine has high adsorption energy and binding affinity with the Twin-BN sheet as compared to the Haeck-BN sheet in both phases but the other two amino acids show good adsorption in only the gas phase. Similar to the case of Ag-doped, His showed good affinity toward Ag-Twin BN sheet in both solvent and gas phase and others showed an affinity with only in the solvent phase. This shows that Histidine has good sensitivity of detection towards both pristine and Ag-doped sheets as compared to other amino acids.[324]

Antibiotics and waste removal from the pharmaceutical industry in water reservoirs are major sources of water pollution. An experimental study was performed for the detection of Tetracycline (TC) through p-BN revealing that the removal of TC from the p-BN sheet after adsorption is 94.25%. The multilayer adsorption isotherm was given by the Freundlich model.[115]

11.4 Analysis of Volatile Organic Compounds (VOCs)

Environmental pollutants like volatile organic compounds (VOCs) can be detected by different 2D nanostructures, like Transition Metal Dichalcogenide (TMDs), which are diverse in their field like photocatalysis and gas sensors. A DFT study for the sensitivity of VOCs over pristine TMD and Janus TMD monolayer, in which acetone found more sensitivity towards sensors than other VOCs due to high adsorption energy -0.35 eV.[335]

Sensing and capturing aromatic organic pollutants by h-BN were studied by DFT and Molecular Dynamic method. In this study, benzene, polyaromatic hydrocarbons and their derivatives adsorbed on top N sites with aromatic rings and their adsorption energies increased by an increase in several aromatic rings. For Brominated compounds, adsorption energy increases with an increase in the degree of bromination as well as by substitution pattern. The hydrophobicity of pollutants was strongly connected with adsorption energy. A theoretical study was performed for the detection of 4-Aminophenol by BNNSs. Study shows that by creating defects in BNNSs the response of 4-Aminophenol towards BNNSs is from 4.7 - 746.0, also having a very short recovery

Materials Advances Accepted Manuscript

View Article Online
DOI: 10.1039/D5MA01210D

Open Access Article. Published on 24 June 2026. Downloaded on 6/26/2026 4:24:14 PM.
This article is licensed under a Creative Commons Attribution 3.0 Unported Licence.

time of 13s for desorption. This increase in the adsorption ability of BNNS by creating defects makes BNNS a strong precursor for sensing devices.[321]

Boron nitride quantum dots (BNDQs) are also synthesized by the up-to-down method using h-BN. These quantum dots are used to detect the toxicity causing organic pollutant 2,4,6-trinitrophenol (TNP) with a limit of detection 0.14 μM. This process is tested by using different ions in a solution of a sample containing the analyte TNP, from all these ions TNP reveals greater reactivity towards BNDQs, showing the good sensitivity of boron nitride quantum dots towards organic pollutants.[336]

For the removal of organic pollutants, a novel mesoporous h-BN fiber was synthesized which has a high surface area and porosity for the detection of organic pollutants. In an experimental study for the detection of methylene blue by h-BN fibre, h-BN is dispersed in methylene blue solution and after stirring methylene blue is separated from the solution and adsorbed by h-BN fibre. Table 6 is explaining adsorption and LOD of different pollutants with BN structure. This study reveals that methylene blue can be removed from the water within only 180 minutes with this h-BN fibre and these pollutants also be removed from h-BN sheets so this fibre can be used several times. h-BN due to its high adsorption capacity and selectivity due to its porous surface make it a good precursor used in sensing devices.[337]

Table 6: Adsorption energy and LOD of different pollutants with BN structures

Structure	Pollutants	Adsorption energy	LOD	Reference.	Nature of Study
p-BN	H2S	-	0.52 μg mL^{-1}	319	Experimental
BCN	Pd (II), Cd (II)	-	Pd (II) 0.93 μg L^{-1}, Cd (II) 0.41 μg L^{-1}	116	Experimental
BNQD	TNP	-	0.14μM	336	Experimental
BNQD	Fe^{3+}	-	0.3 μM	336	Experimental
S-BNNS	NO_2	-	20ppb	329	Experimental
GQD	Pb^{2+}	-	7×10^{-9} M	338	Experimental
Transition Metal Dichalcogenide	methanol, ethanol, acetone and formyl aldehyde	Methanol −0.26 eV, Ethanol −0.25 eV, Acetone -0.35 eV, Formyl aldehyde −0.25 eV	-	335	Computational
Defected BNNT	4-Aminophenol	−19.3 kcal/mol.	-	321	Computational
ABNNR	$COCl_2$	At open-edge −3.085 eV, at closed edge −1.058 eV	-	322	Computational

Materials Advances Accepted Manuscript

View Article Online
DOI: 10.1039/D5MA01210D

Open Access Article. Published on 24 June 2026. Downloaded on 6/26/2026 4:24:14 PM.
This article is licensed under a Creative Commons Attribution 3.0 Unported Licence.

Ni-BNNT	SO_2, SOF_2, SO_2F_2	SO_2 −0.864 eV, SOF_2 −0.522 eV, SO_2F_2 −0.223 eV	-	330	Computational
BNNT	CNCl	Pristine −0.523 eV, Al-BNNT −1.754 eV, Ga-BNNT −1.112 eV	-	332	Computational
CoOOH	H_2S, HF, HCN	H_2S −0.43 eV, HF −0.80 eV, HCN −0.58 eV	-	328	Computational
Co-Graphene	NO, SO_2, NH_3, CO, HCN	NO 4.04 eV, SO_2 2.35 eV, NH_3 1.46 eV, CO 2.19 eV, HCN 2.14 eV	-	327	Computational
BNNT	Cr^{2+}, Mn^{2+}, Fe^{2+}, Cu^{+}, Ag^{+} and Au^{+}	Fe^{2+} −1474.30 eV, Cr^{2+} −1206.95 eV, Mn^{2+} −816.51 eV, Au^{+} −242.15 eV, Cu^{+} −227.47 eV, Ag^{+} −173.25 eV	-	339	Computational

12 h-BN – Heterostructures

Boron nitride (h-BN) aligned well in the development of advanced heterostructures, particularly when combined with other two-dimensional (2D) materials like graphene. The unique properties of h-BN such as high thermal conductivity, excellent electrical insulation, and mechanical strength cater heterostructures with enhanced functionalities. Hence h-BN comprises super structures which align perfectly other materials as well including the metallic oxides and other nanomaterials. These structures undermine the properties of individual system and hence are more suitable in terms of physical, thermal and electronic properties.

Moreover, there is presence of the insulator capabilities in currently known BN phases including the hexagonal, cubic, wurtzite and rhombohedral configurations. Hence the wide band modulations and insulating properties execute a profound hindrance while employing these materials in the manufacture of the electronic devices. Addressing this issue, significant advancements in the computational equipment and regarding technologies equipped the prediction of the BN based hetero materials, well known superstructures are now available with the semiconductor properties and appropriate metallic character to hold the explanation for the excess use of metallic oxides before the discovery and investigation on boron nitride and its analogous structures.

Materials Advances Accepted Manuscript

View Article Online
DOI: 10.1039/D5MA01210D

Open Access Article. Published on 24 June 2026. Downloaded on 6/26/2026 4:24:14 PM.
This article is licensed under a Creative Commons Attribution 3.0 Unported Licence.

The semiconducting efficiencies are well attributed to the presence of the sp^2 hybridizations interactions in the alternating bonds of the nitrogen and boron throughout the expansion of the structures in the three-dimensional network. Few of the assimilation and interactions of other materials with boron nitride have specific properties involving with it. Some of those materials are discussed under below and their structures are presented in figure 12.

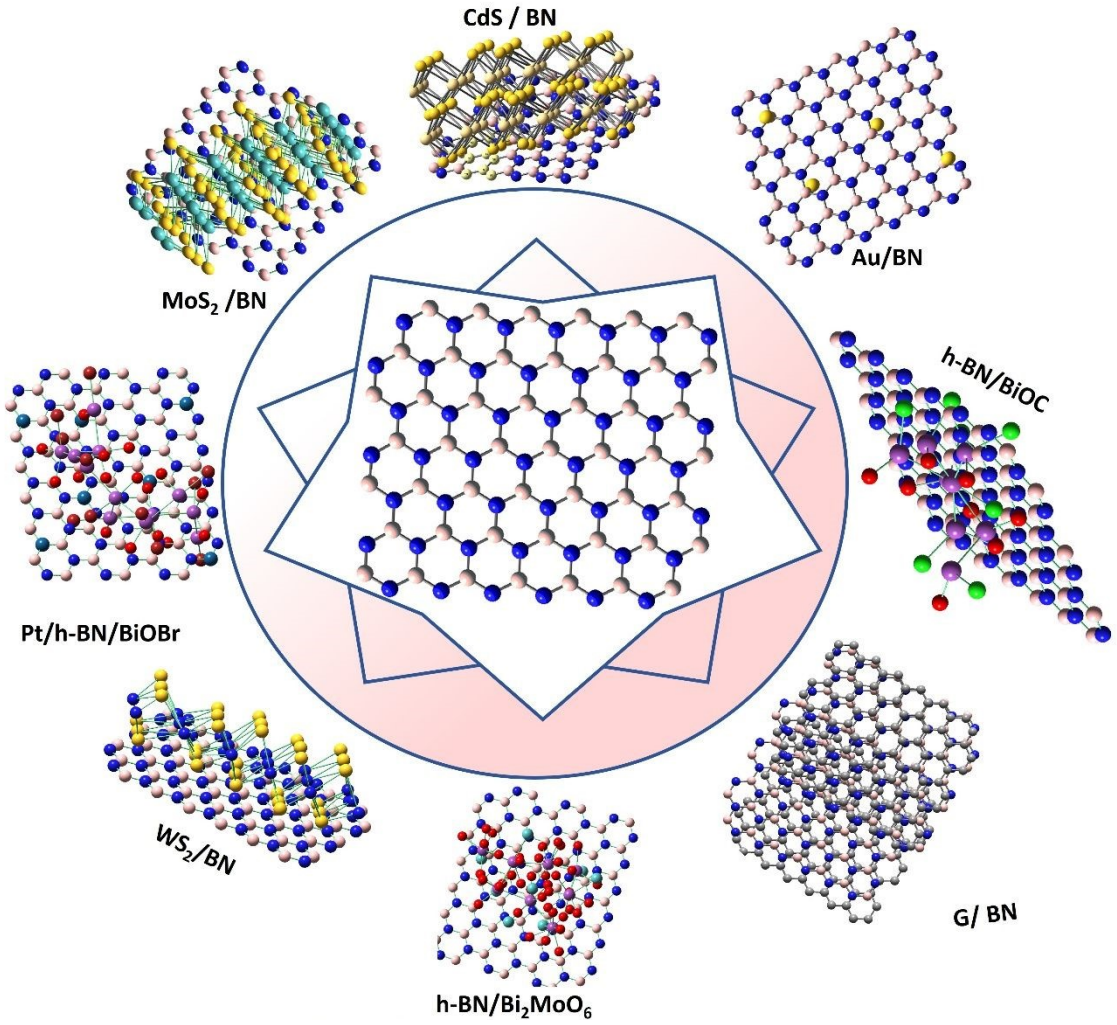

Figure 12: Different heterostructures on the BN sheet

12.1 G/h-BN

Recent advancements in the synthesis of h-BN heterostructures have focused on methods such as chemical vapor deposition (CVD) and mechanical exfoliation. For instance, a one-pot synthesis technique utilizing low-pressure CVD has been successfully employed to grow vertical

Materials Advances Accepted Manuscript

View Article Online
DOI: 10.1039/D5MA01210D

graphene/h-BN heterostructures, demonstrating the modulation of hydrogen partial pressure as a critical factor in achieving high-quality structures.[340] Additionally, in situ growth methods have been explored to create large-area graphene/h-BN films that exhibit excellent electronic transport properties.[341]

There is a keen growing interest in the preparation process of graphene combined hexagonal boron nitride. In particular many of reliable CVD methods had been developed in past few years addressing the incorporations of graphene sections and BN structures. In this regard, the efforts of Dean and colleagues are highly acknowledged in favor of layer by layer attachment process. This method specifically employs the cleaved h-BN segment deposition on SiO_2/Si whilst on polymer coating the graphene segments are deposited perfectly. After the assimilation, the structures are dislodged from the substrate material and a bridge like glass slide is utilized to transfer the graphene to the nanoflakes of boron nitride. The success of this method lead to practical modifications in the synthesis routes via adaptations like placement of optical mask or the use of dry transferred mechanisms.[342] Hence the control of the grain size, defect orientation are critical to steadfast the intrinsic properties of the hetero structure. Otherwise uncontrollable process conditions usually deteriorate the surface properties.

In contrast the direct deposition method is highly advanced in term of preservation of domain size and structural properties. There is uniform thickness and consistency in the adjacent layers therefore this route of synthesis is prevailing with the usage of exfoliated BN as a supporting substrate material for the crystal growth of graphene onto it. For this process, the major focus was use of exfoliated BN layers because of their dielectric properties. However the major concern was the lowered catalytic potential and surface sensitivity which hindered the growth patterns of graphene subsequent layers.[343] In this regard Zhang *et al* made earlier efforts on the crystal growth of graphene stock on BN that were practically aided by energetic plasma.[344]

In contrast the emergence of the gaseous catalysts confers to facilitating the crystal growth of graphene pre-deposited h BN obtained from the process of mechanical exfoliation. With the sufficient growth time of 20 minutes, the domain growth was expected to be 20 micrometer.[345] To make this heterostructures free from the contaminants one batch route was successfully adapted to pass the size limitations of natural BN substrates. Then advancements came via the method of Co segregation which was accompanied by the use of carbon and BN substrate. In this regard the use of Nickel film was used in fabrication process by Liu *et al.* So such heterostructures carry the

Open Access Article. Published on 24 June 2026. Downloaded on 6/26/2026 4:24:14 PM.
This article is licensed under a Creative Commons Attribution 3.0 Unported Licence.

Materials Advances Accepted Manuscript

View Article Online
DOI: 10.1039/D5MA01210D

Open Access Article. Published on 24 June 2026. Downloaded on 6/26/2026 4:24:14 PM.
This article is licensed under a Creative Commons Attribution 3.0 Unported Licence.

properties of graphene and BN thus are well suited to be used in nanoelectronics.[346] Prior the performance efficiency of graphene was declined due to contaminants and other agents thus the assimilation of BN making it dangling free insulation material. Also, the carrier mobility is increased 3 folds (60 000 cm^2/Vs). The reason for three-fold carrier mobility increase is well explained by DFT band structure calculations of graphene/h-BN heterostructures. The band gap of h-BN is about 6 eV approximately and this gap ensures that the valence and conduction bands are energetically remote from the Dirac point of graphene. It also prevents hybridisation between graphene pi-bands and h-BN electronic states. The structure of h-BN substrate is therefore inert electronically, nearly lattice-matched dielectric (with lattice mismatch of 1.8% approximately) and its primary function is to suppress the charged-impurity scattering and surface-optical phonon scattering modes which are responsible to degrade the carrier mobility in graphene supported on SiO_2. Band structure calculations on graphene/h-BN van der Waals heterostructures confirm that the linear Dirac dispersion and near-zero carrier effective mass are preserved with almost negligible perturbation upon the encapsulation of h-BN. It is consistent with the experimentally observed carrier mobilities that do approach 60,000 $cm^2V^{-1}s^{-1}$.[342] All these properties tailored in graphene/BN combination turned out to be promising especially in the manufacture of energy efficient systems and low voltage devices.

The integration of h-BN with graphene into van der Waals heterostructures has resulted in extraordinary electronic properties. The experimental data indicate that these heterostructures can significantly enhance electron mobility due to the high-quality single-crystal form of h-BN, which acts as an effective substrate that suppresses external disorder. The unique band structure and dielectric properties of h-BN allow for the development of devices with improved performance in optoelectronic applications, such as photodetectors, sensors and light-emitting devices.[347, 348]

Heterostructures composed of graphene and h-BN have shown promising results in gas sensing applications. The high surface-to-volume ratio and tunable electronic properties make these materials suitable for detecting toxic gases like SO_2 and CO.[348] Computational studies using density functional theory (DFT) have revealed that specific h-BN/graphene configurations exhibit favorable adsorption energies for these gases, indicating their potential as effective sensors.[349]

12.2 Bi oxide-hBN

Metallic oxides are usually considered the excellent electrocatalyst attributing to the facile synthesis, cost efficiency and chemical stability. Bismuth oxide is one of p type semiconductor

Materials Advances Accepted Manuscript

View Article Online
DOI: 10.1039/D5MA01210D

Open Access Article. Published on 24 June 2026. Downloaded on 6/26/2026 4:24:14 PM.
This article is licensed under a Creative Commons Attribution 3.0 Unported Licence.

owing to the extraordinary sensing capabilities. Depositing of bismuth oxide on BN was a breakthrough in simulation of surface sensitivity in terms of the detection of various compounds including aquatic contaminants. Electrochemical detection process of bismuth oxide on BN was configured via the characterization techniques. Therefore the first study was reported for the detection of FTM using Bi_2O_3/h BN. and to this date there is no computational investigation on this hetero structure to maximize the expected electronics properties.[341]

12.3 MoS_2/h-BN

Molybdenum sulphide and h-BN combination brings about the best properties comparable to those of graphene. Therefore, the report on the density functional theory calculations regarding the layered MoS_2/BN summed up the electronic properties on the resistant effect of dopants. This peculiar presence of dopants imparts the defect stages in the band gap structure which induce the electron transfer between adjacent layers changing the magnetization of the systems. This highlights the intricacies of the doping patterns which contribute to the electronics properties responsible for the manufacturing of tailored and custom made nanoelectronic devices. DFT band alignment calculations also showed that the MoS_2/h-BN heterostructure adopts a type-II (staggered) band alignment. In this alignment, the conduction band minimum of MoS_2 is below that of h-BN and the valence band maximum of MoS_2 is above that of h-BN. Under the phenomenon of photoexcitation, this staggered alignment give spatial separation of photogenerated charge carriers where the electrons do localize preferentially in the MoS_2 layer (the lower conduction band) and the holes migrate toward the h-BN side (lower valence band). Not only the carrier lifetime is prolonged with this built-in interfacial driving force but it also suppresses the recombination of the electrons and holes. The offset of computed conduction band comes out in the range 1.0-1.5 eV and that is subjective with the use of exchange-correlation functional. However, it is large enough to keep interfacial charge transfer to compete effectively with radiative recombination and it happens on timescales of nanoseconds in MoS_2. Thus, this heterostructure is quite a useful platform to be used in solar-driven water splitting and pollutant photodegradation.[350]

12.4 h-BN/$Bi_4O_5Br_2$-LMs

The novel preparation and synthesis of h-BN coupled with the $Bi_4O_5Br_2$-LMs facilitated via the facile route involving ionic liquid in water emulsion in an experimental investigation and there

Materials Advances Accepted Manuscript

View Article Online
DOI: 10.1039/D5MA01210D

Open Access Article. Published on 24 June 2026. Downloaded on 6/26/2026 4:24:14 PM.
This article is licensed under a Creative Commons Attribution 3.0 Unported Licence.

were enough affirmation of the optical properties utilizing the x-ray diffraction and other characterization technique. The strong emphasis on the photocatalytic reactivity through the theoretical calculations predicted the electronic density shifting and regular electron transfer tendencies. The surface properties and other aspects of h-BN made the graphene analogue photocatalysts much more favorable for use in the energy conversions reactions and devices through the photocatalysis.[351]

12.5 BN/BiOBr

The solvothermal process is used to synthesize novel heterostructure for the degradation of antibiotic agents. BN has good interaction with BiOBr explored by XRD and FT-IR analysis shows no separate peak for BN. BN attachment also reduces the bandgap of BiOBr which improves its photocatalytic ability. Its catalytic properties are observed by degradation of a few drugs which shows about 99% degradation for RhB. Ciproflaxacin degrades by 81.5%. The catalyst works for 4 cycles with an efficiency reduction of 5.6%. A 1% concentration of BN in BN/BiOBr displays high photocatalysis, while the increase in BN concentration causes a decrease in its efficiency. This reduction is because more BN covers the BiOBr sheet which decreases the formation of electron-hole pairs by a reduction in light absorption. The study explores how tert-butanol affects photocatalytic activity. O^{2-} and electron pair holes are active sites for the degradation reaction. This catalytic activity is favorable removal of organic pollutants.[352]

12.6 BN/BiOI

A novel photocatalyst BiOI/BN was prepared by facile one-pot solvothermal method. XRD Analysis shows that peaks of BN/BiOI are similar to BiOI, showing that BN content is distributed to BiOI. Its photocatalytic properties were observed by experimenting with different pollutants Rhodamine (RhB), Methylene Blue (MB) and 4-chlorophenol (4-CP) were selected. A catalyst works efficiently with 0.5% concentration of BN, an increase in concentration causes a decrease in its degradation properties. It shows 93% photodegradation activity of RhB at 0.5% while with pristine BiOI it shows 68% degradation. Methylene blue and chlorophenol also have higher degradation with this heterostructure than pristine BiOI. BN increases the catalytic activity of heterostructure by decreasing the band gap of BiOI and increasing its surface area. This study explores information for 3D photocatalyst semiconductors and the degradation of pollutants via photocatalyst.[353]

Materials Advances Accepted Manuscript

View Article Online
DOI: 10.1039/D5MA01210D

Open Access Article. Published on 24 June 2026. Downloaded on 6/26/2026 4:24:14 PM.
This article is licensed under a Creative Commons Attribution 3.0 Unported Licence.

12.7 TiO_2/h-BN

A photocatalyst produced by the heterostructure of TiO_2 with h-BN for water splitting. A theoretical study reveals that its band gap reduces to 2.07eV. The charge transfer in heterostructure is from h-BN to TiO_2 due to the high fermi-level of h-BN. Bandgap reduction and electric field formation with electron-hole pair generation show the enhancement in the light absorption property of TiO_2/h-BN. The difference in strain energy of heterostructure is 0.44eV, indicating strain resistance. The H_2O reduction potential was also calculated which explains that this heterostructure can carry HER and OER processes with different pH values.[354]

12.8 CdS/h-BN

One-step hydrothermal method was used to synthesize a photocatalyst of a heterostructure h-BN/CdS. It has a good degradation property for pollutants like RhB and Cr (VI) ions were studied in an experimental study. CdS causes a reduction in the bandgap of h-BN to 2.29eV. 1.0% of CdS/h-BN has a high resistance of charge transfer and 5 times higher photocurrent density than pure CdS. The degradation of RhB with 1% concentration is 97.5% but with high concentration, it has the same issue of overload on the sheet and blockage of light absorption. While less concentration of 0.5% shows a decrease in the active site for reaction. The reaction rate constant for each concentration of 3%, 1%, 0.5% and pure CdS is 0.03686 min−1, 0.06274 min−1, 0.03473 min−1 and 0.00789 min−1. The reduction of Cr (VI) ions carried out by CdS/h-BN gives 95.1% degradation in 20 minutes. Also, have 4 times recycle ability with less loss in efficiency. This photocatalyst is proficiently used for the degradation of organic pollutants and heavy metals from water.[355]

12.9 h-BN/BiOCl

Semiconductors of BiOCl are used as photocatalysts but their heterostructure with h-BN improves its efficiency. A solvothermal process is used to form h-BN/BiOCl and its catalytic activity was evaluated while experimenting with different pollutants. The concentration of h-BN increases the surface area of the catalyst and increases the formation of active sites for reaction. The surface area for 0.5%, 1%, 1.5% and 2% concentrations of BN are 1.1 m^2g^{-1}, 1m^2g^{-1}, 1.6 m^2g^{-1} and 1.8 m^2g^{-1} respectively. The catalyst shows maximum activity with 1% concentration, a concentration higher than it affects the active sites. The degradation of pollutants RhB and tetracycline (TC) at this heterostructure catalyst is 2.1 times higher and for PFOA is 1.3 times than over the blank

Materials Advances Accepted Manuscript

View Article Online
DOI: 10.1039/D5MA01210D

BiOCl. The rate constant for degradation of RhB and TC are 0.01826 per minute and 0.00577 per minute. The heterostructures have shown good stability for even 5 cycles at different times. This efficient stability of heterostructure makes it a potent applicant for environmental pollutant degradation.[356]

12.10 h-BN/Bi_2MoO_6

A photocatalyst of heterostructure h-BN/Bi_2MoO_6 was prepared by a feasible solvothermal method. The catalyst has a high degradation ability for Tetracycline, oxytetracycline (OTC) and doxycycline (DC) with a ratio of 99.19%, 95.28% and 91.04%. FTIR analysis shows a 50% heterojunction between h-BN and Bi_2MoO_6. h-BN improves the light absorption in the UV region when added to Bi_2MoO_6. Catalyst can be used for about five cycles with a decrease of less than 1% efficiency. Its degradation and absorption capacity make its applications in water pollution removal and cause improvement in solar energy efficiencies.[357]

12.11 Au/h-BN

Noble metals also improve the semiconducting properties of photocatalysts. An experimental study was performed to observe the catalytic properties of Au/h-BN. The XPS analysis shows that the Au nanoparticles form a heterojunction with the h-BN nanocomposites. The degradation of levofloxacin hydrochloride performed by 15% of Au/h-BN displays an 84.4% rate constant. The stability of the catalyst was detected for 5 cycles with an efficiency of 81.6% degradation rate. While the increase in concentration causes a decrease in efficiency because of the overload of active sites. This catalyst improves the HER reaction 61 times, by giving hydrogen production with 61.15 μmol in 5 hours. This catalyst provides perception for the formulation of photocatalyst for degradation of pharma antibiotics and a realistic approach for conversion of solar energy.[358]

12.12 WS_2/h-BN

Direct vapour chemical Deposition is used to form the heterostructure of WS_2 and h-BN. Active sites observed via Raman Spectrum. Photoluminescence peaks were observed which are much brighter for WS_2 growth on h-BN as compared to growth over SiO_2. The heterostructure formed by no chemical bonding between them just energetical interaction makes the large crystal structure.[359]

Open Access Article. Published on 24 June 2026. Downloaded on 6/26/2026 4:24:14 PM.
This article is licensed under a Creative Commons Attribution 3.0 Unported Licence.
Materials Advances Accepted Manuscript

View Article Online
DOI: 10.1039/D5MA01210D

Open Access Article. Published on 24 June 2026. Downloaded on 6/26/2026 4:24:14 PM.
This article is licensed under a Creative Commons Attribution 3.0 Unported Licence.

12.13 Pt/h-BN/BiOBr

A study proposed a photocatalyst for the removal of pollutants from water and gas. The heterostructure of Pt/h-BN/BiOBr was formed experimentally by the process of alcohol-soluble hydrolysis-assisted photoreduction. The rate constant for the degradation of bisphenol was 98.54% with this catalyst which is higher than all possible structures formed by this compound. The XRD analysis shows a good distribution of Pt and h-BN over the support surface, as no separate peak was observed for them. The stability of the catalyst was observed as the catalytic activity reduced to 81.82 for the fourth cycle of degradation. The h-BN and Pt attachment to BiOBr cause an increase in photocurrent. Pt works as an electron capture agent and BN as a hole provider, due to the interaction of both these; its ability for applications of photogenerated carrier improved. This photocatalyst is potent for the removal of pollutants from water.[360]

The future of h-BN heterostructures lies in the exploration of their multifunctional capabilities. The research is ongoing to better understand the role of defects within h-BN. The reason is simple because the defects can be modeled to create new functionalities. Furthermore, the combination of h-BN with other materials such as polymers or metal oxides creates opportunities to develop 2D materials with precisely tailored properties. Thus, the advancements in the synthesis and understanding of h-BN heterostructures are crucial for innovative applications across various fields, including electronics, photonics, and environmental sensing.

Summary and Future Perspectives

Working through all the properties, synthesis, surface interactions and other efficiencies, hexagonal boron nitride has much more potential in the future use as the perfect and economical nanomaterials in suitable applications in various industries. We provide a comprehensive overview of the advances in the surface chemistry of hexagonal boron nitride (h-BN) and its derivatives, focusing on their functionalization, structural properties, and potential applications involving adsorption efficiencies, sensing performance and surface reactivity. Hexagonal Boron Nitride and the related compounds have surface modifications, such as hydroxylation and other chemical functionalization. These introductions of new entities into the regular structure can significantly alter the electronic and mechanical properties of h-BN.

The integration of density functional theory (DFT) calculations with experimental findings is highlighted as a model approach in grasping the concept of interactions at the atomic level. These

Materials Advances Accepted Manuscript

View Article Online
DOI: 10.1039/D5MA01210D

Open Access Article. Published on 24 June 2026. Downloaded on 6/26/2026 4:24:14 PM.
This article is licensed under a Creative Commons Attribution 3.0 Unported Licence.

interactions are useful in predicting how modifications can enhance the performance of h-BN in various applications, including catalysis, sensing, and nanocomposites. Furthermore, recent advancements in synthesis techniques, particularly chemical vapor deposition (CVD) showcase how control overgrowth parameters can lead to improved material quality and functionality.

Although challenges faced in the functionalization of h-BN materials such as achieving uniformity in functional groups and maintaining structural integrity during modifications are difficult to address. However, functionalization can enhance the surface chemical interactions with a wide range of compounds involving the toxic gases, other pollutants, drugs and biological substances.

We propose that future research should focus on developing scalable and efficient functionalization methods that can be easily integrated into existing production processes. Additionally, there is a call for more extensive studies on the interactions between h-BN and other materials to explore new heterostructures that could lead to innovative applications in electronics and photonics. The review concludes by emphasizing the potential of h-BN derivatives to meet the growing demands for high-performance materials in various fields, suggesting that further exploration of their surface chemistry will unlock new functionalities to expand the range of applications over surface.

Looking ahead, the field of h-BN research is poised for significant advancements driven by ongoing developments in computational models and experimental techniques. Future studies should prioritize the exploration of novel functionalization strategies and investigation approaches to probe the mechanisms of oxygen reduction, hydrogen storage and other those not only enhance the properties of h-BN but also ensure environmental sustainability and cost-effectiveness like the detection and sensing efficiencies of pollutants and other toxicological agents. The integration of machine learning algorithms with DFT calculations could streamline the design process for new h-BN derivatives by predicting their properties based on previously established data. This approach could facilitate rapid prototyping of materials tailored for specific applications, such as drug delivery systems or advanced sensors.

Moreover, as the demand for multifunctional materials grows, there is an opportunity to investigate hybrid systems that combine h-BN with other two-dimensional materials like graphene or transition metal dichalcogenides (TMDs). Such heterostructures could cater for the unique properties of each component to create materials with enhanced electronic, optical, or catalytic performance. Research into scalable production methods for this advanced BN based composites

Materials Advances Accepted Manuscript

View Article Online
DOI: 10.1039/D5MA01210D

will be critical to apply this material on commercial scale in addressing global challenges across the development of nanoelectronics technology and environmental sectors.

Acknowledgements

The authors thank Azan Ahmad for useful discussions and technical support.

References:

1. Ahmed, S. F.; Mofijur, M.; Rafa, N.; Chowdhury, A. T. Green approaches in synthesising nanomaterials for environmental nanobioremediation: Technological advancements, applications, benefits and challenges. *Environ. Res.* **2022**, *204*, 111967.
2. Samuel, M. S.; Ravikumar, M.; John J, A.; Selvarajan, E.; Patel, H.; Chander, P. S.; Soundarya, J.; Vuppala, S.; Balaji, R.; Chandrasekar, N. A review on green synthesis of nanoparticles and their diverse biomedical and environmental applications. *Catal.* **2022**, *12* (5), 459.
3. Papageorgiou, D.; Bakoglidis, K. Use of nanomaterials for the improvement of various industrial and biomedical applications. A review. *J. Environ. Prot. Ecol* **2012**, *13* (2), 593-602.
4. Liu, D.; Daniels, C.; Meunier, V.; Every, A. G.; Tománek, D. In-plane breathing and shear modes in low-dimensional nanostructures. *Carbon* **2020**, *157*, 364-370.
5. Wang, L.; Yang, R.; Li, J.; Qu, L.; Harrington, P. d. B. A highly selective and sensitive electrochemical sensor for tryptophan based on the excellent surface adsorption and electrochemical properties of PSS functionalized graphene. *Talanta* **2019**, *196*, 309-316.
6. Tang, L.; He, M.; Na, X.; Guan, X.; Zhang, R.; Zhang, J.; Gu, J. Functionalized glass fibers cloth/spherical BN fillers/epoxy laminated composites with excellent thermal conductivities and electrical insulation properties. *Compos. Commun* **2019**, *16*, 5-10.
7. Hu, W.; Yang, J. Two-dimensional van der Waals heterojunctions for functional materials and devices. *J. Mater. Chem.* **2017**, *5* (47), 12289-12297.
8. Gu, H.; Zhang, H.; Ma, C.; Xu, X.; Wang, Y.; Wang, Z.; Wei, R.; Liu, H.; Liu, C.; Shao, Q. Trace electrosprayed nanopolystyrene facilitated dispersion of multiwalled carbon nanotubes: simultaneously strengthening and toughening epoxy. *Carbon* **2019**, *142*, 131-140.
9. Zhao, S.; Lou, D.; Zhan, P.; Li, G.; Dai, K.; Guo, J.; Zheng, G.; Liu, C.; Shen, C.; Guo, Z. Heating-induced negative temperature coefficient effect in conductive graphene/polymer ternary nanocomposites with a segregated and double-percolated structure. *J. Mater. Chem.* **2017**, *5* (32), 8233-8242.
10. Chen, C.; Chen, H.; Wu, C.; Huang, J.; Duh, J. Heterostructural modulation of in situ growth of iron oxide/holey graphene framework nanocomposites as excellent electrodes for advanced lithium-ion batteries. *Appl. Surf. Sci.* **2019**, *485*, 247-254.
11. Li, B. L.; Wang, J.; Zou, H. L.; Garaj, S.; Lim, C. T.; Xie, J.; Li, N. B.; Leong, D. T. Low-dimensional transition metal dichalcogenide nanostructures based sensors. *Adv. Funct. Mater.* **2016**, *26* (39), 7034-7056.
12. Levendorf, M. P.; Kim, C.-J.; Brown, L.; Huang, P. Y.; Havener, R. W.; Muller, D. A.; Park, J. Graphene and boron nitride lateral heterostructures for atomically thin circuitry. *Nature* **2012**, *488* (7413), 627-632.
13. Clausi, M.; Zahid, M.; Shayganpour, A.; Bayer, I. S. Polyimide foam composites with nano-boron nitride (BN) and silicon carbide (SiC) for latent heat storage. *Adv. Compos. Hybrid Mater.* **2022**, *5* (2), 798-812.

Open Access Article. Published on 24 June 2026. Downloaded on 6/26/2026 4:24:14 PM.
This article is licensed under a Creative Commons Attribution 3.0 Unported Licence.

Materials Advances Accepted Manuscript

View Article Online
DOI: 10.1039/D5MA01210D

Open Access Article. Published on 24 June 2026. Downloaded on 6/26/2026 4:24:14 PM.
This article is licensed under a Creative Commons Attribution 3.0 Unported Licence.

14. Liu, M.; An, H.; Kumamoto, A.; Inoue, T.; Chiashi, S.; Xiang, R.; Maruyama, S. Efficient growth of vertically-aligned single-walled carbon nanotubes combining two unfavorable synthesis conditions. *Carbon* **2019**, *146*, 413-419.
15. Qayyum, M. S.; Hayat, H.; Matharu, R. K.; Tabish, T. A.; Edirisinghe, M. Boron nitride nanoscrolls: Structure, synthesis, and applications. *Appl. Phys. Rev.* **2019**, *6* (2).
16. Yadav, V.; Kulshrestha, V. Boron nitride: a promising material for proton exchange membranes for energy applications. *Nanoscale* **2019**, *11* (27), 12755-12773.
17. Dhungana, K. B.; Pati, R. Boron nitride nanotubes for spintronics. *Sensors* **2014**, *14* (9), 17655-17685.
18. Hirai, M.; Tanaka, N.; Sakai, M.; Yamaguchi, S. Structurally constrained boron-, nitrogen-, silicon-, and phosphorus-centered polycyclic π-conjugated systems. *Chem. Rev.* **2019**, *119* (14), 8291-8331.
19. Kumar, R.; Karkamkar, A.; Bowden, M.; Autrey, T. Solid-state hydrogen rich boron–nitrogen compounds for energy storage. *Chem. Soc. Rev.* **2019**, *48* (21), 5350-5380.
20. Dobrzhinetskaya, L. F.; Wirth, R.; Yang, J.; Green, H. W.; Hutcheon, I. D.; Weber, P. K.; Grew, E. S. Qingsongite, natural cubic boron nitride: The first boron mineral from the Earth's mantle. *Am. Mineral.* **2014**, *99* (4), 764-772.
21. Balmain, W. XLVI. Observations on the formation of compounds of boron and silicon with nitrogen and certain metals. *Lond. Edinb. Dubl. Phil. Mag.* **1842**, *21* (138), 270-277.
22. Balmain, W. Bemerkungen über die Bildung von Verbindungen des Bors und Siliciums mit Stickstoff und gewissen Metallen. *J. Prakt. Chem.* **1842**, *27* (1), 422-430.
23. Pakdel, A.; Bando, Y.; Golberg, D. Nano boron nitride flatland. *Chem. Soc. Rev.* **2014**, *43* (3), 934-959.
24. Bernard, S.; Miele, P. Nanostructured and architectured boron nitride from boron, nitrogen and hydrogen-containing molecular and polymeric precursors. *Mater. Today* **2014**, *17* (9), 443-450.
25. Liu, C.; Li, Q.; Wu, C.; Zhang, J.; Jin, Y.; MacFarlane, D. R.; Sun, C. Single-boron catalysts for nitrogen reduction reaction. *J. Am. Chem. Soc.* **2019**, *141* (7), 2884-2888.
26. Weng, Q.; Wang, X.; Wang, X.; Bando, Y.; Golberg, D. Functionalized hexagonal boron nitride nanomaterials: emerging properties and applications. *Chemical Society Reviews* **2016**, *45* (14), 3989-4012.
27. Mondinos, N.; Altarawneh, M.; Amri, A.; Liew, W. Y. H.; Poinern, G. E. J.; Jiang, Z.-T. Monatomic reactions with single vacancy monolayer h-BN: DFT studies. *RSC advances* **2023**, *13* (43), 30346-30357.
28. Back, S.; Siahrostami, S. Noble metal supported hexagonal boron nitride for the oxygen reduction reaction: a DFT study. *Nanoscale Advances* **2019**, *1* (1), 132-139.
29. He, C.; Liu, M.; Xu, T.; Jin, L.; Ling, H.; Liu, C. Systematic study of rare earth atom-doped double vacancy hexagonal boron nitride as a bifunctional electrocatalyst. *Colloids and Surfaces A: Physicochemical and Engineering Aspects* **2025**, *725*, 137639.
30. Roy, S.; Zhang, X.; Puthirath, A. B.; Meiyazhagan, A.; Bhattacharyya, S.; Rahman, M. M.; Babu, G.; Susarla, S.; Saju, S. K.; Tran, M. K. Structure, properties and applications of two-dimensional hexagonal boron nitride. *Advanced Materials* **2021**, *33* (44), 2101589.
31. Liu, K.; Chen, L.; Zhang, G.; Wu, G.; Ma, F.; Lu, Z. Carbon content and layers number controlling electronic properties of hybridized graphene and boron nitride. *Ceram. Int.* **2019**, *45* (15), 19380-19387.

Materials Advances Accepted Manuscript

View Article Online
DOI: 10.1039/D5MA01210D

32. Bhattacharya, B.; Seriani, N.; Sarkar, U. Raman and IR signature of pristine and BN-doped γ-graphyne from first-principle. *Carbon* **2019**, *141*, 652-662.
33. Tian, Y.; Xu, B.; Yu, D.; Ma, Y.; Wang, Y.; Jiang, Y.; Hu, W.; Tang, C.; Gao, Y.; Luo, K. Ultrahard nanotwinned cubic boron nitride. *Nature* **2013**, *493* (7432), 385-388.
34. Jiang, X.-F.; Weng, Q.; Wang, X.-B.; Li, X.; Zhang, J.; Golberg, D.; Bando, Y. Recent progress on fabrications and applications of boron nitride nanomaterials: a review. *J. Mater. Process. Technol.* **2015**, *31* (6), 589-598.
35. Chakraborty, P.; Xiong, G.; Cao, L.; Wang, Y. Lattice thermal transport in superhard hexagonal diamond and wurtzite boron nitride: A comparative study with cubic diamond and cubic boron nitride. *Carbon* **2018**, *139*, 85-93.
36. Zhang, Z.; Zeng, X. C.; Guo, W. Fluorinating hexagonal boron nitride into diamond-like nanofilms with tunable band gap and ferromagnetism. *J. Am. Chem. Soc.* **2011**, *133* (37), 14831-14838.
37. Liu, H.; Jin, P.; Xue, Y. M.; Dong, C.; Li, X.; Tang, C. C.; Du, X. W. Photochemical synthesis of ultrafine cubic boron nitride nanoparticles under ambient conditions. *Angew. Chem. Int. Ed.* **2015**, *54* (24), 7051-7054.
38. Park, J.-H.; Choi, S. H.; Zhao, J.; Song, S.; Yang, W.; Kim, S. M.; Kim, K. K.; Lee, Y. H. Thickness-controlled multilayer hexagonal boron nitride film prepared by plasma-enhanced chemical vapor deposition. *Curr. Appl. Phys.* **2016**, *16* (9), 1229-1235.
39. Витязь, П.; Сенють, В.; Хейфец, М.; Колмаков, А.; Клименко, С. Synthesis of superhard materials based on sphalerite boron nitride using carbon nanoparticles as a phase conversion catalyst. *Adv. Mater. Technol.* **2020**, (3), 8-17.
40. Chen, C.; Yin, D.; Kato, T.; Taniguchi, T.; Watanabe, K.; Ma, X.; Ye, H.; Ikuhara, Y. Stabilizing the metastable superhard material wurtzite boron nitride by three-dimensional networks of planar defects. *Proc. Natl. Acad. Sci.* **2019**, *116* (23), 11181-11186.
41. Pedersen, H.; Alling, B.; Högberg, H.; Ektarawong, A. Thermodynamic stability of hexagonal and rhombohedral boron nitride under chemical vapor deposition conditions from van der Waals corrected first principles calculations. *J. Vac. Sci. Technol., A* **2019**, *37* (4).
42. Lin, Y.; Connell, J. W. Advances in 2D boron nitride nanostructures: nanosheets, nanoribbons, nanomeshes, and hybrids with graphene. *Nanoscale* **2012**, *4* (22), 6908-6939.
43. Guerra, V.; Wan, C.; Degirmenci, V.; Sloan, J.; Presvytis, D.; McNally, T. 2D boron nitride nanosheets (BNNS) prepared by high-pressure homogenisation: structure and morphology. *Nanoscale* **2018**, *10* (41), 19469-19477.
44. Wang, J.; Ma, F.; Liang, W.; Wang, R.; Sun, M. Optical, photonic and optoelectronic properties of graphene, h-BN and their hybrid materials. *Nanophotonics* **2017**, *6* (5), 943-976.
45. Wang, J.; Ma, F.; Sun, M. Graphene, hexagonal boron nitride, and their heterostructures: properties and applications. *RSC Adv.* **2017**, *7* (27), 16801-16822.
46. Chen, X.; Jia, S.; Ding, N.; Shi, J.; Wang, Z. Capture of aromatic organic pollutants by hexagonal boron nitride nanosheets: density functional theoretical and molecular dynamic investigation. *Environ. Sci. Nano* **2016**, *3* (6), 1493-1503.
47. Dahal, R.; Li, J.; Majety, S.; Pantha, B. N.; Cao, X.; Lin, J.; Jiang, H. Epitaxially grown semiconducting hexagonal boron nitride as a deep ultraviolet photonic material. *Appl. Phys. Lett.* **2011**, *98* (21).
48. Novoselov, K. S.; Jiang, D.; Schedin, F.; Booth, T.; Khotkevich, V.; Morozov, S.; Geim, A. K. Two-dimensional atomic crystals. *Proc. Natl. Acad. Sci.* **2005**, *102* (30), 10451-10453.

Open Access Article. Published on 24 June 2026. Downloaded on 6/26/2026 4:24:14 PM.
This article is licensed under a Creative Commons Attribution 3.0 Unported Licence.

Materials Advances Accepted Manuscript

View Article Online
DOI: 10.1039/D5MA01210D

Open Access Article. Published on 24 June 2026. Downloaded on 6/26/2026 4:24:14 PM.
This article is licensed under a Creative Commons Attribution 3.0 Unported Licence.

49. Shen, H.; Guo, J.; Wang, H.; Zhao, N.; Xu, J. Bioinspired modification of h-BN for high thermal conductive composite films with aligned structure. *ACS Appl. Mater. Interfaces.* **2015**, *7* (10), 5701-5708.
50. Liu, L.; Park, J.; Siegel, D. A.; McCarty, K. F.; Clark, K. W.; Deng, W.; Basile, L.; Idrobo, J. C.; Li, A.-P.; Gu, G. Heteroepitaxial growth of two-dimensional hexagonal boron nitride templated by graphene edges. *Science* **2014**, *343* (6167), 163-167.
51. Terrones, M.; Charlier, J.-C.; Gloter, A.; Cruz-Silva, E.; Terrés, E.; Li, Y.; Vinu, A.; Zanolli, Z.; Dominguez, J.; Terrones, H. Experimental and theoretical studies suggesting the possibility of metallic boron nitride edges in porous nanourchins. *Nano lett.* **2008**, *8* (4), 1026-1032.
52. Chen, Z.-G.; Zou, J.; Liu, G.; Li, F.; Wang, Y.; Wang, L.; Yuan, X.-L.; Sekiguchi, T.; Cheng, H.-M.; Lu, G. Q. Novel boron nitride hollow nanoribbons. *Acs Nano* **2008**, *2* (10), 2183-2191.
53. Zhao, Z.; Yang, Z.; Wen, Y.; Wang, Y. Facile synthesis and characterization of hexagonal boron nitride nanoplates by two-step route. *J. Am. Ceram. Soc.* **2011**, *94* (12), 4496-4501.
54. Ingo, G. M.; Padeletti, G.; de Caro, T.; Riccucci, C.; Faraldi, F.; Curulli, A.; Mezzi, A.; Piccinini, M. Novel route to high-yield synthesis of sp 2-hybridized boron nitride nanoplates on stainless steel. *J. Mater. Chem.* **2011**, *21* (28), 10268-10272.
55. Deepak, F.; Vinod, C.; Mukhopadhyay, K.; Govindaraj, A.; Rao, C. Boron nitride nanotubes and nanowires. *Chem. Phys. Lett.* **2002**, *353* (5-6), 345-352.
56. Qiu, Y.; Yu, J.; Yin, J.; Tan, C.; Zhou, X.; Bai, X.; Wang, E. Synthesis of continuous boron nitride nanofibers by solution coating electrospun templatefibers. *Nanotechnol.* **2009**, *20* (34), 345603.
57. Zheng, M.; Gu, Y.; Xu, Z.; Liu, Y. Synthesis and characterization of boron nitride nanoropes. *Mater. Lett.* **2007**, *61* (8-9), 1943-1945.
58. Yu, Y.; Chen, H.; Liu, Y.; White, T.; Chen, Y. Preparation and potential application of boron nitride nanocups. *Mater. Lett.* **2012**, *80*, 148-151.
59. Siahlo, A. I.; Poklonski, N. A.; Lebedev, A. V.; Lebedeva, I. V.; Popov, A. M.; Vyrko, S. A.; Knizhnik, A. A.; Lozovik, Y. E. Structure and energetics of carbon, hexagonal boron nitride, and carbon/hexagonal boron nitride single-layer and bilayer nanoscrolls. *Phys. Rev. Mater.* **2018**, *2* (3), 036001.
60. Pakdel, A.; Bando, Y.; Golberg, D. Morphology-driven nonwettability of nanostructured BN surfaces. *Langmuir* **2013**, *29* (24), 7529-7533.
61. Weng, Q.; Wang, X.; Zhi, C.; Bando, Y.; Golberg, D. Boron nitride porous microbelts for hydrogen storage. *ACS nano* **2013**, *7* (2), 1558-1565.
62. Yin, J.; Li, X.; Zhou, J.; Guo, W. Ultralight three-dimensional boron nitride foam with ultralow permittivity and superelasticity. *Nano lett.* **2013**, *13* (7), 3232-3236.
63. Huang, B.; Lee, H.; Gu, B.-L.; Liu, F.; Duan, W. Edge stability of boron nitride nanoribbons and its application in designing hybrid BNC structures. *Nano Res.* **2012**, *5*, 62-72.
64. Mukherjee, R.; Bhowmick, S. Edge stabilities of hexagonal boron nitride nanoribbons: a first-principles study. *J. Chem. Theory Comput.* **2011**, *7* (3), 720-724.
65. Zhang, Z.; Liu, Y.; Yang, Y.; Yakobson, B. I. Growth mechanism and morphology of hexagonal boron nitride. *Nano lett.* **2016**, *16* (2), 1398-1403.
66. Tay, R. Y.; Griep, M. H.; Mallick, G.; Tsang, S. H.; Singh, R. S.; Tumlin, T.; Teo, E. H. T.; Karna, S. P. Growth of large single-crystalline two-dimensional boron nitride hexagons on electropolished copper. *Nano lett.* **2014**, *14* (2), 839-846.

Materials Advances Accepted Manuscript

View Article Online
DOI: 10.1039/D5MA01210D

67. Meyer, J. C.; Kisielowski, C.; Erni, R.; Rossell, M. D.; Crommie, M.; Zettl, A. Direct imaging of lattice atoms and topological defects in graphene membranes. *Nano lett.* **2008**, *8* (11), 3582-3586.
68. Ribeiro, R. M.; Peres, N. M. Stability of boron nitride bilayers: Ground-state energies, interlayer distances, and tight-binding description. *Phys. Rev. B: Condens. Matter* **2011**, *83* (23), 235312.
69. Constantinescu, G.; Kuc, A.; Heine, T. Stacking in bulk and bilayer hexagonal boron nitride. *Phys. Rev. Lett.* **2013**, *111* (3), 036104.
70. Shmeliov, A.; Kim, J. S.; Borisenko, K. B.; Wang, P.; Okunishi, E.; Shannon, M.; Kirkland, A. I.; Nellist, P. D.; Nicolosi, V. Impurity induced non-bulk stacking in chemically exfoliated h-BN nanosheets. *Nanoscale* **2013**, *5* (6), 2290-2294.
71. Kim, C.-J.; Brown, L.; Graham, M. W.; Hovden, R.; Havener, R. W.; McEuen, P. L.; Muller, D. A.; Park, J. Stacking order dependent second harmonic generation and topological defects in h-BN bilayers. *Nano lett.* **2013**, *13* (11), 5660-5665.
72. Simon, S.; Duran, M.; Dannenberg, J. How does basis set superposition error change the potential surfaces for hydrogen-bonded dimers? *J. Chem. Phys.* **1996**, *105* (24), 11024-11031.
73. Polo, V.; Gräfenstein, J.; Kraka, E.; Cremer, D. Long-range and short-range Coulomb correlation effects as simulated by Hartree–Fock, local density approximation, and generalized gradient approximation exchange functionals. *Theor. Chem. Acc.* **2003**, *109*, 22-35.
74. Perdew, J. P.; Burke, K.; Ernzerhof, M. Generalized gradient approximation made simple. *Phys. Rev. Lett.* **1996**, *77* (18), 3865.
75. Zhao, Y.; Truhlar, D. G. Density functionals with broad applicability in chemistry. *Acc. Chem. Res.* **2008**, *41* (2), 157-167.
76. Zhao, Y.; Truhlar, D. G. The M06 suite of density functionals for main group thermochemistry, thermochemical kinetics, noncovalent interactions, excited states, and transition elements: two new functionals and systematic testing of four M06-class functionals and 12 other functionals. *Theor. Chem. Acc.* **2008**, *120* (1), 215-241.
77. Kim, C.-J.; Brown, L.; Graham, M. W.; Hovden, R.; Havener, R. W. Stacking order dependent second harmonic generation and topological defects in h-BN bilayers. *Nano lett.* **2013**, *13* (11), 5660-5665.
78. Shmeliov, A.; Kim, J. S.; Borisenko, K. B.; Wang, P.; Okunishi, E. Impurity induced non-bulk stacking in chemically exfoliated h-BN nanosheets. *Nanoscale* **2013**, *5* (6), 2290-2294.
79. Khan, M. H.; Casillas, G.; Mitchell, D. R.; Liu, H. K.; Jiang, L. Carbon-and crack-free growth of hexagonal boron nitride nanosheets and their uncommon stacking order. *Nanoscale* **2016**, *8* (35), 15926-15933.
80. Feng, J.; Deschout, H.; Caneva, S.; Hofmann, S.; Lončarić, I. Imaging of optically active defects with nanometer resolution. *Nano lett.* **2018**, *18* (3), 1739-1744.
81. Hirshfeld, F. L. Bonded-atom fragments for describing molecular charge densities. *Theor. Chem. Acc.* **1977**, *44*, 129-138.
82. Sharma, K. P.; Sharma, S.; Sharma, A. K.; Jaisi, B. P.; Kalita, G.; Tanemura, M. Edge controlled growth of hexagonal boron nitride crystals on copper foil by atmospheric pressure chemical vapor deposition. *Cryst. Eng. Comm.* **2018**, *20* (5), 550-555.
83. Marom, N.; Bernstein, J.; Garel, J.; Tkatchenko, A.; Joselevich, E.; Kronik, L.; Hod, O. Stacking and registry effects in layered materials: the case of hexagonal boron nitride. *Phys. Rev. Lett.* **2010**, *105* (4), 046801.

Open Access Article. Published on 24 June 2026. Downloaded on 6/26/2026 4:24:14 PM.
This article is licensed under a Creative Commons Attribution 3.0 Unported Licence.

Materials Advances Accepted Manuscript

View Article Online
DOI: 10.1039/D5MA01210D

Open Access Article. Published on 24 June 2026. Downloaded on 6/26/2026 4:24:14 PM.
This article is licensed under a Creative Commons Attribution 3.0 Unported Licence.

84. Khan, M. H.; Liu, H. K.; Sun, X.; Yamauchi, Y.; Bando, Y.; Golberg, D.; Huang, Z. Few-atomic-layered hexagonal boron nitride: CVD growth, characterization, and applications. *Mater. Today* **2017**, *20* (10), 611-628.
85. Stone, A.; Wales, D. Theoretical studies of icosahedral C60 and some related species. *Chem. Phys. Lett.* **1986**, *128* (5-6), 501-503.
86. Ma, J.; Alfè, D.; Michaelides, A.; Wang, E. Stone-Wales defects in graphene and other planar sp^2-bonded materials. *Phys. Rev. B: Condens. Matter* **2009**, *80* (3), 033407.
87. Li, Q.; Zou, X.; Liu, M.; Sun, J.; Gao, Y.; Qi, Y.; Zhou, X.; Yakobson, B. I.; Zhang, Y.; Liu, Z. Grain boundary structures and electronic properties of hexagonal boron nitride on Cu (111). *Nano lett.* **2015**, *15* (9), 5804-5810.
88. Gibb, A. L.; Alem, N.; Chen, J.-H.; Erickson, K. J.; Ciston, J.; Gautam, A.; Linck, M.; Zettl, A. Atomic resolution imaging of grain boundary defects in monolayer chemical vapor deposition-grown hexagonal boron nitride. *J. Am. Chem. Soc.* **2013**, *135* (18), 6758-6761.
89. Song, L.; Ci, L.; Lu, H.; Sorokin, P. B.; Jin, C. Large scale growth and characterization of atomic hexagonal boron nitride layers. *Nano lett.* **2010**, *10* (8), 3209-3215.
90. Nozaki, H.; Itoh, S. Structural stability of BC2N. **1996**, *57* (1), 41-49.
91. Pokropivny, V. V.; Skorokhod, V. V.; Oleinik, G. S.; Kurdyumov, A. V.; Bartnitskaya, T. S. Boron nitride analogs of fullerenes (the fulborenes), nanotubes, and fullerites (the fulborenites). *J. Solid State Chem.* **2000**, *154* (1), 214-222.
92. Liu, Y.; Zou, X.; Yakobson, B. I. Dislocations and grain boundaries in two-dimensional boron nitride. *ACS nano* **2012**, *6* (8), 7053-7058.
93. Cretu, O.; Lin, Y.-C.; Suenaga, K. Evidence for active atomic defects in monolayer hexagonal boron nitride: a new mechanism of plasticity in two-dimensional materials. *Nano lett.* **2014**, *14* (2), 1064-1068.
94. Zobelli, A.; Gloter, A.; Ewels, C.; Seifert, G.; Colliex, C. Electron knock-on cross section of carbon and boron nitride nanotubes. *Phys. Rev. B: Condens. Matter* **2007**, *75* (24), 245402.
95. Jin, C.; Lin, F.; Suenaga, K.; Iijima, S. Fabrication of a freestanding boron nitride single layer and its defect assignments. *Phys. Rev. Lett.* **2009**, *102* (19), 195505.
96. Khan, M. H.; Huang, Z.; Xiao, F.; Casillas, G. Synthesis of large and few atomic layers of hexagonal boron nitride on melted copper. *Sci. Rep.* **2015**, *5* (1), 7743.
97. Chen, W.; Li, Y.; Yu, G.; Zhou, Z.; Chen, Z. Electronic structure and reactivity of boron nitride nanoribbons with stone-wales defects. *J. Chem. Theory Comput.* **2009**, *5* (11), 3088-3095.
98. Wang, X.; Wu, J.; Zhang, Y.; Sun, Y.; Ma, K.; Xie, Y.; Zheng, W.; Tian, Z.; Kang, Z.; Zhang, Y. Vacancy defects in 2D transition metal dichalcogenide electrocatalysts: From aggregated to atomic configuration. *Adv. Mater.* **2023**, *35* (50), 2206576.
99. Azzam, S. I.; Parto, K.; Moody, G. Prospects and challenges of quantum emitters in 2D materials. *Appl. Phys. Lett.* **2021**, *118* (24).
100. Dastidar, M. G.; Thekkooden, I.; Nayak, P. K.; Bhallamudi, V. P. Quantum emitters and detectors based on 2D van der Waals materials. *Nanoscale* **2022**, *14* (14), 5289-5313.
101. Innocenzi, P.; Stagi, L. From defects to photoluminescence in h-BN 2D and 0D nanostructures. *Acc. Mater. Res.* **2024**, *5* (4), 413-425.
102. Feng, J.; Deschout, H.; Caneva, S.; Hofmann, S.; Lončarić, I.; Lazić, P.; Radenovic, A. Imaging of optically active defects with nanometer resolution. *Nano lett.* **2018**, *18* (3), 1739-1744.
103. Weitz, R. T.; Yacoby, A. Graphene rests easy. *Nat. Nanotechnol.* **2010**, *5* (10), 699-700.
104. Lei, W.; Portehault, D.; Liu, D.; Qin, S.; Chen, Y. Porous boron nitride nanosheets for effective water cleaning. *Nat. Commun.* **2013**, *4* (1), 1777.

Materials Advances Accepted Manuscript

View Article Online
DOI: 10.1039/D5MA01210D

Open Access Article. Published on 24 June 2026. Downloaded on 6/26/2026 4:24:14 PM.
This article is licensed under a Creative Commons Attribution 3.0 Unported Licence.

105. Kumar, R.; Parashar, A. Fracture toughness enhancement of h-BN monolayers via hydrogen passivation of a crack edge. *Nanotechnology* **2017**, *28* (16), 165702.
106. Fan, M.; Jimenez, J. D.; Shirodkar, S. N.; Wu, J.; Chen, S. Atomic Ru immobilized on porous h-BN through simple vacuum filtration for highly active and selective CO2 methanation. *ACS Catal.* **2019**, *9* (11), 10077-10086.
107. Li, X.; Lin, B.; Li, H.; Yu, Q.; Ge, Y.; Jin, X.; Liu, X.; Zhou, Y.; Xiao, J. Carbon doped hexagonal BN as a highly efficient metal-free base catalyst for Knoevenagel condensation reaction. *Appl. Catal., B* **2018**, *239*, 254-259.
108. Liang, J.; Song, Q.; Lin, J.; Li, G.; Fang, Y.; Guo, Z.; Huang, Y.; Lee, C.-S.; Tang, C. In situ Cu-loaded porous boron nitride nanofiber as an efficient adsorbent for CO2 capture. *ACS Sustain. Chem. Eng.* **2020**, *8* (19), 7454-7462.
109. Zhang, J.; Zhang, H.-l.; Zhou, P.; Qing, P.-h.; Xu, H.-b.; Zhang, Y. Porous hexagonal boron nitride nanosheets with large adsorption capacity for Cu2+ synthesized through a two-step roasting process. *Mater. Lett.* **2018**, *213*, 211-213.
110. Guerra, V.; Wan, C.; McNally, T. Thermal conductivity of 2D nano-structured boron nitride (BN) and its composites with polymers. *Prog. Mater Sci.* **2019**, *100*, 170-186.
111. Sharma, B. B.; Parashar, A. Mechanical and fracture behaviour of hydroxyl functionalized h-BN nanosheets. *J. Mater. Sci.* **2020**, *55* (8), 3228-3242.
112. Li, J.; Jin, P.; Dai, W.; Wang, C.; Li, R.; Wu, T.; Tang, C. Excellent performance for water purification achieved by activated porous boron nitride nanosheets. *Mater. Chem. Phys.* **2017**, *196*, 186-193.
113. Zhao, Y.; Peng, X.; Fu, T.; Huang, C.; Feng, C.; Yin, D.; Wang, Z. Molecular dynamics simulation of nano-indentation of (111) cubic boron nitride with optimized Tersoff potential. *Appl. Surf. Sci.* **2016**, *382*, 309-315.
114. Kvashnin, D.; Ghorbani-Asl, M.; Shtansky, D. Mechanical properties and current-carrying capacity of Al reinforced with graphene/BN nanoribbons: a computational study. *Nanoscale* **2016**, *8* (48), 20080-20089.
115. Song, Q.; Fang, Y.; Liu, Z.; Li, L.; Wang, Y.; Liang, J.; Huang, Y.; Lin, J.; Hu, L.; Zhang, J. The performance of porous hexagonal BN in high adsorption capacity towards antibiotics pollutants from aqueous solution. *Chem. Eng. J.* **2017**, *325*, 71-79.
116. Huang, R.; Lv, J.; Chen, J.; Zhu, Y.; Zhu, J.; Wågberg, T. Three-dimensional porous high boron-nitrogen-doped carbon for the ultrasensitive electrochemical detection of trace heavy metals in food samples. *J. Hazard. Mater.* **2023**, *442*, 130020.
117. Han, T.; Luo, Y.; Wang, C. Effects of temperature and strain rate on the mechanical properties of hexagonal boron nitride nanosheets. *J. Phys. D: Appl. Phys.* **2013**, *47* (2), 025303.
118. Thomas, S.; Ajith, K.; Valsakumar, M. Directional anisotropy, finite size effect and elastic properties of hexagonal boron nitride. *J. Phys.: Condens. Matter* **2016**, *28* (29), 295302.
119. Ding, N.; Wu, C.-M. L.; Li, H. The effect of grain boundaries on the mechanical properties and failure behavior of hexagonal boron nitride sheets. *Phys. Chem. Chem. Phys.* **2014**, *16* (43), 23716-23722.
120. Banhart, F.; Kotakoski, J. Structural defects in graphene. *ACS nano* **2011**, *5* (1), 26-41.
121. Gao, W.; Tkatchenko, A. Sliding mechanisms in multilayered hexagonal boron nitride and graphene: the effects of directionality, thickness, and sliding constraints. *Phys. Rev. Lett.* **2015**, *114* (9), 096101.
122. Falin, A.; Cai, Q.; Santos, E. J.; Scullion, D.; Qian, D. Mechanical properties of atomically thin boron nitride and the role of interlayer interactions. *Nat. Commun.* **2017**, *8* (1), 15815.

Materials Advances Accepted Manuscript

View Article Online
DOI: 10.1039/D5MA01210D

123. Jo, I.; Pettes, M. T.; Kim, J.; Watanabe, K.; Taniguchi, T.; Yao, Z.; Shi, L. Thermal conductivity and phonon transport in suspended few-layer hexagonal boron nitride. *Nano lett.* **2013**, *13* (2), 550-554.
124. Zhou, H.; Zhu, J.; Liu, Z.; Yan, Z. High thermal conductivity of suspended few-layer hexagonal boron nitride sheets. *Nano Res.* **2014**, *7*, 1232-1240.
125. Zheng, J.-C.; Zhang, L.; Kretinin, A. V.; Morozov, S. V.; Wang, Y. B.; Wang, T.; Li, X.; Ren, F.; Zhang, J.; Lu, C.-Y. High thermal conductivity of hexagonal boron nitride laminates. *2D Mater.* **2016**, *3* (1), 011004.
126. Yuan, C.; Li, J.; Lindsay, L.; Cherns, D.; Pomeroy, J. W.; Liu, S.; Edgar, J. H.; Kuball, M. Modulating the thermal conductivity in hexagonal boron nitride via controlled boron isotope concentration. *Phys. Commun.* **2019**, *2* (1), 43.
127. Taha-Tijerina, J.; Narayanan, T. N.; Gao, G.; Rohde, M.; Tsentalovich, D. A.; Pasquali, M.; Ajayan, P. M. Electrically insulating thermal nano-oils using 2D fillers. *ACS nano* **2012**, *6* (2), 1214-1220.
128. Wang, J.; Ma, F. Graphene, hexagonal boron nitride, and their heterostructures: properties and applications. *RSC Adv.* **2017**, *7* (27), 16801-16822.
129. Watanabe, K.; Taniguchi, T.; Kanda, H. Direct-bandgap properties and evidence for ultraviolet lasing of hexagonal boron nitride single crystal. *Nat. Mater.* **2004**, *3* (6), 404-409.
130. Barone, V.; Peralta, J. E. Magnetic boron nitride nanoribbons with tunable electronic properties. *Nano lett.* **2008**, *8* (8), 2210-2214.
131. Gao, R.; Yin, L.; Wang, C.; Qi, Y.; Lun, N.; Zhang, L.; Liu, Y.-X.; Kang, L.; Wang, X. High-yield synthesis of boron nitride nanosheets with strong ultraviolet cathodoluminescence emission. *J. Phys. Chem. C* **2009**, *113* (34), 15160-15165.
132. Satawara, A. M.; Shaikh, G. A.; Gupta, S. K.; Gajjar, P. Structural, electronic and optical properties of hexagonal boron-nitride (h-BN) monolayer: An Ab-initio study. *Mater. Today Proc.* **2021**, *47*, 529-532.
133. Ravan, B. A.; Jafari, H. DFT study on electronic and optical properties of halogen-adsorbed hexagonal boron nitride. *Comput. Condens. Matter* **2019**, *21*, e00416.
134. Laleyan, D. A.; Mengle, K.; Zhao, S.; Wang, Y.; Kioupakis, E.; Mi, Z. Effect of growth temperature on the structural and optical properties of few-layer hexagonal boron nitride by molecular beam epitaxy. *Opt. Express* **2018**, *26* (18), 23031-23039.
135. Wang, G.; Cheng, Y.; Chen, J.; Meng, J.; Zeng, L.; Yin, Z.; Wu, J.; Zhang, X. Luminescence properties of the hexagonal boron nitride epilayer. *Adv. Opt. Mater.* **2023**, *11* (23), 2301034.
136. Blase, X.; Rubio, A.; Louie, S. G.; Cohen, M. L. Quasiparticle band structure of bulk hexagonal boron nitride and related systems. *Physical review B* **1995**, *51* (11), 6868.
137. Arnaud, B.; Lebègue, S.; Rabiller, P.; Alouani, M. Huge excitonic effects in layered hexagonal boron nitride. *Physical review letters* **2006**, *96* (2), 026402.
138. Wirtz, L.; Marini, A.; Rubio, A. Excitons in boron nitride nanotubes: dimensionality effects. *Physical review letters* **2006**, *96* (12), 126104.
139. Watanabe, K.; Taniguchi, T.; Kanda, H. Direct-bandgap properties and evidence for ultraviolet lasing of hexagonal boron nitride single crystal. *Nature materials* **2004**, *3* (6), 404-409.
140. Liao, L.; Lin, Y.-C.; Bao, M.; Cheng, R.; Bai, J.; Liu, Y.; Qu, Y.; Wang, K. L.; Huang, Y.; Duan, X. High-speed graphene transistors with a self-aligned nanowire gate. *Nature* **2010**, *467* (7313), 305-308.

Open Access Article. Published on 24 June 2026. Downloaded on 6/26/2026 4:24:14 PM.
This article is licensed under a Creative Commons Attribution 3.0 Unported Licence.

Materials Advances Accepted Manuscript

View Article Online
DOI: 10.1039/D5MA01210D

141. Kınacı, A.; Haskins, J. B.; Sevik, C.; Çağın, T. Thermal conductivity of BN-C nanostructures. *Phys. Rev. B: Condens. Matter* **2012**, *86* (11), 115410.
142. Lu, J.; Zhang, K.; Feng Liu, X.; Zhang, H.; Chien Sum, T.; Castro Neto, A. H.; Loh, K. P. Order–disorder transition in a two-dimensional boron–carbon–nitride alloy. *Nature commun.* **2013**, *4* (1), 2681.
143. Lyalin, A.; Nakayama, A.; Uosaki, K.; Taketsugu, T. Theoretical predictions for hexagonal BN based nanomaterials as electrocatalysts for the oxygen reduction reaction. *Phys. Chem. Chem. Phys.* **2013**, *15* (8), 2809-2820.
144. Yang, Y.; Fu, Q.; Wei, M.; Bluhm, H.; Bao, X. Stability of BN/metal interfaces in gaseous atmosphere. *Nano Res.* **2015**, *8*, 227-237.
145. Bai, W.; Cao, C.; Yang, S.; Yan, S. Hydrolysis stability and its mechanism of porous boron nitride fibers in a watery environment. *J. Taiwan Inst. Chem. Engrs.* **2023**, *150*, 105061.
146. Feng, P. X.; Chavez, E.; Malca, C. Super stable pollution gas sensor based on functionalized 2D boron nitride nanosheet materials for high humidity environments. *Chemosensors* **2018**, *6* (4), 49.
147. Kostoglou, N.; Tampaxis, C.; Charalambopoulou, G.; Constantinides, G.; Ryzhkov, V.; Doumanidis, C.; Matovic, B.; Mitterer, C.; Rebholz, C. Boron nitride nanotubes versus carbon nanotubes: A thermal stability and oxidation behavior study. *Nanomaterials* **2020**, *10* (12), 2435.
148. Chen, X.; Dmuchowski, C. M.; Park, C.; Fay, C. C.; Ke, C. Quantitative characterization of structural and mechanical properties of boron nitride nanotubes in high temperature environments. *Scientific report* **2017**, *7* (1), 11388.
149. Nigam, S.; Majumder, C. CO oxidation by BN− fullerene cage: effect of impurity on the chemical reactivity. *ACS nano* **2008**, *2* (7), 1422-1428.
150. Wasey, A. A.; Chakrabarty, S.; Das, G.; Majumder, C. h-BN monolayer on the Ni (111) surface: a potential catalyst for oxidation. *ACS Appl. Mater. Interfaces.* **2013**, *5* (21), 10404-10408.
151. Laskowski, R.; Blaha, P. Ab initio study of h-BN nanomeshes on Ru (001), Rh (111), and Pt (111). *Phys. Rev. B: Condens. Matter* **2010**, *81* (7), 075418.
152. Mahvash, F.; Eissa, S.; Bordjiba, T.; Tavares, A.; Szkopek, T.; Siaj, M. Corrosion resistance of monolayer hexagonal boron nitride on copper. *Scientific report* **2017**, *7* (1), 42139.
153. Li, H.; Zhu, S.; Zhang, M.; Wu, P. Tuning the chemical hardness of boron nitride nanosheets by doping carbon for enhanced adsorption capacity. *ACS omega* **2017**, *2* (9), 5385-5394.
154. Liu, Y.; Zhan, G.; Wang, Q.; He, D.; Zhang, J. Hardness of Polycrystalline Wurtzite boron nitride (wBN) compacts. *Scientific report* **2019**, *9* (1), 10215.
155. Li, L. H.; Cervenka, J.; Watanabe, K.; Taniguchi, T.; Chen, Y. Strong oxidation resistance of atomically thin boron nitride nanosheets. *ACS nano* **2014**, *8* (2), 1457-1462.
156. Bosak, A.; Serrano, J.; Krisch, M.; Watanabe, K.; Taniguchi, T.; Kanda, H. Elasticity of hexagonal boron nitride: Inelastic x-ray scattering measurements. *Phys. Rev. B: Condens. Matter* **2006**, *73* (4), 041402.
157. Hamdi, I.; Meskini, N. Ab initio study of the structural, elastic, vibrational and thermodynamic properties of the hexagonal boron nitride: performance of LDA and GGA. *Phys. Rev. B: Condens. Matter* **2010**, *405* (13), 2785-2794.
158. Lebedev, A. V.; Lebedeva, I. V.; Knizhnik, A. A.; Popov, A. M. Interlayer interaction and related properties of bilayer hexagonal boron nitride: ab initio study. *RSC Adv.* **2016**, *6* (8), 6423-6435.

Open Access Article. Published on 24 June 2026. Downloaded on 6/26/2026 4:24:14 PM.
This article is licensed under a Creative Commons Attribution 3.0 Unported Licence.

Materials Advances Accepted Manuscript

View Article Online
DOI: 10.1039/D5MA01210D

159. Zhao, Y.-M.; Zhang, C.; Shin, S.; Shen, L. Thermal conductivity of sliding bilayer h-BN and its manipulation with strain and layer confinement. *J. Mater. Chem.* **2023**, *11* (32), 11082-11090.
160. Zhou, L.; Zhang, J.; Li, S.; Tian, Y.; Wang, J.; Huang, M.; Yuan, Q.; Li, X.; Kou, Z.; He, D. Effects of hardness and grain size on wear resistance of polycrystalline cubic boron nitride. *Int. J. Refract. Met. Hard Mater.* **2023**, *111*, 105766.
161. Xu, H.; Zhou, J.; Li, Y.; Jaramillo, R.; Li, J. Optomechanical control of stacking patterns of h-BN bilayer. *Nano Res.* **2019**, *12*, 2634-2639.
162. Ding, S.; Chang, W.; Wang, W.; Gong, P. Fluorinated Boron Nitride Nanosheets-Based Solid Lubricating Coating for Tribological Applications at Elevated Temperatures. *ACS Appl. Nano Mater.* **2024**, *7* (18), 21871-21881.
163. Escobedo-Morales, A.; Salazar-Villanueva, M.; Guatemala-Vera, H. Structural and Physicochemical Properties of Carbon Doped Boron Nitride Fullerenes: Effect of Doping Level and Atomic Arrangement. *ADV. THEOR. SIMUL.* **2024**, *7* (3), 2300698.
164. Esrafili, M. D.; Rad, F. A. Carbon-doped boron nitride nanosheets as highly sensitive materials for detection of toxic NO and NO2 gases: a DFT study. *Vacuum* **2019**, *166*, 127-134.
165. Ouyang, H.; Li, W.; Long, Y. Carbon-doped h-BN for the enhanced electrochemical determination of dopamine. *Electrochim. Acta* **2021**, *369*, 137682.
166. Xiao, M.; Li, X.; Du, B. Electronic and optical properties of C-doped BN nanotubes by adsorption of typical decomposition products of C_3F_7CN gas. *Appl. Surf. Sci.* **2019**, *491*, 698-706.
167. Guo, F.; Yang, P.; Pan, Z. Carbon-doped BN nanosheets for the oxidative dehydrogenation of ethylbenzene. *Angew. Chem.* **2017**, *129* (28), 8343-8347.
168. Zhao, J.; Chen, Z. Carbon-doped boron nitride nanosheet: an efficient metal-free electrocatalyst for the oxygen reduction reaction. *J. Phys. Chem. C* **2015**, *119* (47), 26348-26354.
169. Nguyen, D. B.; Tran, L. N. Assessment of electrocatalytic performance of metal-free C-doped BN nanoflakes for oxygen reduction and hydrogen evolution reactions: A comparative study. *J. Phys. Chem. C* **2018**, *122* (37), 21124-21131.
170. Ri, M.; Choe, K.; Kim, K.; Gao, Y.; Tang, Z. C-doping into h-BN at low annealing temperature by alkaline earth metal borate for photoredox activity. *RSC Adv.* **2018**, *8* (73), 42109-42115.
171. Anindya, K. N.; Rochefort, A. Collective Magnetism in 2D Polymer Made of C-Doped Triangular Boron Nitride Nanoflakes. *ADV. THEOR. SIMUL.* **2021**, *4* (5), 2100028.
172. Jalilian, J.; Kanjouri, F. Structural, electronic and magnetic properties of carbon doped boron nitride nanowire: Ab initio study. *J. Solid State Chem.* **2016**, *243*, 232-240.
173. Gao, M.; Adachi, M.; Lyalin, A.; Taketsugu, T. Long range functionalization of h-BN monolayer by carbon doping. *J. Phys. Chem. C* **2016**, *120* (29), 15993-16001.
174. Pang, J.; Chao, Y.; Chang, H.; Li, H. Tuning electronic properties of boron nitride nanoplate via doping carbon for enhanced adsorptive performance. *J. Colloid Interface Sci.* **2017**, *508*, 121-128.
175. Wang, B.; Qu, X.; Zheng, K. C and O doped BN nanoflake and nanowire hybrid structures for tuneable photoluminescence. *J. Alloys Compd.* **2017**, *705*, 691-699.
176. Xiong, J.; Yang, L.; Chao, Y.; Pang, J.; Zhang, M.; Zhu, W.; Li, H. Boron nitride mesoporous nanowires with doped oxygen atoms for the remarkable adsorption desulfurization performance from fuels. *ACS Sustain. Chem. Eng.* **2016**, *4* (8), 4457-4464.

Open Access Article. Published on 24 June 2026. Downloaded on 6/26/2026 4:24:14 PM.
This article is licensed under a Creative Commons Attribution 3.0 Unported Licence.

Materials Advances Accepted Manuscript

View Article Online
DOI: 10.1039/D5MA01210D

Open Access Article. Published on 24 June 2026. Downloaded on 6/26/2026 4:24:14 PM.
This article is licensed under a Creative Commons Attribution 3.0 Unported Licence.

177. Liu, F.; Li, S.; Yu, D. Template-free synthesis of oxygen-doped bundlelike porous boron nitride for highly efficient removal of heavy metals from wastewater. *ACS Sustain. Chem. Eng.* **2018**, *6* (12), 16011-16020.
178. Noura, M.; Rahdar, A.; Taimoory, S. M. A theoretical first principles computational investigation into the potential of aluminum-doped boron nitride nanotubes for hydrogen storage. *Int. J. Hydrogen Energy* **2020**, *45* (19), 11176-11189.
179. Ibrahim, M. A.; Rady, A.-s. S.; Mandarawe, A. M. Adsorption of chlormethine anti-cancer drug on pure and aluminum-doped boron nitride nanocarriers: A comparative DFT study. *J. Pharm. Sci.* **2022**, *15* (10), 1181.
180. Darwish, A. A.; Fadlallah, M. M.; Badawi, A.; Maarouf, A. A. Adsorption of sugars on Al- and Ga-doped boron nitride surfaces: a computational study. *Appl. Surf. Sci.* **2016**, *377*, 9-16.
181. Piya, A. A.; Shamim, S. U. D.; Uddin, M. N.; Munny, K. Adsorption behavior of cisplatin anticancer drug on the pristine, Al-and Ga-doped BN nanosheets: A comparative DFT study. *Comput. Theor. Chem.* **2021**, *1200*, 113241.
182. Soleymani, R. The Effect of Aluminum, Gallium, Indium-Doping on the Zigzag (5, 0) Boron-Nitride Nanotubes: DFT, NMR, Vibrational, Thermodynamic Parameters and Electrostatic Potential Map with Electrophilicity Studies. **2016**.
183. Doust Mohammadi, M.; Abdullah, H. Y. Theoretical study of the adsorption of amantadine on pristine, Al-, Ga-, P-, and As-doped boron nitride nanosheets: a PBC-DFT, NBO, and QTAIM study. *Theor. Chem. Acc.* **2020**, *139* (10), 158.
184. Behmagham, F.; Vessally, E.; Massoumi, B. A computational study on the SO2 adsorption by the pristine, Al, and Si doped BN nanosheets. *Superlattices Microstruct.* **2016**, *100*, 350-357.
185. Vessally, E.; Farajzadeh, P.; Najafi, E. Possible sensing ability of boron nitride nanosheet and its Al–and Si–doped derivatives for methimazole drug by computational study. *IJCCE.* **2021**, *40* (4), 1001-1011.
186. Zhuang, C.; Li, L.; Ban, C. Synthesis, analysis and electrical properties of silicon doped BN nanowires. *J. Alloys Compd.* **2018**, *731*, 84-89.
187. Hussain, A.; Rafique, H. M.; Tayyab, M. Computational study of Be-doped hexagonal boron nitride (h-BN): Structural and electronic properties. *Comput. Condens. Mater.* **2020**, *23*, e00474.
188. Farmanzadeh, D.; Rezainejad, H. Adsorption of diazinon and hinosan molecules on the iron-doped boron nitride nanotubes surface in gas phase and aqueous solution: A computational study. *Appl. Surf. Sci.* **2016**, *364*, 862-869.
189. Asif, Q. u. A.; Hussain, A.; Nabi, A. Computational study of X-doped hexagonal boron nitride (h-BN): structural and electronic properties (X= P, S, O, F, Cl). *J. Mol. Model.* **2021**, *27*, 1-15.
190. Ikram, M.; Wakeel, M.; Hassan, J.; Haider, A.; Naz, S. Impact of Bi doping into boron nitride nanosheets on electronic and optical properties using theoretical calculations and experiments. *Nanoscale Res. Lett.* **2021**, *16* (1), 82.
191. Xia, S.-Y.; Tao, L.-Q.; Jiang, T. Rh-doped h-BN monolayer as a high sensitivity SF6 decomposed gases sensor: A DFT study. *Appl. Surf. Sci.* **2021**, *536*, 147965.
192. Muhammad, R.; Shuai, Y.; Tan, H.-P. A first-principles study on alkaline earth metal atom substituted monolayer boron nitride (BN). *J. Phys. Chem. C* **2017**, *5* (32), 8112-8127.
193. Wang, W.-Y.; Ma, N.-N.; Wang, C.-H. Enhancement of second-order nonlinear optical response in boron nitride nanocone: Li-doped effect. *J. Mol. Graphics Modell.* **2014**, *48*, 28-35.

Materials Advances Accepted Manuscript

View Article Online
DOI: 10.1039/D5MA01210D

Open Access Article. Published on 24 June 2026. Downloaded on 6/26/2026 4:24:14 PM.
This article is licensed under a Creative Commons Attribution 3.0 Unported Licence.

194. Iqbal, J.; Ayub, K. Enhanced electronic and non-linear optical properties of alkali metal (Li, Na, K) doped boron nitride nano-cages. *J. Alloys Compd.* **2016**, *687*, 976-983.
195. Hossain, M. R.; Hasan, M. M.; Nishat, M. DFT and QTAIM investigations of the adsorption of chlormethine anticancer drug on the exterior surface of pristine and transition metal functionalized boron nitride fullerene. *J. Mol. Liq.* **2021**, *323*, 114627.
196. Bibi, S.; Ur-Rehman, S.; Khalid, L.; Bhatti, I. A. Investigation of the adsorption properties of gemcitabine anticancer drug with metal-doped boron nitride fullerenes as a drug-delivery carrier: a DFT study. *RSC Adv.* **2022**, *12* (5), 2873-2887.
197. Hassan, J.; Ikram, M.; Ul-Hamid, A. Application of chemically exfoliated boron nitride nanosheets doped with co to remove organic pollutants rapidly from textile water. *Nanoscale Res. Lett.* **2020**, *15*, 1-13.
198. Basharnavaz, H.; Habibi-Yangjeh, A. A DFT study for adsorption of CO on Ni, Pd and Pt atoms doped (7, 0) boron nitride nanotube. *Mol. Phys.* **2018**, *116* (2), 204-211.
199. Tabtimsai, C.; Wanno, B. Theoretical investigation on 5–fluorouracil anti–cancer drug adsorption on Sc–and Ti–doped armchair and zigzag boron nitride nanotubes. *J. Mol. Liq.* **2021**, *337*, 116596.
200. Kang, Y.; Chen, L.; Liu, C. Enhancement of n-type conductivity of hexagonal boron nitride films by in-situ co-doping of silicon and oxygen. *J. Phys.: Condens. Matter* **2022**, *34* (38), 384002.
201. Liang, J.; Song, Q.; Lin, J.; Li, G.; Fang, Y. In situ Cu-loaded porous boron nitride nanofiber as an efficient adsorbent for CO2 capture. *ACS Sustain. Chem. Eng.* **2020**, *8* (19), 7454-7462.
202. Al-Sunaidi, A. Adsorption of SO_2 and NO_2 on metal-doped boron nitride nanotubes: a computational study. *Comput. Theor. Chem.* **2016**, *1092*, 108-113.
203. Hassan, J.; Naz, S.; Haider, A.; Raza, A.; Ul-Hamid, A. h-BN nanosheets doped with transition metals for environmental remediation; a DFT approach and molecular docking analysis. *Mater. Sci. Eng., B* **2021**, *272*, 115365.
204. Mananghaya, M.; Yu, D.; Santos, G. N. Hydrogen adsorption on boron nitride nanotubes functionalized with transition metals. *Int. J. Hydrogen Energy* **2016**, *41* (31), 13531-13539.
205. Abbasi, M.; Nemati-Kande, E.; Mohammadi, M. D. Doping of the first row transition metals onto B12N12 nanocage: A DFT study. *Comput. Theor. Chem.* **2018**, *1132*, 1-11.
206. Najafi, M. P-doped carbon nanotube and Ge-doped boron nitride nanotube as a real catalysts for N2O+ SiO reaction: DFT examination. *Appl. Surf. Sci.* **2017**, *420*, 243-251.
207. Bahari, A.; Bagheri, M.; Amiri, M. First principles study of electronic and structural properties of single walled zigzag boron nitride nanotubes doped with the elements of group IV. *Solid State Commun.* **2017**, *267*, 1-5.
208. Matin, M. A.; Alauddin, M.; Islam, M. M. Investigation of transition metals (Ag, Au, Pd, Pt and Ru)-doped boron nitride nanocarrier for drug delivery process of favipiravir: An intuition from DFT. *J. Mol. Liq.* **2024**, *407*, 125244.
209. Abedi, M.; Eslami, M.; Ghadiri, M. An insight into the electro-chemical properties of halogen (F, Cl and Br) doped BP and BN nanocages as anodes in metal-ion batteries. *Scientific reports* **2020**, *10* (1), 19948.
210. Li, H.; Ran, H.; Li, Y.; Lv, N.; Yin, J.; Zhang, J. Comparative study of halogen-doped (XCl, Br, I) hexagonal boron nitride: A promising strategy to enhance the capacity of adsorptive desulfurization. *J. Environ. Chem. Eng.* **2021**, *9* (5), 105886.

Materials Advances Accepted Manuscript

View Article Online
DOI: 10.1039/D5MA01210D

Open Access Article. Published on 24 June 2026. Downloaded on 6/26/2026 4:24:14 PM.
This article is licensed under a Creative Commons Attribution 3.0 Unported Licence.

211. Cui, Q.; Qin, G.; Wang, W.; Sun, L.; Du, A. Mo-doped boron nitride monolayer as a promising single-atom electrocatalyst for CO2 conversion. *Beilstein J. Nanotechnol.* **2019**, *10* (1), 540-548.
212. Özkapı, S. G.; Özkapı, B.; Dalgıç, S. Electronic properties of Cr and Mn doped BN nanowires. In *Mater. Sci. Forum*, 2018; Trans Tech Publ: Vol. 916, pp 69-73.
213. Muhammad, R.; Uqaili, M. A.; Shuai, Y.; Mahar, M.; Ahmed, I. Ab-initio investigations on the physical properties of 3d and 5d transition metal atom substituted divacancy monolayer h-BN. *Appl. Surf. Sci.* **2018**, *458*, 145-156.
214. Debebe, M. M.; Hailemariam, S. M. Computational study on the impact of Nb doping on electronic structure, magnetic and optical properties of hexagonal bilayer BN. *Mater. Res. Express.* **2023**, *10* (1), 016301.
215. Derdare, M.; Boudjahem, A.-G. Adsorption of the guanine molecule over the pristine, Nb-, and Au-doped boron nitride nanosheets: a DFT study. *Struct. Chem.* **2021**, *32* (6), 2159-2173.
216. Taherpour, A. A.; Shahri, Z.; Rezaei, O.; Jamshidi, M.; Fellowes, T. Adsorption, intercalation and sensing of helium on yttrium functionalized open edge boron nitride: A first principle DFT and TDDFT study. *Chem. Phys. Lett.* **2018**, *691*, 231-237.
217. Zhukovskii, Y. F.; Piskunov, S.; Kazerovskis, J.; Makaev, D. V.; D'yachkov, P. N. Comparative theoretical analysis of BN nanotubes doped with Al, P, Ga, As, In, and Sb. *J. Phys. Chem. C* **2013**, *117* (27), 14235-14240.
218. Fu, Y.; Zhang, W.; Fan, Z.; Jiang, H.; Hou, Y.; Luo, Q.; Wang, Y. Investigation of Electronic and Optical Properties of (Cs, Br, Cs-Br) Doped Mono-Layer Hexagonal Boron Nitride Using First Principles. *Crystals* **2022**, *12* (10), 1406.
219. Lu, Q.; Wei, S.; Yin, G.; Bai, P.; Li, Y. Doping Dy improves magnetism and electricity in hexagonal boron nitride. *Appl. Surf. Sci.* **2024**, *645*, 158887.
220. Ran, H.; Yin, J.; Zhang, J.; Zhang, Y.; He, J.; Lv, N.; Li, H.; Li, H. Group IIIA Single-Metal Atoms Anchored on Hexagonal Boron Nitride for Selective Adsorption Desulfurization via S–M Bonds. *Inorg. Chem.* **2023**, *62* (12), 4883-4893.
221. Yang, P.; Zha, J.; Gao, G.; Zheng, L.; Huang, H.; Xia, Y.; Xu, S.; Xiong, T.; Zhang, Z.; Yang, Z. Growth of tellurium nanobelts on h-BN for p-type transistors with ultrahigh hole mobility. *Nanomicro Lett.* **2022**, *14* (1), 109.
222. Ayub, A. R.; Zeshan, M.; Khan, M. A.; Kalsoom, S. Nonlinear Optical Properties of Hybrid Materials of Neodymium Metal Doped Boron Nitride: Comprehensively Study via Silico-Technique. *J. Inorg. Organomet. Polym.* **2023**, *33* (9), 2681-2697.
223. Wang, X.; Liu, Z.; Shi, X.; Jia, Y.; Zhu, G.; Peng, J.; Wang, Q. Optical and photocatalytic characteristics of Se-doped h-boron nitride: Experimental assessments and DFT calculations. *J. Alloys Compd.* **2022**, *909*, 164791.
224. da Silva, W. M.; Ferreira, T. H.; de Morais, C. A.; Leal, A. S.; Sousa, E. M. B. Samarium doped boron nitride nanotubes. *Appl. Radiat. Isot.* **2018**, *131*, 30-35.
225. Wang, X.; Zhi, C.; Li, L.; Zeng, H.; Li, C.; Mitome, M.; Golberg, D.; Bando, Y. "Chemical blowing" of thin-walled bubbles: High-throughput fabrication of large-area, few-layered BN and C x-BN nanosheets. *Adv. Mater.* **2011**, *23* (35), 4072-4076.
226. Song, L.; Liu, Z.; Reddy, A. L. M.; Narayanan, N. T.; Taha-Tijerina, J.; Peng, J.; Gao, G.; Lou, J.; Vajtai, R. Binary and ternary atomic layers built from carbon, boron, and nitrogen. *Adv. Mater.* **2012**, *24* (36), 4878-4895.

Materials Advances Accepted Manuscript

View Article Online
DOI: 10.1039/D5MA01210D

Open Access Article. Published on 24 June 2026. Downloaded on 6/26/2026 4:24:14 PM.
This article is licensed under a Creative Commons Attribution 3.0 Unported Licence.

227. Krivanek, O. L.; Chisholm, M. F.; Nicolosi, V.; Pennycook, T. J.; Corbin, G. J.; Dellby, N.; Murfitt, M. F.; Own, C. S.; Szilagyi, Z. S. Atom-by-atom structural and chemical analysis by annular dark-field electron microscopy. *Nature* **2010**, *464* (7288), 571-574.
228. Qiu, N.-x.; Tian, Z.-y.; Guo, Y.; Zhang, C.-h.; Luo, Y.-p. A first-principle study of calcium-decorated BC2N sheet doped by boron or carbon for high hydrogen storage. *Int. J. Hydrogen Energy* **2014**, *39* (17), 9307-9320.
229. Huang, C.; Chen, C.; Zhang, M.; Lin, L.; Ye, X.; Lin, S.; Antonietti, M.; Wang, X. Carbon-doped BN nanosheets for metal-free photoredox catalysis. *Nature commun.* **2015**, *6* (1), 7698.
230. Sevak Singh, R.; Yingjie Tay, R.; Leong Chow, W.; Hon Tsang, S.; Mallick, G.; Tong Teo, E. H. Band gap effects of hexagonal boron nitride using oxygen plasma. *Appl. Phys. Lett.* **2014**, *104* (16).
231. Singh, R. S. Influence of oxygen impurity on electronic properties of carbon and boron nitride nanotubes: A comparative study. *AIP Adv.* **2015**, *5* (11).
232. Silva, L. A.; Guerini, S. C.; Lemos, V. Electronic and structural properties of oxygen-doped BN nanotubes. *IEEE Trans. Nanotechnol.* **2006**, *5* (5), 517-522.
233. Wu, J.; Zhang, W. Tuning the magnetic and transport properties of boron-nitride nanotubes via oxygen-doping. *Solid State Commun.* **2009**, *149* (11-12), 486-490.
234. Han, W.-Q.; Yu, H.-G.; Zhi, C.; Wang, J.; Liu, Z.; Sekiguchi, T.; Bando, Y. Isotope effect on band gap and radiative transitions properties of boron nitride nanotubes. *Nano lett.* **2008**, *8* (2), 491-494.
235. Gou, G.; Pan, B.; Shi, L. The nature of radiative transitions in O-doped boron nitride nanotubes. *J. Am. Chem. Soc.* **2009**, *131* (13), 4839-4845.
236. Melo Oliveira, L.; Santos, O.; Martins, J.; Azevedo, S.; Kaschny, J. Electronic and optical properties of Ge doped graphene and BN monolayers. *Appl. Phys. A* **2019**, *125*, 1-8.
237. Wu, J.; Zhang, W. Magnetism in germanium-doped boron-nitride nanotubes. *Chem. Phys. Lett.* **2008**, *457* (1-3), 169-173.
238. Lu, S.; Shen, P.; Zhang, H.; Liu, G.; Guo, B. Towards n-type conductivity in hexagonal boron nitride. *Nature commun.* **2022**, *13* (1), 3109.
239. Feng, C.; Tang, L.; Deng, Y.; Zeng, G.; Wang, J.; Liu, Y.; Chen, Z.; Yu, J.; Wang, J. Enhancing optical absorption and charge transfer: synthesis of S-doped h-BN with tunable band structures for metal-free visible-light-driven photocatalysis. *Appl. Catal., B Environ.* **2019**, *256*, 117827.
240. Feng, L.; Qin, Z.; Huang, Y.; Peng, K.; Wang, F.; Yan, Y.; Chen, Y. Boron-, sulfur-, and phosphorus-doped graphene for environmental applications. *Sci. Total Environ.* **2020**, *698*, 134239.
241. Zhao, G.; Wang, A.; He, W.; Xing, Y.; Xu, X. 2D new nonmetal photocatalyst of sulfur-doped h-BN nanosheeets with high photocatalytic activity. *Adv. Mater. Interfaces.* **2019**, *6* (7), 1900062.
242. Tan, B.; Wu, Y.; Gao, F.; Yang, H.; Hu, Y.; Shang, H.; Zhang, X.; Zhang, J.; Li, Z.; Fu, Y. Engineering the optoelectronic properties of 2D hexagonal boron nitride monolayer films by sulfur substitutional doping. *ACS Appl. Mater. Interfaces.* **2022**, *14* (14), 16453-16461.
243. Liu, B.; Lee, J. Y.; Yan, S. J. C. Enhanced Catalytic Oxidation of CO on Sulfur-Doped Boron Nitride. *Chem. Nano. Mat.* **2020**, *6* (2), 223-231.
244. Liu, Y.; Wang, M.; Nie, Y.; Zhang, Q.; Ma, Q. Sulfur regulated boron nitride quantum dots electrochemiluminescence with amplified surface plasmon coupling strategy for BRAF gene detection. *Anal. Chem.* **2019**, *91* (9), 6250-6258.

Materials Advances Accepted Manuscript

View Article Online
DOI: 10.1039/D5MA01210D

Open Access Article. Published on 24 June 2026. Downloaded on 6/26/2026 4:24:14 PM.
This article is licensed under a Creative Commons Attribution 3.0 Unported Licence.

245. Kokulnathan, T.; Vishnuraj, R.; Wang, T.-J.; Kumar, E. A.; Pullithadathil, B. Heterostructured bismuth oxide/hexagonal-boron nitride nanocomposite: A disposable electrochemical sensor for detection of flutamide. *Ecotoxicol. Environ. Saf.* **2021**, *207*, 111276.
246. Zhang, Q.; Li, Z.; Li, X.; Yu, L.; Wu, Z. Boron nitride nanosheets decorated by bismuth ferrite particles: preparation, characterization, and effect on flame-retardant performance of epoxy resin. *Mater. Res. Express.* **2018**, *5* (9), 095019.
247. Chen, Z.; Chen, X.; Di, J.; Liu, Y.; Yin, S.; Xia, J.; Li, H. Graphene-like boron nitride modified bismuth phosphate materials for boosting photocatalytic degradation of enrofloxacin. *J. Colloid Interface Sci.* **2017**, *492*, 51-60.
248. Radha, A.; Wang, S.-F. Bismuth sulfide microstructures decorated with functionalized boron nitride composite for electrochemical detection of sulfadiazine. *Microchem. J.* **2022**, *189* (11), 429.
249. Mosavi, M. Adsorption behavior of mephentermine on the pristine and Si, Al, Ga-doped boron nitride nanosheets: DFT studies. *J. Chem. Lett.* **2020**, *1* (4), 164-171.
250. Nemati-Kande, E.; Karimian, R.; Goodarzi, V.; Ghazizadeh, E. Feasibility of pristine, Al-doped and Ga-doped Boron Nitride nanotubes for detecting SF4 gas: A DFT, NBO and QTAIM investigation. *Appl. Surf. Sci.* **2020**, *510*, 145490.
251. Doust Mohammadi, M.; Abdullah, H. Y. The adsorption of chlorofluoromethane on pristine, and Al-and Ga-doped boron nitride nanosheets: a DFT, NBO, and QTAIM study. *J. Mol. Model.* **2020**, *26*, 1-15.
252. Itas, Y. S.; Razali, R.; Tata, S.; Alrub, S. A. DFT Studies of Photocatalytic Properties of Silicon-and Boron-doped Gallium-nitride Nanotubes for Hydrogen Evolution and Carbondioxide Capture. *Silicon* **2024**, *16* (6), 2757-2770.
253. Baei, M. T.; Hashemian, S.; Torabi, P.; Gharehbaghi, A. Electronic structure study of gallium and indium doped (4, 4) armchair single-walled boron nitride nanotubes for production of solid-state devices. *FULLER NANOTUB CAR N* **2015**, *23* (1), 68-77.
254. Soleymani, R. The Effect of Aluminum, Gallium, Indium-Doping on the Zigzag (5, 0) Boron-Nitride Nanotubes: DFT, NMR, Vibrational, Thermodynamic Parameters and Electrostatic Potential Map with Electrophilicity Studies. *J. Phys. Theor. Chem.* **2016**.
255. Ran, H.; Yin, J.; Zhang, J.; Zhang, Y.; He, J. Group IIIA Single-Metal Atoms Anchored on Hexagonal Boron Nitride for Selective Adsorption Desulfurization via S–M Bonds. *Inorg. Chem.* **2023**, *62* (12), 4883-4893.
256. Yu, S.; Li, L.; Lai, Z.; Hao, J.; Zhang, K. A coupling effects of vacancy and Al (Ga, In) dopant on electronic structures of hexagonal boron nitride monolayer. *Mater. Res. Express.* **2017**, *4* (11), 116302.
257. Peyghan, A. A.; Baei, M. T.; Moghimi, M.; Hashemian, S. Phenol adsorption study on pristine, Ga-, and In-doped (4, 4) armchair single-walled boron nitride nanotubes. *Comput. Theor. Chem.* **2012**, *997*, 63-69.
258. Mohammadi, M. D.; Abdullah, H. Y.; Kalamse, V.; Chaudhari, A. Interaction of Fluorouracil drug with boron nitride nanotube, Al doped boron nitride nanotube and BC2N nanotube. *Comput. Theor. Chem.* **2022**, *1212*, 113699.
259. Nemati-Kande, E.; Abbasi, M.; Mohammadi, M. D. DFT studies on the interactions of pristine, Al and Ga-doped boron nitride nanosheets with CH3X (X= F, Cl and Br). *J. Mol. Struct.* **2020**, *1199*, 126962.
260. Shakerzadeh, E.; Noorizadeh, S. A first principles study of pristine and Al-doped boron nitride nanotubes interacting with platinum-based anticancer drugs. *Physica E* **2014**, *57*, 47-55.

Materials Advances Accepted Manuscript

View Article Online
DOI: 10.1039/D5MA01210D

Open Access Article. Published on 24 June 2026. Downloaded on 6/26/2026 4:24:14 PM.
This article is licensed under a Creative Commons Attribution 3.0 Unported Licence.

261. Nemati-Kande, E.; Karimian, R.; Goodarzi, V. Feasibility of pristine, Al-doped and Ga-doped Boron Nitride nanotubes for detecting SF4 gas: A DFT, NBO and QTAIM investigation. *Appl. Surf. Sci.* **2020**, *510*, 145490.
262. Zhang, J.; Zhang, B.; Yu, Y.; Wang, C.-M. Regulating the electronic and optic properties of hexagonal boron nitride nanosheets via phosphorus doping. *Europhys. Lett.* **2020**, *129* (3), 37001.
263. Lin, B.; Xu, F.; Mei, Y.; Liu, Y.; Zou, Y. Phosphorus-doped h-boron nitride as an efficient metal-free catalyst for direct dehydrogenation of ethylbenzene. *Catal. Sci. Technol.* **2021**, *11* (16), 5590-5597.
264. Liu, Y.; Xu, F.; Yuan, N.; Lin, B.; Zhou, Y. Revealing the Effect of Mass Transfer on Direct Dehydrogenation of Ethylbenzene Catalyzed by Phosphorous-doped Boron Nitride: Comparative Study. *Chem. Cat. Chem.* **2022**, *14* (2), e202101676.
265. Weng, Q.-H.; He, Q.; Liu, T.; Huang, H.-Y. Simple combustion production and characterization of octahydro [60] fullerene with a non-IPR C_{60} cage. *J. Am. Chem. Soc.* **2010**, *132* (43), 15093-15095.
266. Sainsbury, T.; O'Neill, A.; Passarelli, M. K.; Seraffon, M. Dibromocarbene functionalization of boron nitride nanosheets: Toward band gap manipulation and nanocomposite applications. *Chem. Mater.* **2014**, *26* (24), 7039-7050.
267. Shin, H.; Guan, J.; Zgierski, M. Z.; Kim, K. S.; Kingston, C. T. Covalent functionalization of boron nitride nanotubes via reduction chemistry. *ACS nano* **2015**, *9* (12), 12573-12582.
268. Zhi, C.; Bando, Y.; Terao, T.; Tang, C.; Kuwahara, H.; Golberg, D. J. C. A. A. J. Chemically activated boron nitride nanotubes. **2009**, *4* (10), 1536-1540.
269. Lin, Y.; Williams, T. V.; Xu, T.-B.; Cao, W.; Elsayed-Ali, H. E. Aqueous dispersions of few-layered and monolayered hexagonal boron nitride nanosheets from sonication-assisted hydrolysis: critical role of water. *J. Phys. Chem. C* **2011**, *115* (6), 2679-2685.
270. Xiao, F.; Naficy, S.; Casillas, G.; Khan, M. H. Hydrogels: Edge-Hydroxylated Boron Nitride Nanosheets as an Effective Additive to Improve the Thermal Response of Hydrogels (Adv. Mater. 44/2015). *Adv. Mater.* **2015**, *27* (44), 7247-7247.
271. Weng, Q.; Ide, Y.; Wang, X.; Wang, X. Design of BN porous sheets with richly exposed (002) plane edges and their application as TiO2 visible light sensitizer. *Nano Energy* **2015**, *16*, 19-27.
272. Krepel, D.; Hod, O. Effects of edge oxidation on the structural, electronic, and magnetic properties of zigzag boron nitride nanoribbons. *J. Chem. Theory Comput.* **2014**, *10* (1), 373-380.
273. Kim, D.; Nakajima, S.; Sawada, T. Sonication-assisted alcoholysis of boron nitride nanotubes for their sidewalls chemical peeling. *Chem. Commun.* **2015**, *51* (33), 7104-7107.
274. Ikuno, T.; Sainsbury, T.; Okawa, D.; Fréchet, J. Amine-functionalized boron nitride nanotubes. *Solid State Commun.* **2007**, *142* (11), 643-646.
275. Xie, S.-Y.; Wang, W.; Fernando, K. S.; Wang, X.; Lin, Y. Solubilization of boron nitride nanotubes. *Chem. Commun.* **2005**, (29), 3670-3672.
276. He, Z.; Zhao, J.; Li, F.; Zhang, D.; Guo, F.; Guo, H.; Wang, X. In situ synthesis of polymer-modified boron nitride nanosheets via anionic polymerization. *Appl. Surf. Sci.* **2021**, *537*, 147966.
277. Dai, J.; Wu, X.; Yang, J. Unusual metallic microporous boron nitride networks. *J. Phys. Chem. Lett.* **2013**, *4* (20), 3484-3488.
278. Zhi, C.; Bando, Y.; Tang, C.; Honda, S.; Sato, K.; Kuwahara, H. Covalent functionalization: towards soluble multiwalled boron nitride nanotubes. *Angew. Chem. Int. Ed.* **2005**, *44* (48), 7932-7935.

Materials Advances Accepted Manuscript

View Article Online
DOI: 10.1039/D5MA01210D

Open Access Article. Published on 24 June 2026. Downloaded on 6/26/2026 4:24:14 PM.
This article is licensed under a Creative Commons Attribution 3.0 Unported Licence.

279. Huang, X.; Zhi, C.; Jiang, P.; Golberg, D.; Bando, Y.; Tanaka, T. Polyhedral oligosilsesquioxane-modified boron nitride nanotube based epoxy nanocomposites: an ideal dielectric material with high thermal conductivity. *Adv. Funct. Mater.* **2013**, *23* (14), 1824-1831.
280. Bhattacharya, A.; Bhattacharya, S.; Das, G. Band gap engineering by functionalization of BN sheet. *Phys. Rev. B: Condens. Matter* **2012**, *85* (3), 035415.
281. Li, X.; Zhao, J.; Yang, J. Semihydrogenated BN sheet: a promising visible-light driven photocatalyst for water splitting. *Scientific reports* **2013**, *3* (1), 1858.
282. Tang, C.; Bando, Y.; Huang, Y.; Yue, S.; Gu, C.; Xu, F.; Golberg, D. Fluorination and electrical conductivity of BN nanotubes. *J. Am. Chem. Soc.* **2005**, *127* (18), 6552-6553.
283. Sun, W.; Meng, Y.; Fu, Q.; Wang, F.; Wang, G.; Gao, W.; Huang, X.; Lu, F. High-yield production of boron nitride nanosheets and its uses as a catalyst support for hydrogenation of nitroaromatics. *ACS Appl. Mater. Interfaces.* **2016**, *8* (15), 9881-9888.
284. Grant, J. T.; Carrero, C. A.; Goeltl, F.; Venegas, J. Selective oxidative dehydrogenation of propane to propene using boron nitride catalysts. *Science* **2016**, *354* (6319), 1570-1573.
285. Wang, L.; Wang, Y.; Zhang, R.; Ding, R.; Chen, X. Edge-activating CO2-mediated ethylbenzene dehydrogenation by a hierarchical porous BN catalyst. *ACS Catal.* **2020**, *10* (12), 6697-6706.
286. Wang, Y.; Wang, J.; Zheng, P.; Sun, C.; Luo, J. Boosting selectivity and stability on Pt/BN catalysts for propane dehydrogenation via calcination & reduction-mediated strong metal-support interaction. *J. Energy Chem.* **2022**, *67*, 451-457.
287. Torii, S.; Jimura, K.; Hayashi, S.; Kikuchi, R. Utilization of hexagonal boron nitride as a solid acid–base bifunctional catalyst. *J. Catal.* **2017**, *355*, 176-184.
288. Mao, X.; Zhou, S.; Yan, C.; Zhu, Z. A single boron atom doped boron nitride edge as a metal-free catalyst for N 2 fixation. *Phys. Chem. Chem. Phys.* **2019**, *21* (3), 1110-1116.
289. Liu, Y.; Zhang, H.; Cheng, X. Unveiling the mechanism of nitrogen fixation by single-atom catalysts and dual-atom catalysts anchored on defective boron nitride nanotubes. *Energy Fuels* **2023**, *37* (17), 13271-13281.
290. Zhang, Y.; Du, H.; Ma, Y.; Ji, L. Hexagonal boron nitride nanosheet for effective ambient N 2 fixation to NH 3. *Nano Res.* **2019**, *12*, 919-924.
291. Lu, L.; He, J.; Wu, P.; Wu, Y.; Chao, Y. Taming electronic properties of boron nitride nanosheets as metal-free catalysts for aerobic oxidative desulfurization of fuels. *Green Chem.* **2018**, *20* (19), 4453-4460.
292. Wu, P.; Wu, Y.; Chen, L.; He, J.; Hua, M. Boosting aerobic oxidative desulfurization performance in fuel oil via strong metal-edge interactions between Pt and h-BN. *Chem. Eng. J.* **2020**, *380*, 122526.
293. Zhang, Y.; Yao, Y.-F.; Qiao, Y.-Y.; Wang, G.-C. First-principles theoretical study on dry reforming of methane over perfect and boron-vacancy-containing h-BN sheet-supported Ni catalysts. *Phys. Chem. Chem. Phys.* **2021**, *23* (1), 617-627.
294. Xu, Y.; An, Z.; Yu, X.; Yao, J.; Lv, Q.; Yang, H.; Lv, Z.; Guo, H.; Jiang, Q. Enhanced catalytic stability and structural evolution of Rh-BN interface in dry reforming of methane under intensified CO2 partial pressure. *J. Catal.* **2023**, *427*, 115094.
295. Ma, C.; Liu, B.; Yan, S. Enhanced catalytic activity for CO oxidation by Fe-Adsorbing on BN under mild condition: A promising single-atom catalyst. *Mol. Catal.* **2020**, *495*, 111165.
296. Lu, Z.; Lv, P.; Yang, Z.; Li, S.; Ma, D. A promising single atom catalyst for CO oxidation: Ag on boron vacancies of h-BN sheets. *Phys. Chem. Chem. Phys.* **2017**, *19* (25), 16795-16805.

Materials Advances Accepted Manuscript

View Article Online
DOI: 10.1039/D5MA01210D

Open Access Article. Published on 24 June 2026. Downloaded on 6/26/2026 4:24:14 PM.
This article is licensed under a Creative Commons Attribution 3.0 Unported Licence.

297. Datta, J.; Majumder, C. Stabilizing Co, Ni and Cu on the h-BN surface: Using OO bond activation to probe their performance as single atom catalyst. *Catal. Today* **2021**, *370*, 75-82.
298. Sredojevic, D. N.; Belic, M. R.; Sljivancanin, Z. Hydrogen evolution reaction over single-atom catalysts based on metal adatoms at defected graphene and h-BN. *J. Phys. Chem. C* **2020**, *124* (31), 16860-16867.
299. Ma, Z.; Cui, Z.; Xiao, C.; Dai, W. Theoretical screening of efficient single-atom catalysts for nitrogen fixation based on a defective BN monolayer. *Nanoscale* **2020**, *12* (3), 1541-1550.
300. Deng, C.; He, R.; Shen, W. A single-atom catalyst of cobalt supported on a defective two-dimensional boron nitride material as a promising electrocatalyst for the oxygen reduction reaction: a DFT study. *Phys. Chem. Chem. Phys.* **2019**, *21* (13), 6900-6907.
301. Sharker, S. M. Hexagonal boron nitrides (white graphene): a promising method for cancer drug delivery. *Int. J. Nanomed.* **2019**, 9983-9993.
302. Majedi, S.; Behmagham, F.; Vakili, M. Theoretical view on interaction between boron nitride nanostructures and some drugs. *J. Chem. Lett.* **2020**, *1* (1), 19-24.
303. Ciofani, G. Potential applications of boron nitride nanotubes as drug delivery systems. *Expert Opin Drug Deliv.* **2010**, *7* (8), 889-893.
304. Hosseinian, A.; Vessally, E.; Yahyaei, S.; Edjlali, L.; Bekhradnia, A. A density functional theory study on the Interaction between 5-Fluorouracil Drug and C 24 Fullerene. *J. Cluster Sci.* **2017**, *28*, 2681-2692.
305. Nejati, K.; Vessally, E.; Nezhad, P. D. K.; Mofid, H.; Bekhradnia, A. The electronic response of pristine, Al and Si doped BC2N nanotubes to a cathinone molecule: Computational study. *J. Phys. Chem. Solids* **2017**, *111*, 238-244.
306. Nejati, K.; Hosseinian, A.; Vessally, E.; Bekhradnia, A. A comparative DFT study on the interaction of cathinone drug with BN nanotubes, nanocages, and nanosheets. *Appl. Surf. Sci.* **2017**, *422*, 763-768.
307. Permyakova, E. S.; Antipina, L. Y.; Kovalskii, A. M.; Zhitnyak, I. Y. Experimental and theoretical study of doxorubicin physicochemical interaction with BN (O) drug delivery nanocarriers. *J. Phys. Chem. C* **2018**, *122* (46), 26409-26418.
308. Gnatyuk, O.; Dovbeshko, G.; Yershov, A.; Karakhim, S. 2D-BN nanoparticles as a spectroscopic marker and drug delivery system with protection properties. *RSC Adv.* **2018**, *8* (53), 30404-30411.
309. Vatanparast, M.; Shariatinia, Z. Hexagonal boron nitride nanosheet as novel drug delivery system for anticancer drugs: Insights from DFT calculations and molecular dynamics simulations. *J. Mol. Graphics Modell.* **2019**, *89*, 50-59.
310. Weng, Q.; Wang, B.; Wang, X.; Hanagata, N.; Li, X. Highly water-soluble, porous, and biocompatible boron nitrides for anticancer drug delivery. *ACS nano* **2014**, *8* (6), 6123-6130.
311. Zhitnyak, I. Y.; Bychkov, I. N.; Sukhorukova, I. V.; Kovalskii, A. M. Effect of BN nanoparticles loaded with doxorubicin on tumor cells with multiple drug resistance. *ACS Appl. Mater. Interfaces.* **2017**, *9* (38), 32498-32508.
312. Goyal, A.; Aggarwal, D.; Kapoor, S.; Goel, N.; Singhal, S.; Shukla, J. A comprehensive experimental and theoretical study on BN nanosheets for the adsorption of pharmaceutical drugs. *New J. Chem.* **2020**, *44* (10), 3985-3997.
313. Makiabadi, B.; Zakarianezhad, M.; Behjatmanesh-Ardakani, R. Investigating the performance of BN nanotubes as drug delivery systems for Azacitidine and decitabine anti-cancer drugs: a theoretical study. *Comput. Theor. Chem.* **2024**, *1231*, 114429.

Materials Advances Accepted Manuscript

View Article Online
DOI: 10.1039/D5MA01210D

314. Sukhorukova, I. V.; Zhitnyak, I. Y.; Kovalskii, A. M.; Matveev, A. T. Boron nitride nanoparticles with a petal-like surface as anticancer drug-delivery systems. *ACS Appl. Mater. Interfaces.* **2015**, *7* (31), 17217-17225.
315. Hassan, J.; Naz, S.; Haider, A.; Raza, A.; Ul-Hamid, A.; Qumar, U.; Haider, J.; Goumri-Said, S. h-BN nanosheets doped with transition metals for environmental remediation; a DFT approach and molecular docking analysis. *Mater. Sci. Eng., B* **2021**, *272*, 115365.
316. Zeng, Y.; Lin, S.; Gu, D.; Li, X. Two-dimensional nanomaterials for gas sensing applications: The role of theoretical calculations. *Nanomaterials* **2018**, *8* (10), 851.
317. Chen, X.; Jia, S.; Ding, N.; Shi, J. Capture of aromatic organic pollutants by hexagonal boron nitride nanosheets: density functional theoretical and molecular dynamic investigation. *Environ. Sci. Nano* **2016**, *3* (6), 1493-1503.
318. Rahman, Z.; Singh, V. P. The relative impact of toxic heavy metals (THMs)(arsenic (As), cadmium (Cd), chromium (Cr)(VI), mercury (Hg), and lead (Pb)) on the total environment: an overview. *Environ. Monit. Assess.* **2019**, *191*, 1-21.
319. Bian, Y.; Li, L.; Song, H.; Su, Y.; Lv, Y. Porous boron nitride: A novel metal-free cataluminescence material for high performance H2S sensing. *Sens. Actuators, B* **2021**, *332*, 129512.
320. Ahmad, R.; Tripathy, N.; Khosla, A.; Khan, M.; Mishra, P. Recent advances in nanostructured graphitic carbon nitride as a sensing material for heavy metal ions. *J. Electrochem. Soc.* **2019**, *167* (3), 037519.
321. Li, L.; Zhao, J. Defected boron nitride nanosheet as an electronic sensor for 4-aminophenol: A density functional theory study. *J. Mol. Liq.* **2020**, *306*, 112926.
322. Srivastava, P.; Sharma, V.; Jaiswal, N. K. Adsorption of COCl2 gas molecule on armchair boron nitride nanoribbons for nano sensor applications. *Microelectron. Eng.* **2015**, *146*, 62-67.
323. Mohammadi, M.; Alirezapour, F.; Khanmohammadi, A. Adsorption of transition metal cations (Cr2+, Mn2+, Fe2+, Cu+, Ag+ and Au+) on boron nitride nanotube: structural analysis and electronic properties. *Adv. J. Chem. Sect., A* **2024**, *7* (4), 355-373.
324. Roondhe, B.; Ahuja, R.; Luo, W. Investigation of the adsorption behaviour of toxic heavy metals and bacteria on two allotropes of low dimensional boron nitride: Implications for detection and elimination. *Appl. Surf. Sci.* **2024**, *667*, 160404.
325. Bian, Y.; Li, L.; Song, H.; Su, Y.; Lv, Y. Porous boron nitride: A novel metal-free cataluminescence material for high performance H2S sensing. *Sens. Actuators, B* **2021**, *332*, 129512.
326. Yoosefian, M.; Etminan, N.; Moghani, M. Z.; Mirzaei, S. The role of boron nitride nanotube as a new chemical sensor and potential reservoir for hydrogen halides environmental pollutants. *Superlattices Microstruct.* **2016**, *98*, 325-331.
327. Tang, Y.; Chen, W.; Li, C.; Pan, L.; Dai, X. Adsorption behavior of Co anchored on graphene sheets toward NO, SO2, NH3, CO and HCN molecules. *Appl. Surf. Sci.* **2015**, *342*, 191-199.
328. Opoku, F.; Govender, P. P. Two-dimensional CoOOH as a highly sensitive and selective H2S, HCN and HF gas sensor: a computational investigation. *Electroanalysis* **2020**, *32* (12), 2764-2774.
329. He, Y.; Li, D.; Gao, W.; Yin, H.; Chen, F.; Sun, Y. High-performance NO_2 sensors based on spontaneously functionalized hexagonal boron nitride nanosheets via chemical exfoliation. *Nanoscale* **2019**, *11* (45), 21909-21916.

Open Access Article. Published on 24 June 2026. Downloaded on 6/26/2026 4:24:14 PM.
This article is licensed under a Creative Commons Attribution 3.0 Unported Licence.

Materials Advances Accepted Manuscript

View Article Online
DOI: 10.1039/D5MA01210D

Open Access Article. Published on 24 June 2026. Downloaded on 6/26/2026 4:24:14 PM.
This article is licensed under a Creative Commons Attribution 3.0 Unported Licence.

330. Pi, S.; Zhang, X.; Chen, D.; Tang, J. Sensing properties of Ni-doped boron nitride nanotube to SF6 decomposed components: a DFT study. *AIP Adv.* **2019**, *9* (9).
331. Deng, Z.-Y.; Zhang, J.-M.; Xu, K.-W. First-principles study of SO2 molecule adsorption on the pristine and Mn-doped boron nitride nanotubes. *Appl. Surf. Sci.* **2015**, *347*, 485-490.
332. Movlarooy, T.; Fadradi, M. A. Adsorption of cyanogen chloride on the surface of boron nitride nanotubes for CNCl sensing. *Chem. Phys. Lett.* **2018**, *700*, 7-14.
333. Huo, B.; Liu, B.; Chen, T.; Cui, L.; Xu, G.; Liu, M. One-step synthesis of fluorescent boron nitride quantum dots via a hydrothermal strategy using melamine as nitrogen source for the detection of ferric ions. *Langmuir* **2017**, *33* (40), 10673-10678.
334. Azamat, J.; Sattary, B. S.; Khataee, A.; Joo, S. W. Removal of a hazardous heavy metal from aqueous solution using functionalized graphene and boron nitride nanosheets: Insights from simulations. *J. Mol. Graphics Modell.* **2015**, *61*, 13-20.
335. Yeh, C.-H. Computational study of Janus transition metal dichalcogenide monolayers for acetone gas sensing. *ACS omega* **2020**, *5* (48), 31398-31406.
336. Peng, D.; Zhang, L.; Li, F.-F.; Cui, W.-R.; Liang, R.-P.; Qiu, J.-D. J. A. A. M.; Interfaces. Facile and green approach to the synthesis of boron nitride quantum dots for 2, 4, 6-trinitrophenol sensing. *ACS Appl. Mater. Interfaces.* **2018**, *10* (8), 7315-7323.
337. Xue, L.; Lu, B.; Wu, Z.-S.; Ge, C.; Wang, P.; Zhang, R.; Zhang, X.-D. J. C. E. J. Synthesis of mesoporous hexagonal boron nitride fibers with high surface area for efficient removal of organic pollutants. *Chem. Eng. J.* **2014**, *243*, 494-499.
338. Zhou, C.; Jiang, W.; Via, B. K. Facile synthesis of soluble graphene quantum dots and its improved property in detecting heavy metal ions. *Colloids Surf., B* **2014**, *118*, 72-76.
339. Mohammadi, M.; Alirezapour, F.; Khanmohammadi, A. Adsorption of transition metal cations (Cr2+, Mn2+, Fe2+, Cu+, Ag+ and Au+) on boron nitride nanotube: structural analysis and electronic properties. *Adv J Chem Sect A* **2024**, *7* (4), 355-373.
340. Lu, Z.; Yao, Q.; Ying, H.; Li, T.; Zhang, J.; Wang, L. One-pot synthesis of vertical graphene/h-BN heterostructure utilizing the passivation role of hydrogen. *Results Phys.* **2022**, *35*, 105404.
341. Martini, L.; Mišeikis, V.; Esteban, D.; Azpeitia, J.; Pezzini, S. Scalable high-mobility graphene/hBN heterostructures. *ACS Appl. Mater. Interfaces.* **2023**, *15* (31), 37794-37801.
342. Dean, C. R.; Young, A. F.; Meric, I.; Lee, C.; Wang, L. Boron nitride substrates for high-quality graphene electronics. *Nat. Nanotechnol.* **2010**, *5* (10), 722-726.
343. Tang, S.; Ding, G.; Xie, X.; Chen, J.; Wang, C. Nucleation and growth of single crystal graphene on hexagonal boron nitride. *Carbon* **2012**, *50* (1), 329-331.
344. Yang, W.; Chen, G.; Shi, Z.; Liu, C.-C. Epitaxial growth of single-domain graphene on hexagonal boron nitride. *Nat. Mater.* **2013**, *12* (9), 792-797.
345. Tang, S.; Wang, H.; Wang, H. S.; Sun, Q.; Zhang, X. Silane-catalysed fast growth of large single-crystalline graphene on hexagonal boron nitride. *Nat. Commun.* **2015**, *6* (1), 6499.
346. Zhang, C.; Zhao, S.; Jin, C.; Koh, A. L.; Zhou, Y. Direct growth of large-area graphene and boron nitride heterostructures by a co-segregation method. *Nat. Commun.* **2015**, *6* (1), 6519.
347. Toksumakov, A. N.; Ermolaev, G. A.; Tatmyshevskiy, M. K.; Klishin, Y. A.; Slavich, A. S.; Begichev, I. V. Anomalous optical response of graphene on hexagonal boron nitride substrates. *Commun. Phys.* **2023**, *6* (1), 13.
348. Mawwa, J.; Shamim, S. U. D.; Khanom, S.; Hossain, M. K.; Ahmed, F. In-plane graphene/boron nitride heterostructures and their potential application as toxic gas sensors. *RSC Adv.* **2021**, *11* (52), 32810-32823.

Materials Advances Accepted Manuscript

View Article Online
DOI: 10.1039/D5MA01210D

349. Chernozatonskii, L. A.; Kochaev, A. I. Bilayer C60 Polymer/h-BN Heterostructures: A DFT Study of Electronic and Optic Properties. *Polymers* **2024**, *16* (11), 1580.
350. Gillen, R.; Robertson, J.; Maultzsch, J. Electronic properties of MoS2/h-BN heterostructures: impact of dopants and impurities. *Phys. Status Solidi* **2014**, *251* (12), 2620-2625.
351. Ding, S.; Mao, D.; Yang, S.; Wang, F.; Meng, L. Graphene-analogue h-BN coupled Bi-rich Bi4O5Br2 layered microspheres for enhanced visible-light photocatalytic activity and mechanism insight. *Appl. Catal., B* **2017**, *210*, 386-399.
352. Di, J.; Xia, J.; Ji, M.; Wang, B. Advanced photocatalytic performance of graphene-like BN modified BiOBr flower-like materials for the removal of pollutants and mechanism insight. *Appl. Catal., B* **2016**, *183*, 254-262.
353. Liu, D.; Jiang, Z.; Zhu, C.; Qian, K.; Wu, Z.; Xie, J. Graphene-analogue BN-modified microspherical BiOI photocatalysts driven by visible light. *Dalton Trans.* **2016**, *45* (6), 2505-2516.
354. Li, D.; Li, R.; Zhou, D.; Zeng, F.; Yan, W.; Cai, S. The charge transfer feature and high photocatalytic activity of S-scheme TiO2/h-BN heterostructure from first-principles. *Appl. Surf. Sci.* **2022**, *586*, 152765.
355. Song, L.; Jia, H.; Zhang, H.; Cao, J. Graphene-like h-BN/CdS 2D/3D heterostructure composite as an efficient photocatalyst for rapid removing rhodamine B and Cr (Ⅵ) in water. *Ceram. Int.* **2020**, *46* (15), 24674-24681.
356. Li, H.; Luo, R.; Zhong, J.; Huang, S.; Li, M.; Li, J. In-situ construction of h-BN/BiOCl heterojunctions with rich oxygen vacancies for rapid photocatalytic removal of typical contaminants. *Colloids Surf., A. Physicochem. Eng. Asp.* **2023**, *659*, 130756.
357. Du, Z.; Feng, L.; Guo, Z.; Yan, T.; Hu, Q.; Lin, J. Ultrathin h-BN/Bi2MoO6 heterojunction with synergetic effect for visible-light photocatalytic tetracycline degradation. *J. Colloid Interface Sci.* **2021**, *589*, 545-555.
358. He, Y.; Xu, N.; Junior, L. B.; Hao, X.; Yao, B.; Yang, Q. Construction of AuNPs/h-BN nanocomposites by using gold as interfacial electron transfer mediator with highly efficient degradation for levofloxacin hydrochloride and hydrogen generation. *Appl. Surf. Sci.* **2020**, *520*, 146336.
359. Okada, M.; Sawazaki, T.; Watanabe, K.; Taniguch, T.; Hibino, H.; Shinohara, H.; Kitaura, R. Direct chemical vapor deposition growth of WS2 atomic layers on hexagonal boron nitride. *Acs Nano* **2014**, *8* (8), 8273-8277.
360. Ahmed, S. F.; Mofijur, M.; Rafa, N.; Chowdhury, A. T.; Chowdhury, S.; Nahrin, M.; Islam, A. S.; Ong, H. C. Green approaches in synthesising nanomaterials for environmental nanobioremediation: Technological advancements, applications, benefits and challenges. *Environ. Res.* **2022**, *204*, 111967.

Open Access Article. Published on 24 June 2026. Downloaded on 6/26/2026 4:24:14 PM.
This article is licensed under a Creative Commons Attribution 3.0 Unported Licence.

Materials Advances Accepted Manuscript

View Article Online
DOI: 10.1039/D5MA01210D

No primary research results, software or code have been included and no new data were generated or analysed as part of this review.

Open Access Article. Published on 24 June 2026. Downloaded on 6/26/2026 4:24:14 PM.
This article is licensed under a Creative Commons Attribution 3.0 Unported Licence.

Materials Advances Accepted Manuscript